MECHANICAL AND THERMAL PROPERTIES OF TWO-DIMENSIONAL MATERIAL

by

Dan Jia

A dissertation submitted to the faculty of
The University of North Carolina at Charlotte
in partial fulfillment of the requirements
for the degree of Doctor of Philosophy in
Mechanical Engineering

Charlotte

2015

Approved by:

_____

Dr. Alireza Tabarraei

_____

Dr. Ronald E. Smelser

_____

Dr. Harish P. Cherukuri

_____

Dr. Jian Zhang

ABSTRACT

The aim of this dissertation is to investigate the mechanical and thermal properties of two-dimensional materials. The discovery of the fantastic properties of graphene, such as high mechanical strength and excellent electronic properties, has stimulated interests in exfoliating other two-dimensional graphene-like materials. Laminated materials such as hexagonal boron nitride or MoO_3 which are composed of stacked layers with the van der Waals force between adjacent sheets and strong covalent bonds within each layer have received the most attention. In laminated materials, the weak bonding between layers allows an easy isolation of free-standing single or few-atom-thick sheets. The isolated stable free-standing sheets are known as two-dimensional materials which exhibit properties distinct from their corresponding three-dimensional bulk material counterparts.

The high specific surface area of two-dimensional materials along with their attractive physical, electrical and mechanical properties make them important for a variety of applications such as supercapacitors, optoelectronics, spintronics, lithium ion batteries, sensors and nanocomposites. The use of two-dimensional materials in such sensitive devices necessitates a fundamental understanding of their physical and mechanical properties. It is the objective of this dissertation to investigate the mechanical and thermal properties of two-dimensional materials with special focus on MoO_3, graphyne and hybrid graphene-boron nitirde.

Ideally, the properties of two-dimensional materials should be characterized experimentally. However, designing and performing experiments at nanoscales is very complicated. Computational studies, on the other hand, can provide valuable insights about the behavior of two-dimensional materials. In this dissertation density functional theory (DFT) and molecular dynamics (MD) simulations are used to study the properties of two-dimensional materials. In the first part of this dissertation, DFT is used to develop and propose a hyperelastic constitutive model for modeling the mechanical behavior of MoO_3. Such a constitutive model pave the way toward finite element modeling of monolayer MoO_3 and can substantially reduce the computational costs in comparison with atomistic simulations. In the second part of the dissertation, molecular dynamics is utilized to study the mechanical and thermal properties of both graphyne and hybrid graphene-boron nitride nanoribbons. Using MD simulations, the impacts of nanoribbons width, length and chirality on their properties are investigated. Furthermore, the effects of defects on the properties of ribbons are studied and the strain engineering of the thermal conductivity of ribbons is investigated.

ACKNOWLEDGEMENTS

I would never have been able to finish my dissertation wihout the gudiance of committee members, help from friends, and support from my parents.

My sincere gratitude goes towards my academic advisor Dr. Alireza Tabarraei, for his help on my research. I would also to thank Dr. Ronald E. Smelser, Dr. Harish P. Cherukuri and Dr. Jian Zhang for serving on my dissertation committee.

I would like to thank Dr. Hodgins and Franklin, who as the lab leading mentors, has helped me so much through my teaching assistant work. Many thanks to Rodrigo and other TAs' in the labs for helping me learn instrumentation knowledge.

I would like to thank Lisa Yu, as my best friend, who is always willing to help and give me the best suggestions. I would like to specially thank Tish Barber, Jerry Barber, Jerry and Lynn, Min, Jing, for their never-end care and encouragement supporting me go through the harsh times.

Finally, I would like to thank my parents. They were always there and gave me all the love and encouragement.

TABLE OF CONTENTS

LIST OF FIGURES

LIST OF TABLES

CHAPTER 1: INTRODUCTION

In this chapter, a literature review of studies investigating two-dimensional materials will be presented. Primarily, the background of two-dimensional materials up-to-date studies and obstacles are stated. We review the achievements and applicable methodologies for studying of graphene, MoO_3, graphyne and other related two dimensional materials. Thereafter, we state the research objectives of this dissertation and tasks to investigate two dimensional materials, specifically MoO_3 and graphyne. Finally, issues pertaining to the mechanical properties and thermal properties of the two-dimensional materials will be addressed.

1.1   Background and Motivation

1.1.1   Graphene

Since the first two-dimensional graphene was successfully produced in 2004, extensive research has been put into studying mechanical, thermal, chemical and photonic properties in monolayer graphene sheets [32,48]. Graphene is a single-layer of carbon atoms that is extracted from graphite, and packed into a dense honeycomb crystal structure, which can be viewed as an individual atomic plane [130]. Graphene can be prepared by exfoliating graphite through dispensation of graphite on the surface of an organic solvent, grown on a metal base [64,99]. The size of graphene samples obtained by exfoliation is relatively small due to defects. Fig. 1 shows the two-

dimensional graphene, a one-dimensional fullerrance ball and the three-dimensional graphite. The two-dimensional materials have attracted great interest among researchers due to their unique chemical, mechanical, thermal and photonic properties [32, 45, 48, 51].
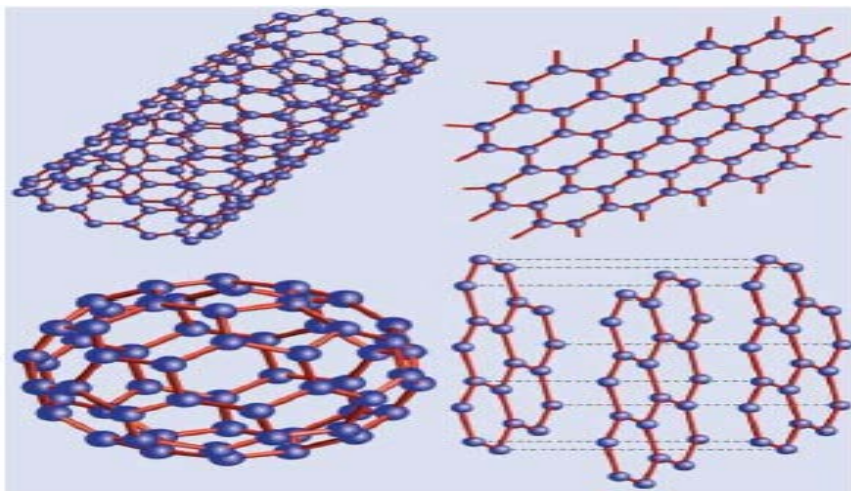
Figure 1: Graphene and its carbon allotropes [152]

The success in obtaining monolayer graphene has shown that it is possible to create stable, single or few-atom-thick layers of two-dimensional materials with weak van der Waals-like coupling between layers. Although the mechanical properties of graphene have been entensively investigated with both computational methods and experimental tests, strength of graphene is still limited by the presence of defects. Large-scale efficient production of graphene is the prerequisite to putting this single-layer crystal into structural and mechanical applications. With the improvement of experimental techniques, small-scale graphene is available by exfoliating bulk graphite. However,

researchers are still investigating how to obtain large-scale graphene with dispersing methodologies. By transforming or folding the two-dimensional graphene, one-dimensional nanotubes and zero-dimensional buckyballs can be obtained [80].

Fig. 1 has shown an example of graphene being made into variable forms. Obviously, it's inevitable to have defects during the preparation of two-dimensional material. Additional defects occur during the process of folding or wrapping mono-layer graphene membranes into different shapes. Defects can increase the chemical reactivity of graphene [40] but reduce the mechanical strength of this material.

Many studies have examined the mechanical properties of graphene in recent years [51, 95, 98, 136, 207]. Lee's research group measured the free-standing monolayer graphene membranes' breaking strength (42 Nm^{-1}) and Young's modulus (E=1.0 TPa) [95]. High strength graphene has been used to make films for stretchable and transparent electrodes [86, 99]. By depositing graphene on the base of a copper foil or a silicon composite, large-scale graphene has been obtained to be used as anodes for batteries [6, 99, 175]. To fully exploit the mechanical properties of graphene, graphene is used as filler in polymer matrices [48, 146]. Mechanical properties of graphene based composites can be enhanced by controlling the content of graphene [136, 145, 207]. It broadens the area in stable, light weight and functional composites.

Furthermore, the remarkable thermal properties of two-dimensional graphene have renewed researchers' interest in inorganic two-dimensional materials [176]. Graphene's high thermal conductivity is an alternative way of solving the microelectronic devices' high-temperature detachment problems. Moreover, two-dimensional graphene can be cut into various shapes, such as graphene nano-ribbons to be applicable to nanosize

devices. With the increasing demand for the microelectronics devices, good understanding and managing the thermal behavior of material used in these devices is important to the success of the microelectronics and other industries [1,4,47,61,75,211].

Graphene's super hign in-plabe thermal conductivity is related to the sp^2 carbon-carbon bondings; while the out-of plane heat flow is constrained by weak van der Waals coupling [143]. The outstanding mechanical, thermal and photonic properties of mono-layer graphene have broaden the range of its potential applications of carbon materials in nano-scale devices [32, 48, 51].

Nika's research group studied the thermal conductivity of two-dimensional graphene and compared it with the bulk graphite [127]. The heat transport in two-dimensional graphene is distinguished from that of the bulk graphite. In bulk graphite, there's no need to consider other scattering mechanism when calculating the thermal conductivity integral. However, for two-dimensional graphene, the heat transports in two-dimensional only till certain low-bound cut-off frequency [88, 89, 127].

The study of thermal conductivity of graphene can be summarized in the following key parameters.

∗ Thermal conductivity's dependent on nanoribbons' length and width

Guo's group studied the thermal conductivity of graphene nanoribbons. They stated that the length, width and uni-axial strains dependence of thermal conductivity is essential to the study of low-dimensional system's thermal conduction [61]. Li's group also showed that thermal conductivity of nanostructures are dependent on the stress and strain. Applying strain on the material can provides a mechanism to

tune the thermal conductivity to a desired rate [101]. William's group investigated the correlation between graphene sheet and thermal conductivity, including size's and width's effect [47]. Besides study the thermal conductivity's dependent on nanoribbons of graphene, researchers have even achieved tuning or rectification the thermal conductivity by edge passivation and isotope engineering [70, 192].

∗ Thermal conductivity's dependent on nanoribbons' edge

Hu's research team found out that the thermal conductivity of graphene nanoribbons depends on the edge-chirality and can be affected by defects. The thermal conductivity varies with the chirality angle of graphene ribbon [69]. William's group investigated the correlation between graphene sheet and thermal conductivity, including the smooth and the rough edge's effect [47]. Hao's group also investigated defects' effect on both mechanical and thermal properties of graphene. [62]. The zigzag graphene nanoribbonds is shown to have larger thermal conductivity compared to that of the armchair graphene [61, 69].

∗ Thermal conductivity's dependent on temperature, strain and defects

Most measurements on nanotube materials indicate that thermal conductivity increases monotonically with increasing temperature even above ambient temperature [108]. Remarkable decreasing of thermal conductivity is observed when tensile or compression strain is applied on the two-dimensional nanoribbons [61, 101]. Defects can cause the decrement of thermal conductivity of graphene [62, 69].

1.1.2 Other Two-dimensional Materials

∗ Two-dimensional MoO_3
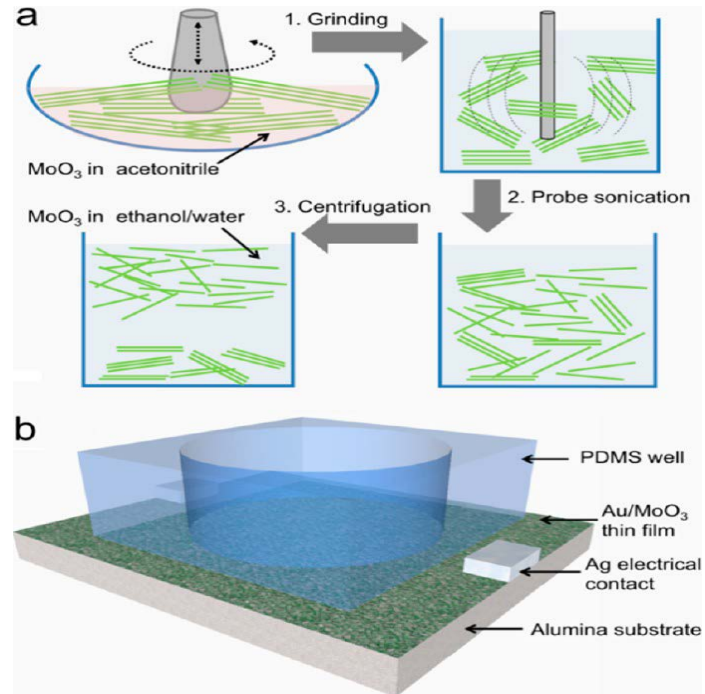
Figure 2: Exfoliation schematic of 2D MoO_3 [10]

Two-dimensional MoO_3 is applicable to semiconductors [54,115,188], energy storage systems [19, 185], photochromism [43, 50] and oxidation catalyst [30, 118]. MoO_3 is also a promising material in optical devices, sensors, lubricants, lithium batteries, and information storage [72]. Two-dimensional MoO_3 is usually used as both functional material and structural support material in those applications. Two-dimensional MoO_3's application area requires a good understanding of its mechanical properties, such as Young's modulus and yield strength. Traditional methods for understanding mechanical properties of materials rely on experiments. Performing experiments on two-dimensional MoO_3 is challenging, time consuming and expensive. Two-dimensional MoO_3 has been successfully ex-foliated [10,174]. The process of exfoliating two-dimensional MoO_3 in the experiment is shown in Fig. 2. Usually, the two-dimensional MoO_3 is obtained through dispersing liquid mixed with pow-

dered MoO_3 onto a metal base. Thereafter, the dried one-layer MoO_3 is exfoliated from the base.

However, defects are inevitable during the exfoliation. It's critical to understand the mechanical properties of two-dimensional MoO_3 to properly apply it as functional material or structural support material. Until now, some researchers use experiments to investigate the structural and mechanical properties of two-dimensional MoO_3. Some research groups studied the structural properties of MoO_3 catalyst supported by a base such as Al_2O_3 experimentally, since the structure of MoO_3 affects the reaction [30, 72, 197]. Moreover, MoO_3 is superior in charge storage systems due to its ability of intercalating ions in a wide range, which requires it being made into thin films [19, 212]. MoO_3 is a most important member of the interstitial-free transitional metal oxides, which is a promising anode for lithium-ion batteries [141, 177]. MoO_3 meets the requirement of such batteries having high capacity ability, high thermal and chemical stability [177].

It's important to understand the mechanical strength of MoO_3 to produce a good performance of the whole system. Although some studies have been done on the chemical, photonic or electrical properties of MoO_3, most of the methods are based on experiments or computational methods including density functional theory [19, 30, 176]. However,there are rare publications on the general model that can predict the mechanical properties of MoO_3. We propose to use the computational method DFT to study mechanical properties of two-dimensional MoO_3. We will then propose a constitutive model for MoO_3 based on the DFT results.

Table 1: Summary of elastic properties of MoO_3

MoO_3 type	thickness	Young's modulus [GPa]	Method and Potential
nanoflake [174] %	N/A	176.3 ± 4.1	Experiment(nano-indentation)
nanoflake [10]	0.14 nm	N/A	Experiment

∗ Graphyne

Since graphyne has a hexagonal structure analogous to that of mono-layer graphene; yet graphyne has the carbon-carbon triple-bond linkage. Graphyne may have similar or even superior thermal and mechanical properties compared to graphene due to the presence of triple-bond linkage.

There exist many other carbon allotropes which are two-dimensional, such as graphyne, graphdiyne, graphyne-2, graphyne-3 and graphyne-4. Two-dimensional graphyne and its family of materials are predicted to be applicable to micro-scale devices due to their structural similarity to graphene. Graphyne is a superior heat conductor with room temperature thermal conductivity up to 5300W/mK, which allows it to be used in thermal management applications in nano-electronic circuits, even in micro-electronics, photonics, and bioengineering [8,56,155,190]. Two-dimensional graphyne and its family of materials are likely to have similar or even superior mechanical or thermal properties compared to the well-known graphene. Anomalous large thermal conductivity of two-dimensional graphene has been observed and obtained from experiments; while in three-dimensional bulk materials, the thermal conductivity has a finite value [12,55]. The crystal's anharmonisity mainly affects the thermal conductivity of bulk graphene; however, the two-dimensional graphene's thermal conductivity

varies due to structural and other factors. Usually, the thermal condcutivity of 2D graphene diverges in a logarithmic way. The finite-size thermal conductivity $\kappa(N, T)$ behaves a correlation with the size of the system, shown by $\kappa\ ln(N)$. N is the number of atoms in the two-dimensional graphene system. Since the thermal conductivity of two-dimensional graphene has been shown to be dependent on the structural and other factors; graphyne, as an allotrope, may have similar thermal properties. Since there is no two-dimensional graphyne available, little attention has been paid to the analysis of mechanical properties of graphyne until recent few years [85, 193, 199].

Furthermore, thermal properties, such as thermal conductivity of two-dimensional materials, are also very important to further utilize the two-dimensional graphyne in the microelectronics industry. Thermal conductivity is the property of a material to transmit heat. The fundamental way of calculating thermal conductivity is $J = -\kappa \bigtriangledown T$, where J is heat flux, κ is thermal conductivity and $\bigtriangledown T$ is the temperature gradient. Yet, there are few published papers on the thermal properties of two-dimensional graphyne. We noticed that in 2012 Ouyang's group studied the thermal transportation in graphyne nanoribbons [132]. Thereafter, there're still no publications on the thermal properties of two-dimensional graphyne. However, thermal dispavity is the most important for microeletronics devices. A good understanding of the thermal properties of promising microeletronics materials will be crucial to assure the proper performance of the whole system. It's also crucial to avoid the malfunction caused by overheating issues. There is a demand to understand the mechanical and thermal properties of two-dimensional graphyne and its family materials. We propose to use the computational molecular dynamics simulation to study mechanical

and thermal properties of two-dimensional graphyne and its family of materials.

∗ Boron nitride

Boron nitride has attracted researchers due to the atomic sheets that are the structural analogue of carbon. It is an atomic two-dimensional structure consisting of three atoms: boron nitride atoms and graphene atoms. Boron nitride is composed of both hexagonal- and cubic-bonded structures [133]. The heat dissipation problem for microelectronic packaging is becoming increasingly important as the demands in denser and faster circuits intensify [74, 213]. In order to improve the thermal conductivity of the substrates, traditionally, people put thermally conductive ceramic materials in polymers. A lot of researchers have been investigating the electrical, mechanical and thermal properties of boron nitride nanosheets [39, 130, 168, 178].

Boron nitride is a promising deep ultraviolet light emitter [93, 178]. The specialized structural consisting of boron nitride and graphite, numerous kinds of two-dimensional hybrid graphene-boron nitride sheets can be obtained. Pacile stated that the hexagonal boron nitride(h-BN) phase is isostructural to graphite except for the various stacking sequences of the atomic planes [133]. Dean and the research group studied the appealing substrate made of hexagonal boron nitride, which is a great improvement in the quality of graphene eletronics. Boron nitride has an atomically smooth surface and exhibits superior characteristics [39].

∗ Hybrid Graphene-Boron Nitride

There are few published papers on the properties of two-dimensional hybrid graphene boron nitride nanoribbons. The discovery of carbon nanotubes boron nitride has

attracted many researchers to investigate the properties and applications of two-dimensional hybrid graphene-boron nitride nanosheets. The thermal conductivity of boron nitride increases with applied strain; while the thermal conductivity of graphene decreases. It's interesting to investigate the hybrid graphene-boron nitride's thermal conductivity, which may not change with strain applied. Both theoretical prediction and experimental realization have proved that hybrid graphene boron nitride is achievable.

1.2   Current Problems

The mechanical properties, such as the Young's modulus, E, of a bulk material in tension can be obtained by $E = \frac{\sigma}{\varepsilon}$. This is the conventional way of evaluating the Young's modulus of a bulk material. Yet obtaining the Young's modulus for two-dimensional materials, such as graphene, MoO_3 or graphyne, is limited by many factors. Similarly, it's difficult to obtain the thermal properties of two-dimensional materials by experiments. Herein, we propose several key factors that limit the experimental methodologies. Firstly, two-dimensional material demands specific technical support to prepare. Until now, two-dimensional graphene has been successfully produced and been studied [32, 48, 51]. Yet, two-dimensional MoO_3 has been produced and studied on the surface with other supported materials [30, 107]. There are few published papers on the production of two-dimensional graphyne and its family materials. Secondly, even if the two-dimensional materials can be successfully produced, applying tensile stress on the samples are challenged by the current instruments and control. Moreover, defects are inevitable during the preparation of two-dimensional

materials, which demands more efforts in the study. Finally, it's time-consuming and laborintensive to post-process the experiment data.

Although there are many publications about thermal and mechanical properties of graphene; however, until now, there are few published papers on the mechanical and thermal properties of two-dimensional MoO_3 and graphyne. Computational methods are capable of defining two-dimensional perfect sample sheets. Furthermore, the cost and labor is less due to the availability of modern computers. In this study, we address the mechanical or thermal properties of two-dimensional MoO_3 and two-dimensional graphyne.

1.3   Research Objectives

The goal of our study is to analyze the mechanical and thermal properties of two dimensional MoO_3 and graphyne. In order to achieve our main goal, we (i) propose a constitutive model for MoO_3 that can predict the mechanical propeties such as Young's modulus and Possion's ratio. (ii) study the mechanical properties of graphyne using molecular dynamics simulation. (iii) study the thermal properties of graphyne, such as thermal conductivity using molecular dynamics simulation.

To achieve these goals and objectives, we address these problems for the two-dimensional MoO_3 and graphyne. The mechanical properties of two-dimensional MoO_3 are found using density functional theory (DFT) to study the mechanical properties (such as Young's modulus) of two dimensional MoO_3. We propose constitutive equations for MoO_3 based on the DFT results that predict the mechanical properties of two-dimensional MoO_3.

The mechanical properties of two-dimensional graphyne are found using molecular dynamics simulation. We analyze the mechanical properties of non-defective graphyne and its family materials (such as gradiphyne, graphyne-3, graphyne-4). We also use molecular dynamics simulation to analyze the mechanical properties of defective graphyne. The defects are created by deleting atoms from the perfect sheet. There are several types of defects, including random defects, bond defects and area defects. Bond defects are investigated into zero degree bond-defect and sixty degree bond-defect. Area defect will be studied by the size of the defective area.

The thermal properties of two-dimensional graphyne are studied using the molecular dynamics simulation. We analyze thermal properties (such as thermal conductivity) of non-defective graphyne and its family of materials (such as gradiphyne, graphyne-3, graphyne-4). We also use molecular dynamics to investigate the thermal conductivity dependence on the applied strain. We use molecular dynamics to investigate the thermal conductivity dependence on the variance of graphyne' length and width. We also use molecular dynamics simulation to analyze the thermal properties of defective graphyne. All the simulations are performed using two different potentials, listed as the Airebo potential and the Tersoff potential. The studies are taken to obtain the thermal conductivity of armchair and zigzag graphyne.

The study of mechanical and thermal properties of two-dimensional hybrid graphene-boron nitride sheets are divided into steps. We use the molecular dynamics simulation to analyze the thermal properties (such as thermal conductivity) of alternating non-defective hybrid graphene-boron nitride. We analyze the thermal properties (such as thermal conductivity) of laterally non-defective hybrid graphene-boron nitride.

1.4   Outline of Dissertation

Chapter I serves as the introduction to the background for two-dimensional materials. In this chapter, we review current studies of two-dimensional materials. Background of two-dimensional materials' investigation and obstacles are stated. We review the achievements and applicable methodologies for MoO_3, graphene, graphyne and other related two dimensional materials. We propose problems that need to be addressed. Thereafter, we propose the research objectives of this dissertation and tasks to investigate the two dimensional materials, including MoO_3 and graphyne. Finally, the mechanical properties and thermal properties of the two-dimensional materials are addressed in Chapter II, Chapter III and Chapter IV.

Chapter II reviews the study of current methodologies of two-dimensional materials. Then we introduce the applications of those methodologies. Based on the review, we list the present limitations on the methodologies analysis of two-dimensional materials. We state the problem that we solved in our study. Finally, we propose the applicable methodology framework for our research and the tasks to address the proposed problem.

Chapter III focuses on the mechanical property analysis of the two-dimensional MoO_3. We review the current investigations on MoO_3. We propose the limitations that remain to be addressed. We analyze the mechanical properties of MoO_3 with density functional theory. Finally, we propose a mathematical model that matches with the DFT results.

Chapter IV presents the analysis of the mechanical properties of two-dimensional

graphyne. First, we summarize the previous research on the mechanical properties of graphyne and its family of materials. Then we propose an unsolved problem for the mechanical properties of graphyne. Finally, we use molecular dynamics to address this problem.

Chapter V is used to analyze the thermal properties of two dimensional graphyne. We review the current studies on the thermal properties of graphyne and its family of materials. Then we propose an unsolved problem for the thermal properties of graphyne. Finally, we use molecular dynamics to solve this problem.

Chapter VI analyzes the thermal and mechanical properties of two-dimensional hybrid graphene-boron nitride. First, we review the current research on the thermal properties of hybrid graphene-boron nitride. We propose an unsolved problem for the thermal properties of hybrid graphene-boron nitride. Finally, we use molecular dynamics to address the thermal properties of both alternating and laterally nanoribbons.

Chapter VII summarizes the achievements in this dissertation and make conclusions based on the results.

CHAPTER 2: INTRODUCTION OF METHODOLOGIES

In this chapter, we outline the current state of methodologies used in the analysis of two-dimensional materials. Basically, there are three types of approaches in the investigation process of two dimensional materials: (i) theoretical metho, (ii) experimental method and (iii) computational method.

The single-layer crystal form of carbon is named graphene, and, ironically, it is probably the best-studied carbon allotrope theoretically and experimentally [52, 65, 80, 144, 191]. Experimental methods are used a lot in the analysis of bulk materials. Yet for micro-scale materials, studying the properties of two-dimensional materials is limited by the size of nanoribbons. The measured results are limited by the accuracy of instruments and some other factors, such as environmental factors and human control accuracy. Computational methods can have large size-scale and time-scale advantages, which are usually hard to achieve by experiments. The computational simulation can make well ordered two-dimensional material without defects, which is almost inevitable for experiments. The predicted mechanical or thermal conductivity obtained by computational simulation might be larger than the experimental results due to the initial length and time scale definition. Yet, computational methods still exhibits superior abilities in predicting the two-dimensional materials' mechanical and thermal properties. The most commonly used computational methods are molecular dynamics and density functional theory. Besides, Khare [84] used quantum me-

chanical or molecular mechanical modeling to study the defective graphene sheets. Herein, we introduce the commonly used experimental methodology and computational methodology.

2.1   Experimental Methodology

Graphene, consisting of a two-dimensional honey-comb carbon-carbon bonded structure, has been successfully produced in experiments   [52, 65, 144, 191]. Small size graphene can be made of by exfoliating single-layer crystal sheet from bulk graphite; while large size graphene can be obtained by dispensing graphite in the organic solvent and then growing mono-layer graphene on metal base. As defects are inevitable during the making process of graphene, it's important to understand the mechanical properties such as Young's modulus and yield strength. It'd also critical to investigate the correlation between defects and graphene's mechanical properties. Since two-dimensional graphite and its family of materials are still not available, it's not practical to address the mechanical or thermal properties via experimental methods.

We reviewed the previous experimental methods that have been taken to study the mechanical and thermal properties of graphene. Firstly, we focus on the experimental methods on the mechanical properties of graphene. Lee's research group studied the elastic properties and strength of graphene by nanoindentation by applying microscale atomic force   [95]. In the nanoindetation experiment, a round single layer graphene film is fixed on the edge while the rest is free-standing. By indenting the area around the centre of the graphene repeatedly, mechanical-displacement correlation data can be obtained. Thereafter, the Young's modulus E of graphene can be evaluated from

the stress-strain correlation, which is $E = 1TPa$ shown in Table 2. Graphene's mechanical properties, especially Youg's modulus have been successfully measured with experiments. Table 2 also shows the experimental results of graphene match with the results obtained from the computational methods.

Besides nanoindentation experimental method, Lee, Yoon and Cheong proposed to use raman spectroscopy to measure the direct strain applied on graphene by loading various pressure [96]. Fig. 3 is the schematic of the experiment of raman spectroscopy. By applying the atmosphheric pressure, the graphene membrane will bulge upward like a balloon; a Raman band G_1 is obtained. Look at Fig. 3, the red-curve will shift if the graphene membrane is pumped upward from the flattened status. Then, by vacuum the pressure until the graphene get flattened, another Raman band G_2 is got. The strain applied on the graphene can be derived by comparison the difference of G_1 and G_2, since the bulging of graphene membrane cause the tension.

The experimental method studying the thermal conductivity shows in Table 3. Obviously, it exhibits that laser focused excitation or microwave excitation are the mainly used experimental methods to study the thermal conductivity of graphene. Graphene's thermal conductivity is measured through the excitation laser light focused on a graphene layer, which shows graphene has very high thermal conductivity [8, 56].
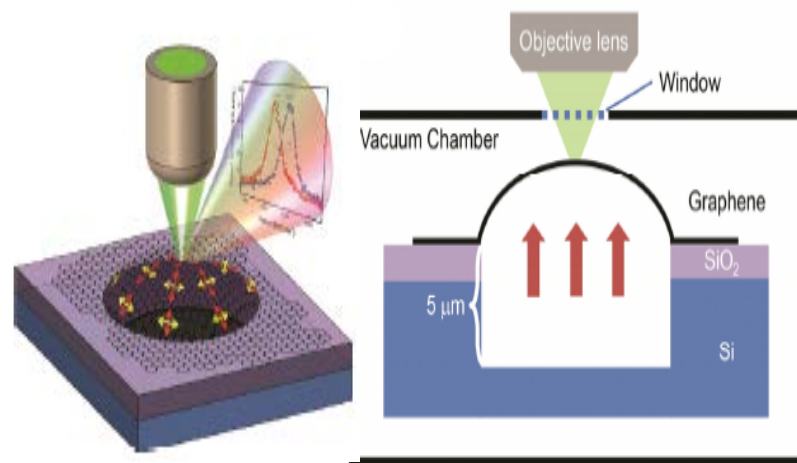
Figure 3: Schematic of the experiment of raman spectroscopy [96]

Table 2: Young's modulus of graphene

Material	Young's Modulus E(TPa)	Method
Graphene [95]	1	Nanoindentation
Graphene [96]	2-2.8	Raman spectroscopy
Graphene [78]	0.95	MD
Graphene [171]	1.11	Ab initio
Carbon nanotube [158]	1.033-1.042	nanoscale continuum mechanics

Thirdly, we reviewed the previous study of electrical properties of graphene with experimental methodology. There are lots of experiments are taken to investigate electrical properties of graphene [25, 98, 153, 202]. The electronic bandgap is an intrinsic property of semiconductors and insulators that largely determines their transport and

optical properties [202]. Graphene, despite its mono-layer crystal structure and even without coating protection, is proved to be a good semiconductor, whose electronic bandgap is tunable by the electric field effect [25, 111, 131, 202]. In conventioanl bulk materials, the bandgap is a constant, which is fixed by their structure. However, graphene has a tunable wide range of bandgap, which opens the applications of bandgap controllable nanoelectronic and nanophonic devices based on graphene [111, 202]. [111] even stated that by adjusting the position of graphene, bandgap can be diminished to zero, which is very helpful when we do not need the charge carrier to be activated.

Furthermore, researchers investigate other study of electrical properties of graphene with experiments, such as the quantum effect and eletrodes effect. Graphene's charge carriers behavior mimic relativistic particles with zero rest mass, having the speed of light [130]. Graphene's resistance, carrier density, and mobility were measured to study the quantum Hall effect and Berry's phase in graphene [201]. The quantum experiments observations showed it is possible to change the carrier type or concentration in microsope and to control the macroscope behavior of electronic devices.

2.2 Computational Methodology

Density functional theory (DFT) and molecular dynamics (MD) are two most widely used computational methods for studying the two-dimensional materials.

2.2.1 Introduction of Density Functional Theory

Kohn stated in his Nobel lecture that DFT has been most useful for systems of very many electrons where wave function methods encounter and are stopped by the

exponential wall [36,91]. Electronic structure calculations based on density functional theory have greatly contributed to our understanding of atomic, molecule and solid problems [24, 184]. DFT is capable of providing an accurate description of the chemical bond correlation in a large variety of systems, yet is computationally efficient [21, 36]. It is difficult to obtain the stress-strain behavior of single-layer systems by experiments, especially the manufacturing of some two-dimensional material is not applicable. Furthermore, defects are inevitable during the process of preparation. Yet DFT can build a connection between the external energy and the internal energy of the atomic system.

The simplest DFT correlation is based on the Thomas-Fermi model [44]. The current DFT correlation was initially proposed in a study of the movement of inhomogeneous electron gas, which is called the Hohenberg-Kohn theorems [67]. DFT evolved from two theorems: the Hohenberg theorem and the Kohn theorem. It can also be called the first H-K theorems. The Hohenberg theorem states that the electron density determines all properties of a non-degenerate ground state of an atom or a molecule. The basic concept of the Hohenberg-Kohn theorems considers that electrons are moving in an enclosed box. The movement of the electrons are randomly. The electrons are under the influence of an external potential $v(\boldsymbol{r})$ and the mutual Coulomb repulsion. The ground-state energy is obtained at an external potential. The evaluation process is shown in Eq. (1), where H is the Hanmilton, T is the kinetic energy, V is the potential energy from the external field due to positively charged nuclei, and U is the electron-electron interaction energy. The interpretation of the many-electron wave-function is: probability for finding the electrons in an in-

finitesimal volume element around configration x_i if the nuclei are at rest at positions R_i and the systems are in the electronic eigenstate [124].

$$H = T + V + U \tag{1}$$

$$T = \sum_{i=1}^{N} \left(-\frac{h^2}{2m_i^2}\nabla^2\right) \tag{2}$$

$$V = \sum_{i=1}^{N} v(r_i) \tag{3}$$

$$U = \sum_{i<j}^{N} u(r_i, r_j) \tag{4}$$

$$H\phi = (T + V + U)\phi = E\phi \tag{5}$$

Thereafter, researchers invent a new method called Hohenberg-Kohn-Sham DFT based on the former DFT methods. The second HK theorem defines an energy functional for the system and proves that the correct ground state electron density minimizes this energy functional. The framework of Hohenberg-Kohn-Sham DFT (HKS DFT) mainly comes from the H-K theorem [13].

Shortly after the appearance of Hohenberg-Kohn-Sham DFT, another DFT method called Kohn-Sham DFT was developed. Within the profile of Kohn-Sham DFT (KS DFT), the intractable many-body problem of interacting electrons in a static external potential is reduced to a tractable problem of non-interacting electrons moving in an effective potential. The profundity lies in that the potential where all the many-body effects are incorporated [63]. The effective potential includes the external potential and the effects of the Coulomb interactions between the electrons: the exchange and correlation interactions. Modelling the latter two interactions is the difficulty in KS

DFT. The simplest approximation is the local-density approximation (LDA), which is based upon the exact exchange of energy for a uniform electron gas. This can be obtained from the Thomas-Fermi model, and from fits to the correlation energy for a uniform electron gas. Non-interacting systems are relatively easy to solve as the wavefunction can be represented as a Slater determinant of orbitals. Further, the kinetic energy functional of such a system is known exactly. The exchange-correlation part of the total-energy functional remains unknown and must be approximated.

Another approach, less popular than KS DFT but arguably more closely related to the spirit of the original H-K theorems, is orbital-free density functional theory (OFDFT), in which approximate functional are also used for the kinetic energy of the non-interacting system. OFDFT is not accurate compared to the KS DFT. However, it's applicable to large systems due to its fast and efficient characteristics.

Although the DFT has been widely used in the study of electronic structure in material science, it has some limitations. First, it can become very computationally consuming due to large scale atomic systems. Molecular dynamics simulation is preferable. Second, the application of DFT still suffers from errors due to deficiencies of the currently used approximate exchange-correlation functional [36]. The deficiencies of the functions include the de-localization error, neglecting the fractional charges, static correlation errors and fractional spins. As a result, DFT is not suitable for metal dimers. Third, the potential will affect the accuracy of the calculation.

2.2.2 Introduction of Molecular Dynamics

Classical molecular dynamics (MD) is a computational method that stimulates the behavior of a group of atoms by simultaneously solving Newton's second law of motion for the atoms with a given set of potentials [109], as shown in Eq. (6)

$$- \bigtriangledown \phi = \overrightarrow{F} = m\frac{d^2\overrightarrow{r}}{dt^2} \tag{6}$$

where ϕ is the potential energy, $\overrightarrow{F}$ is force, m is atomic mass, $\overrightarrow{r}$ is position vector and t is time. To understand the mechanical and thermal properties of two-dimensional materials via MD, we need to consider the energy correlation of the whole system. There are many investigations on the thermal conductivities of two-dimensional materials using MD, shown in Table 3. Usually, the total empirical inter-atomic potential energy of a molecular system is composed with the energies related to bond, angle, electrostatic interactions and van der Waals force.

Table 3: Summary of thermal conductivity of graphene

Material	thermal conductivity (W/mK)	Method and Potential
Graphyne [137]	N/A	DFT
Graphene [8]	4840-0.44 5300+0.48	Experiment
Graphene [127]	3000-5000	Analytical Model
Graphene nanoribbons [61]	armchair(zigzag)460(590)	MD, Tersoff potential
Graphene membrane [49]	600	Experiment
Graphene nanotube [14]	6600	MD, Carbon potential
Mutilayer graphene [76]	2800-1300 (2-4 layer)	MD, Tersoff potential

There are four types of methods to compute the thermal conductivity using molecular dynamics. All four methods can be categorized into non-equilibrium methods and equilibrium methods. The basic concept of these methods for the evaluation of thermal conductivity is to induce a temperature gradient or heat flux and monitor the other quantity. The non-equilibrium methods includ (i) direct thermostatting method of Ikeshoji and Hafskjold, (ii) reverse perturbation method of Muller-Plathe, and (iii) aggregate variant of Muller-Plathe method. The equilibrium method refers to Green-Kubo formalism.

The direct thermostatting method was studied initially in a liquid by Ikeshoji and Hafskjold [73]. The schematic of thermal conduct behavior of armchair direction is shown in Fig. 4.
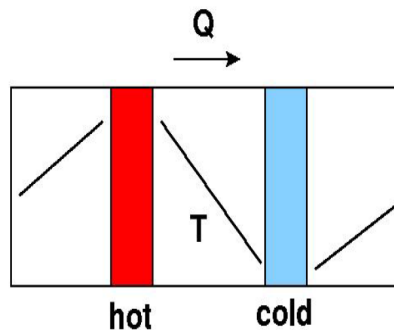
Figure 4: Schematic of direct thermostatting method

The systems are divided into "hot", "cold" and "middle" regions. For the zigzag direction thermal conduct behavior, the system will be grouped into "hot", "cold" ad "middle" regions along the zigzag direction. The energy flows in the armchair or zigzag direction from the hot to the cold region passing through the middle region. A constant amount of kinetic energy is applied to the hot region at each time step.
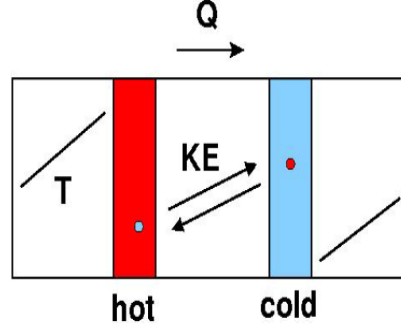
Figure 5: Schematic of Muller-Plathe method

Meanwhile, the same amount of energy is obtained from the cold region by scaling the velocities of the particles in these regions. As a result, the thermal conductivity can be derived as follows:

$$\lambda = -\frac{J_e}{dT/dx} \tag{7}$$

where λ is the thermal conductivity, J_e is the heat flux and dT/dx is the temperature gradient along x-direction.

The Muller-Plathe reverse perturbation method was presented initially in liquid by Muller-Plathe in 1997 [119]. This method has the disadvantage that it's difficult to converge the heat flux J_t and the autocorrelation function. The schematic of Muller-Plathe method is shown in Fig. 5. The systems are divided into "hot" and "cold" regions. The heat flux is generated by exchanging the velocity vectors of an atom in the "cold" region and one in the "hot" region where the temperature increases in the "hot" region and decreases in the "cold" region.

The Muller-Plathe reverse perturbation method allows the energy to flow in two directions while the former method only has one direction. It means the energy can flow from the "hot" region to the "cold" region or in the opposite way. This method

initially focuses on finding the "hottest" atom in the "cold" region and the "coldest" atom in the "hot" region. In this method, energy flows unphysically from the "cold" region to the "hot" region. The reason is the distribution of atomic kinetic energy is much wider than the temperature difference between the "hot" region and the "cold" region. Then the velocity vector of the "hottest" atom and the "hottest" atom will be swapped. In this case, the total kinetic energy and the total energy of the system will not be changed. The instantaneous local kinetic temperature T_k in region k is shown as:

$$T_k = \frac{1}{3n_k k_B} \sum_{i \subset k}^{2} n_k m_i v_i^2 \tag{8}$$

n_k is the number of atoms in the region k. m_i and v_i is the atomic mass and velocity of the ith atom in region k. k_B is Boltzmann's constant. The temperature T is thereafter calculated by the average of T_k during the simulation time. The thermal conductivity is obtained by

$$\lambda = -\frac{\sum_{transfers} \frac{m}{2}(v_h^2 - v_c^2)}{2t L_x Ly < \partial T / \partial z >} \tag{9}$$

m is the identical mass of the "hottest" atom or the "coldest" atom. v_h is the velocity of the "hottest" atom in the cold region; while v_c is the "coldest" atom in the "hot" region. t is the simulation time. L_x and L_y is the box length along the armchair direction and the zigzag direction, respectively. The Muller-Plathe reverse perturbation method shows that the energy can flow from the "hot" region to the "cold" region or in the opposite way. Obviously, this method double the area to transport the heat flux, which make its a effective way compared to the direct

thermostatting method.

The variant of Muller-Plathe reverse perturbation method was presented initially in liquid by Muller-Plathe in 1999 [166]. Fig. 6 shows the thermal conduction in variant of Muller-Plathe reverse method.
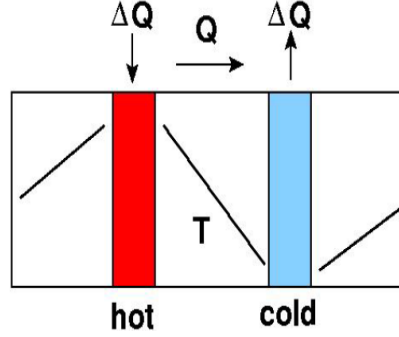
Figure 6: Schematic of variant Muller-Plathe method

In this case, the cause and effect are reversed compared to former Muller-Plathe reverse perturbation method. The systems are grouped into "hot" and "cold" regions. Energy will be added or subtracted continuously to all the atoms in both regions. The total energy and total momentum of the system will not change due to the positions of the atoms are not changing. Energy will still flow from the "hot" regions to the "cold" regions. Herein, the amount of momentum and energy transported from the "hot" region to the "cold" region will be preciously known. The thermal conductivity can be obtained by the energy differentiation,

$$\lambda = -\frac{1}{2AV} \sum_{i}^{2} n_k \frac{\partial E}{\partial t} \qquad (10)$$

where V is the volume. A is the cross-sectional area.

The Green-Kubo method relates the ensemble average of auto-correlation of the energy to the thermal conductivity [59, 92]. Fig. 7 shows the thermal conduction
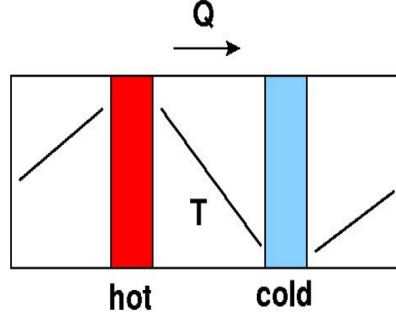
Figure 7: Schematic of Green-Kubo method

process in Green-Kubo method. The thermal conductivity is obtained by

$$\lambda = \frac{V}{k_B T^2} \int_0^\infty < J_x(0) J_x(t) > dt \tag{11}$$

where J is calculated as follows

$$J = \frac{1}{V} [\sum_i e_i \boldsymbol{v}_i + \frac{1}{2} \sum_{i<j} (\boldsymbol{f}_{ij}(\boldsymbol{v}_i + \boldsymbol{v}_j)) \boldsymbol{x}_{ij}] \tag{12}$$

To calculate the thermal conductivity of two-dimensional graphyne, we use the RNEMD. This is due to the following reasons. Firstly, RNEMD conserves the total energy and the total linear momentum of the system with swapping the "hottest" atom and the "coldest" atom with identical mass. Thus, the microcanonicity of Newton's equation of motion can be conserved. Secondly, thermostatting is not required in RNEMD. There are always two types of regions, the "hot" region and the "cold" region, which leads to a self-thermostatting [120].

All the molecular dynamics simulations are performed using LAMMPS (Large-scale Atomic/Molecular Massively Parallel Simulator). The core part of the LAMMPS is the input script, which defines all the boundary conditions and loading conditions. LAMPPS is an open source code, which provides many examples that can be edited

to meet the practical demanding.

The basic input script of LAMMPS has the following four parts: (i) initialization, (ii) atom definition, (iii) settings, and (iv) run a simulation. To begin, we set all the initial parameters in the initialization section. This section includes the factors such as units, dimensions, atom type and so on. Second, in the atom definition part, the coordinate system of the atoms will be built. There are usually two ways to set up the atomic systems. Users can either create all the atoms on a lattice or read the atomic coordination data from a file. Next comes the core part of the input script. Basically, there are four parts need to be set up, which include force field coefficients, simulation parameters, boundary conditions and output script.

Apendix C shows the input LAMMPS scripts for the thermal conductivity calculation based on the RNEMD simulations. The LAMMPS input scripts for the two-dimensional graphyne can be suitable for the two-dimensional hybrid graphene-boron nitride's thermal conductivity calculation.

When the simulation in LAMMPS is done, the thermal conductivity of the material can be obtained be post-processing with two types of output files. One is called the "log" file, and the other is called the temperature "profile". The calculation of thermal conductivity based on the former four methods are shown as follows.

2.3   Conclusion

Although experimental methods are used a lot in the analysis of bulk materials. Yet studying the properties of two-dimensional materials is limited by the size of nanoribbons. Computational methods, such as DFT and molecular dynamics can

have large size-scale and time-scale advantages, which are usually hard to achieve by experiments.

CHAPTER 3: STUDY OF MECHANICAL PROPERTIES OF MoO$_3$

In this chapter, a detailed description of the analysis of the mechanical properties of MoO$_3$ is presented. First, the background of mechanical analysis on the MoO$_3$'s properties and gaps are stated. We review the achievements and applicable methodologies for MoO$_3$ and related two-dimensional materials. Secondly, we state the research objectives and tasks to investigate the mechanical properties of MoO$_3$. Finally, the results obtained using density functional theory are presented.

3.1 Introduction

Two-dimensional MoO$_3$ is applicable to semiconductors [54, 115, 188], energy storage systems [19, 185], photochromism [43, 50] and oxidation catalyst [30, 118]. Two-dimensional MoO$_3$ is also a promising material in optical devices, sensors, lubricants, lithium batteries, and information storage [72].

MoO$_3$ is superior in charge storage systems due to its ability to intercalate ions in a wide range, which requires its being made into thin films [19, 212]. MoO$_3$ is also a most important member of the interstitial-free transitional metal oxides, which is the promising anode for lihthium-ion batteries [141, 177]. MoO$_3$ meets the requirement of such batteries due to its high capacity, high thermal and chemical stability [177].

Fig. 8 and Fig. 9 show the crystal structure of MoO$_3$ [9]. There are two types of MoO$_3$: α-MoO$_3$ and β-MoO$_3$. Since β-MoO$_3$ is not stable and always transforms
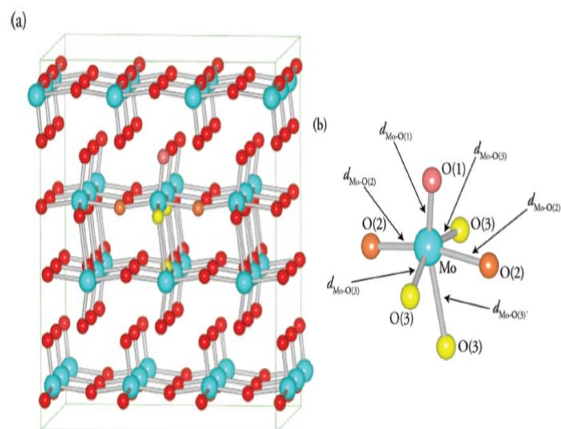
Figure 8: Schematic of MoO$_3$ [150]

into α-MoO$_3$. Our research on the two-dimensional MoO$_3$ focuses on α-MoO$_3$. Since two-dimensional MoO$_3$ is used as both functional material and structural support material in applications, a good understanding of its mechanical properties is required. Traditional methods for understanding mechanical properties of materials relies on experiments. Performing experiments on two-dimensional MoO$_3$ is challenging, time consuming, and expensive. Two-dimensional MoO$_3$ has been successfully exfoliated [10, 174].
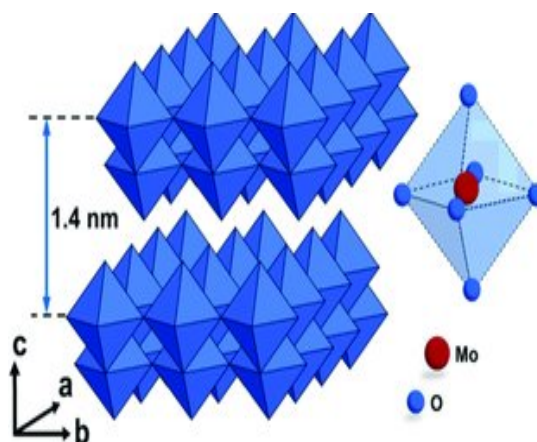
Figure 9: Schematic of MoO$_3$ [9]

It is important to understand the mechanical strength of MoO$_3$ to ensure the good

performance of the whole system. Although some studies have been done on the chemical, photonic or electrical properties of MoO_3, most of the methods are based on experiments or computational methods including density functional theory (DFT) [19, 30, 176]. However,there are few publications on general model that can predict the mechanical properties of MoO_3. We use the computational method DFT to study mechanical properties of two-dimensional MoO_3. We use the DFT results to propose a constitutive model for MoO_3.

3.2   Purpose and Tasks

We use DFT simulations to study the mechanical properties of MoO_3 and to obtain stress-strain curves of MoO_3, under the uniaxial and biaxial loadings. Using the stress-strain relations obtained from the DFT simulations, we propose a hyperelastic constitutive model, which can predict the mechanical properties of MoO_3. Finally, we compare the DFT results with the results obtained from the constitutive model.

3.3   DFT Simulation and Continuum Model

All the DFT simulations are performed using SIESTA code [160]. To compute the mechanical properties of two-dimensional MoO_3, a number of boundary conditions for tensile loadings are considered. The sample of two-dimensional MoO_3 is the unit cell consisting of 8 atoms, including two Mo atoms and six oxygen atoms. Herein the DFT simulation, we set the unit cell lattice constants as x=3.72 Å, y=3.94 Å and z=12.855 Å [11]. Fig. 10 shows the unit cell used in the DFT simulation.
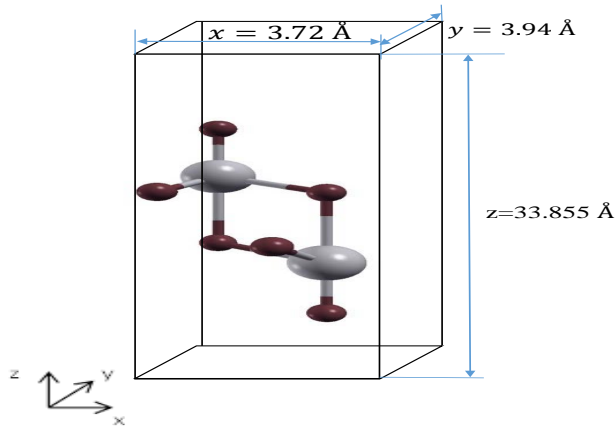
Figure 10: Unitcell of two-dimensional MoO_3 used in DFT simulation

To remove the interaction between periodic images in the z-direction, the unit cell size in the z-direction is defined as 32.855 Åin the DFT simulation. To obtain the stress-strain relations, strain is applied in the x-direction and y-direction of MoO_3.

In the DFT simulation, the k-point grid is $30 \times 30 \times 1$ with a cutoff energy of 500 eV. The whole simulation system is relaxed to make sure two-dimensional MoO_3 is in a undeformed equilibrium state, where energy and stress are minimized as a function of the in-plane lattice vector and out-of plane O atom heights. The stress computed in the Siesta are expressed as true stress, also known as Cauchy stress. The program code for DFT simulation is shown in Appendix A.

3.4   DFT Results

Fig. 11 shows the energy density-strain and stress-strain curves of MoO_3 under the uni-X direction tensile loading. The two-dimensional unit cell was stretched along the x-direction while the y-direction is fixed, as shown in the left figure in Fig. 11. As the increment of strain from 0 % up to 15 %, MoO_3's energy density increases

nonlinearly.
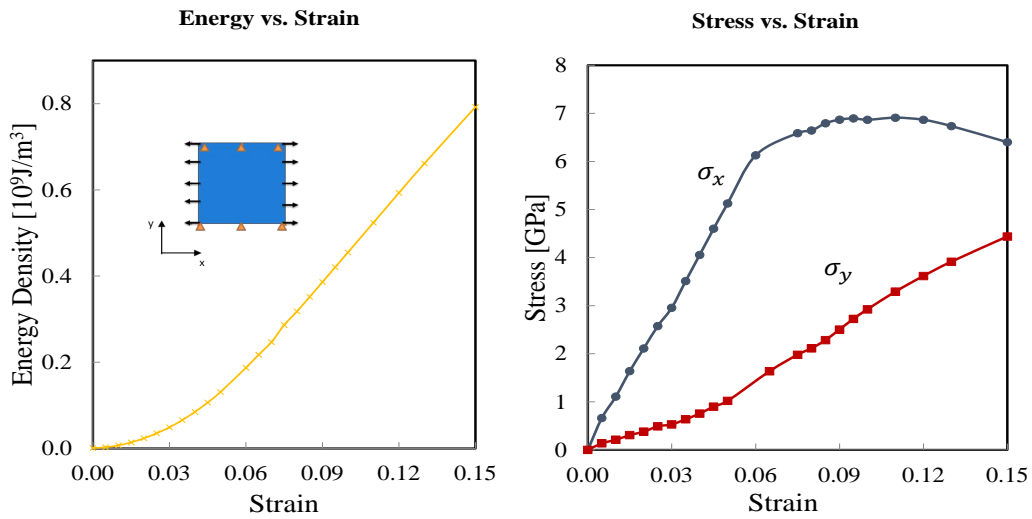
Figure 11: Energy density-strain and stress-strain results of uniaxial tension in the x-direction of two-dimensional MoO_3

Meanwhile, the stress-strain curves show that two-dimensional MoO_3 in the x-direction is sensitive to the applied strain compared to the y-direction.
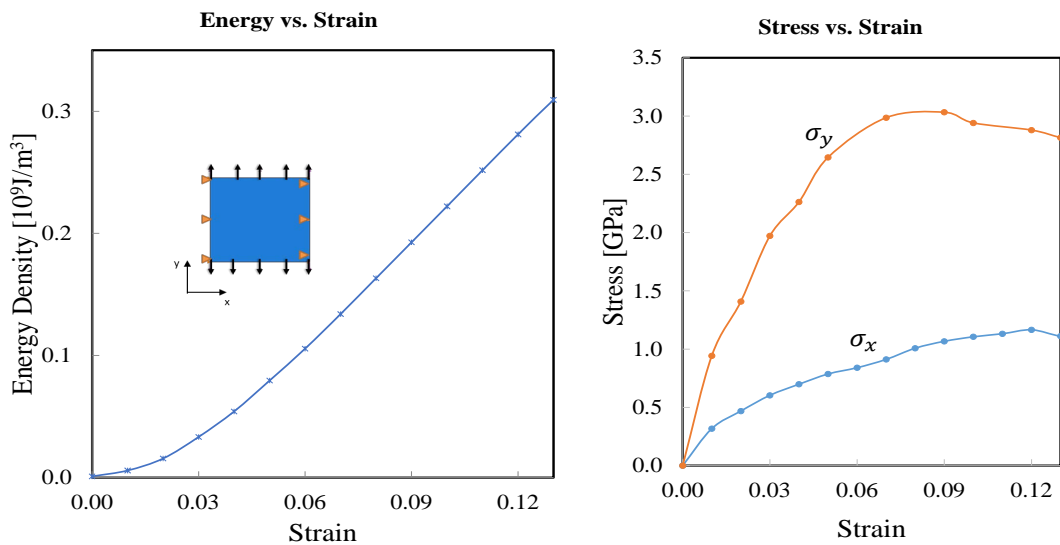
Figure 12: Energy-strain and stress-strain results of uniaxial tension in the y-direction of two-dimensional MoO_3
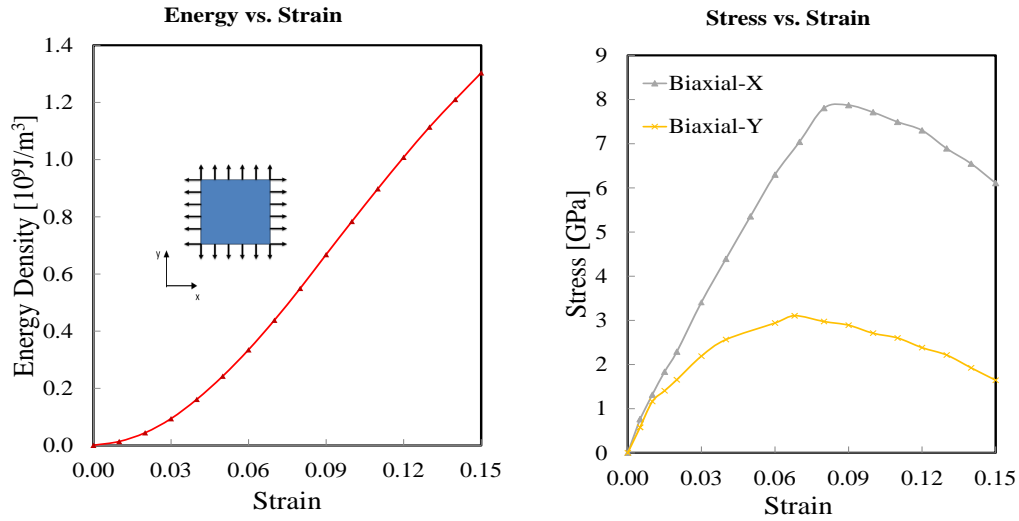
Figure 13: Energy-strain and stress-strain results of biaxial tension of two-dimensional MoO_3

Fig. 12 shows the energy density-strain and stress-strain curves of MoO_3 under the uniaxial tensile loading in the y-direction. The two-dimensional unit cell was stretched along the y-direction while its x-direction is fixed, as shown in the left figure in Fig. 12. As the increment of strain from 0 % up to 12 %, MoO_3's energy density increases nonlinearly.

Consider both Fig. 11 and Fig. 12, it's interesting to note that the anisotropy of two-dimensional MoO_3 is very dependent on the structure itself. The atoms in the y-direction is predominent by the Mo-O bond connections, which is easier to elongated yet not easily broken. However, the atoms in the x-direction is consisted of Mo-O rigid angle connection. Although the angle bond connection can store more strain energy, yet it's more sensitive to the strain that tends to tear the angle up. Fig. 13 shows the energy density-strain and stress-strain curves of MoO_3 under the biaxial tensile loading. The two-dimensional unit cell was stretched along both of the x-direction

and y-direction at the same time, as shown in the left figure in Fig. 13.

As the increment of strain from 0 % up to 15 %, MoO_3's energy density increases nonlinearly. The stress-strain curves show that two-dimensional MoO_3 in the x-direction has higher strength compared to the y-direction of MoO_3. Up to 1 % of the strain , both x-direction and y-direction MoO_3 exhibit the same stress-strain curves, which mean the Young's modulus in the x-direction and y-direction are the same before 1 % strain. We assume MoO_3 is isotropic material before 1 % strain and it's anisotropic characteristics become dominant under large deformation.
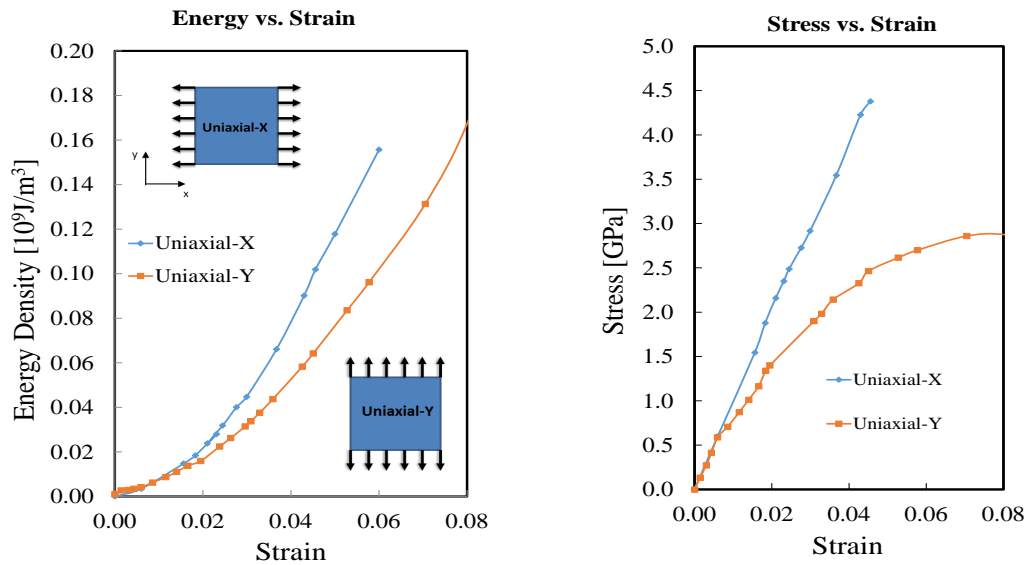
Figure 14: Energy-strain and stress-strain results of uniaxial tension along x-direction while y-direction free

Fig. 14 shows the energy density verses strain and stress verses strain curves of MoO_3 under the uniaxial x-direction or y-direction tensile loading. The two-dimensional MoO_3 was stretched along the x-direction while the y-direction is free to move, as shown in the left figure in Fig. 14.

Up to 1 % of the strain , both x-direction and y-direction MoO_3 exhibit the same

stress-strain curves, Young's modulus are the same before 1 % strain. The Young's modulus of the isotropic state is 95 GPa. Consider both Fig. 13 and Fig. 14, obviously we notice that MoO_3 is isotropic material before 1 % strain and it's anisotropic characteristics become the dominant properties under large deformation.

3.5   A Constitutive Model

We assume that two-dimensional MoO_3 is a hyperelastic material. We propose the elastic strain energy density constitutive model can be expressed as,

$$\phi(I_1, I_2, E_1, E_2) = \sum_{N_1}^{i=1} c_i(I_1 - 2)^2 + \sum_{N_2}^{k=1} d_k(lnJ)^{2k} - 2\sum_{N_2}^{k=1} m_k(lnJ)^k$$

$$+ H(E_1 - E_2)H(E_1E_2)\sum_{i=1}^{3} p_i E_1^i E_2 + \sum_{i=1}^{3} b_i E_2^{i+1}$$

$$+ H(E_2 - E_1)H(E_1E_2)\sum_{i=1}^{3} q_i E_2^i E_1$$

$$+ n_1 E_1^{a_1} E_2^{1.5-a_1} n_2 E_1^{a_2} E_2^{2-a_2} + n_3 E_1^{a_2} E_2^{2.5-a_2} + n_4 E_1^{a_4} E_2^{3-a_4}$$

$$+ H(-E_1E_2)H(-E_2)\sum_{i=1}^{4} s_i E_1^i + H(-E_1E_2)H(-E_1)\sum_{i=1}^{2} t_i E_1 E_2^{i+1} \quad (13)$$

where $\sum_{N_1}^{i=1} c_i(I_1 - 2)^2 + \sum_{N_2}^{k=1} d_k(lnJ)^{2k} - 2\sum_{N_2}^{k=1} m_k(lnJ)^k$

$+ H(E_1 - E_2)H(E_1E_2)\sum_{i=1}^{3} p_i E_1^i E_2 + \sum_{i=1}^{3} b_i E_2^{i+1}$ are the isotropic terms of two-dimensional MoO_3. The rest terms in Eq. (13) are used to fit the anisotropic properties of MoO_3. I_1 and I_2 are the first and the second principal invariants. E_1 and E_2 are the Green strain. N_1 and N_2 are the polynomial terms. c_i, d_k, m_k, p_i, b_i, q_i, n_i, a_i, s_i and t_i are all the unknown parameters, which need to be calculated through fitting the continuum model to the DFT results. $J = det(\boldsymbol{F}) = \sqrt{I_2}$, where $\boldsymbol{F}$ is the deformation gradient.

Since the stress results obtained from the DFT simulation is Cauchy stress, we use the second Piola-Kirhchhoff (PK2) stress tensor, which is defined as the derivative relation of the strain energy over the right Cauchy-Green tensor to find the stress-strain relation. The second Piola-Kirhchhoff (PK2) stress tensor is shown as follows,

$$\boldsymbol{S} = 2\frac{\partial \phi}{\partial \boldsymbol{C}} = 2[\frac{\partial \phi}{\partial I_1} + \frac{\partial I_1}{\partial \boldsymbol{C}} + \frac{\partial \phi}{\partial I_2} + \frac{\partial I_2}{\partial \boldsymbol{C}} + \frac{\partial \phi}{\partial E_1} + \frac{\partial E_1}{\partial \boldsymbol{C}} + \frac{\partial \phi}{\partial E_2} + \frac{\partial E_2}{\partial \boldsymbol{C}}] \quad (14)$$

where $\boldsymbol{C}$ is the right Cauchy-Green tensor expressed as,

$$\boldsymbol{C} = \boldsymbol{F^T F} = 2\boldsymbol{E} + 1 \quad (15)$$

The left Cauchy-Green tensor is $\boldsymbol{B} = \boldsymbol{F F^T}$. Meanwhile, the first order deformation gradient I_1 and the second order deformation gradient I_2 are $I_1 = \lambda_1^2 + \lambda_2^2 + \lambda_3^2$ and $I_2 = \lambda_1^2\lambda_2^2 + \lambda_2^2\lambda_3^2 + \lambda_3^2\lambda_1^2$. For two-dimensional MoO$_3$, we can ignore the deformation in z-axis. It means $\lambda_3 = 0$; so that the deformation gradients are $I_1 = \lambda_1^2 + \lambda_2^2$ and $I_2 = \lambda_1^2$. Herein, we can derive that $\frac{\partial I_1}{C} = \boldsymbol{I}$ and $\frac{\partial I_2}{C} = I + 2\boldsymbol{C^{-1}}$. Insert all the related correlations into cauchy stress equation

$$\boldsymbol{\sigma} = J^{-1}\boldsymbol{FSF} = 2J^{-1}\frac{\partial \phi}{\partial I_1}\boldsymbol{B} + I_2\frac{\partial \phi}{\partial I_2}\boldsymbol{I} \quad (16)$$

We obtain the Cauchy-stress continuum model as,

$$\sigma_x = 2J^{-1}\sum_{N_1}^{i=1} ic_i(I_1 - 2)^{i-1}\lambda_1^2 + 2J^{-1}\sum_{N_2}^{k=1} kd_k(lnJ)^{2k-1} - 2J^{-1}\sum_{N_2}^{k=1} km_k(lnJ)^{k-1} + \phi_{x0}^{'}$$

$$(17)$$

$$\sigma_y = 2J^{-1}\sum_{N_1}^{i=1} ic_i(I_1 - 2)^{i-1}\lambda_2^2 + 2J^{-1}\sum_{N_2}^{k=1} kd_k(lnJ)^{2k-1} - 2J^{-1}\sum_{N_2}^{k=1} km_k(lnJ)^{k-1} + \phi_{y0}^{'}$$

$$(18)$$

where $\phi_{x0}^{'}$ and $\phi_{y0}^{'}$ are the derivative of the heavyside terms in the strain energy

continuum model. Those two parameters are used to make the constitutive stress-strain model fit to the anisotropic properties of MoO_3 under large strain conditions.

3.6   Fitting Curve Results

All the unknown parameters are obtained through fitting the constitutive model to the DFT results, as shown in Table 4.

Table 4: Fitting parameters

i	1	2	3	4
c_i	2.52	13.50	-21.92	-
d_i	2.52	2.52	-	-
m_i	2.51	1.17	-	-
b_i	-18.45	-79.05	543.00	-
n_i	-6.70	-42.18	-257.34	1319.70
a_i	1.46	0.77	0.43	1.10
p_i	-99.76	845.47	-1094.5	-
q_i	-82.52	300.27	820.22	-
s_i	0.5	25	-166.67	1250
t_i	2500	3333.33	-	-

By applying strain on the x-direction while restricting y-direction, we assume $E_2 = 0$. The stress constitutive model is simplified to Eq. (19) and Eq. (20),

$$\sigma_x = 2J^{-1}\sum_{N_1}^{i=1} ic_i(I_1-2)^{(i-1)}\lambda_1^2 + 2J^{-1}\sum_{N_2}^{k=1} kd_k(lnJ)^{2k-1} - 2J^{-1}\sum_{N_2}^{k=1} km_k(lnJ)^{(k-1)}$$

$$(19)$$

$$\sigma_y = 2J^{-1}\sum_{N_1}^{i=1} ic_i(I_1-2)^{(i-1)}\lambda_2^2 + 2J^{-1}\sum_{N_2}^{k=1} kd_k(lnJ)^{2k-1} - 2J^{-1}\sum_{N_2}^{k=1} km_k(lnJ)^{k-1}$$

$$+ J^{-1}(p_1E_1 + p_2E_1^2 + p_3E_1^3)$$

$$(20)$$
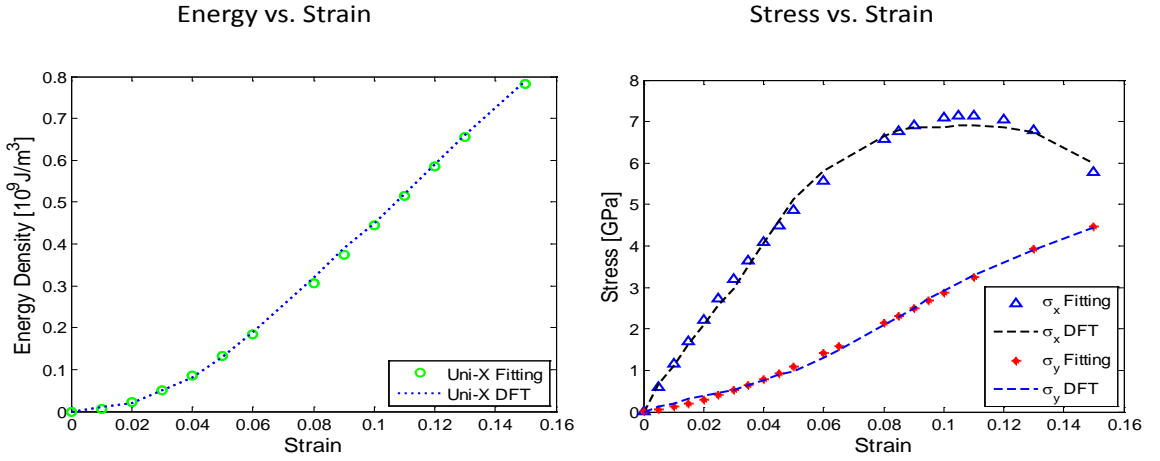
Figure 15: Fitting curve results of uni-X axial tension of two-dimensional MoO_3

We use the nonlinear least square method to fit Eq. (19) and Eq. (20) to the DFT results. Fig. 15 shows the fitting curves of uniaxial tension along x-direction of two-dimensional MoO_3. The marker shows the DFT results and the solid lines exhibits the continuum model results. It implies that the constitutive model matches well with the DFT results. The constitutive model is capable of predicting the uni-X axial tension of MoO_3 under large strain.

All the fitting parameters are obtained through three to six simulations until we obtain the converging results. There are other combinations of the fitting parameters,

we try to reduce the number of fitting parameters to make the constitutive model simple.

Similarly, when we apply strain on the y-direction while keep the x-direction fixed, we can assume $E_1 = 0$. Fig. 16 shows the fitting energy density-strain and stress-strain curves of MoO_3. It shows the constitutive model fits well with the DFT results. It also implies the constitutive can successfully predict the stress behavior of two-dimensional MoO_3.
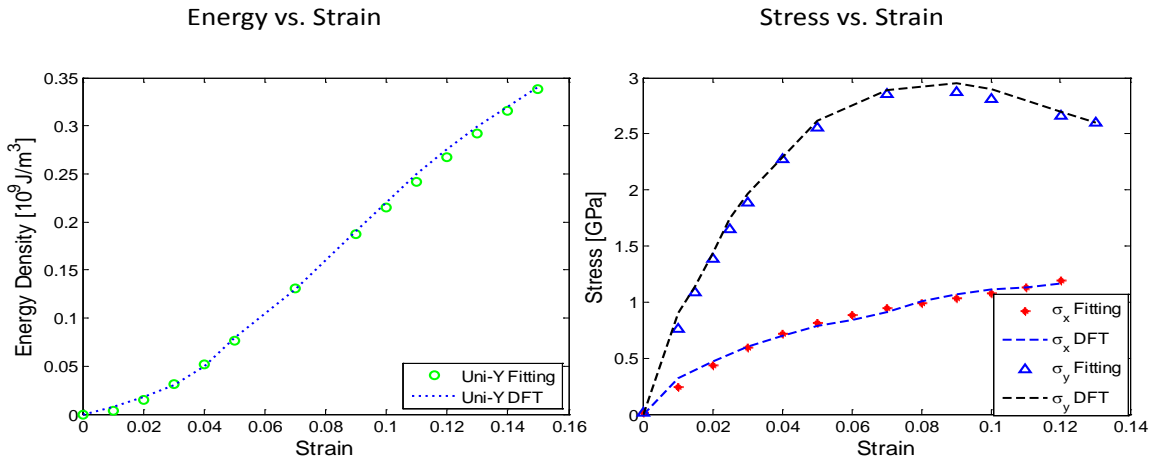
Figure 16: Fitting curve results of uni-Y axial tension of two-dimensional MoO_3

Fig. 17 shows the energy density-strain and stress-strain fitting curves of two-dimensional MoO_3 under biaxial loading. we can assume $E_1 = E_2$. The constitutive model matches well with the DFT results in predicting the stress-strain behavior of two-dimensional MoO_3 under biaxial loading. Fig. 17 also implies that two-dimensional MoO_3 has higher strength in the x-direction than that of the y-direction. The anisotropic properties of MoO_3 become more obvious under large strain.
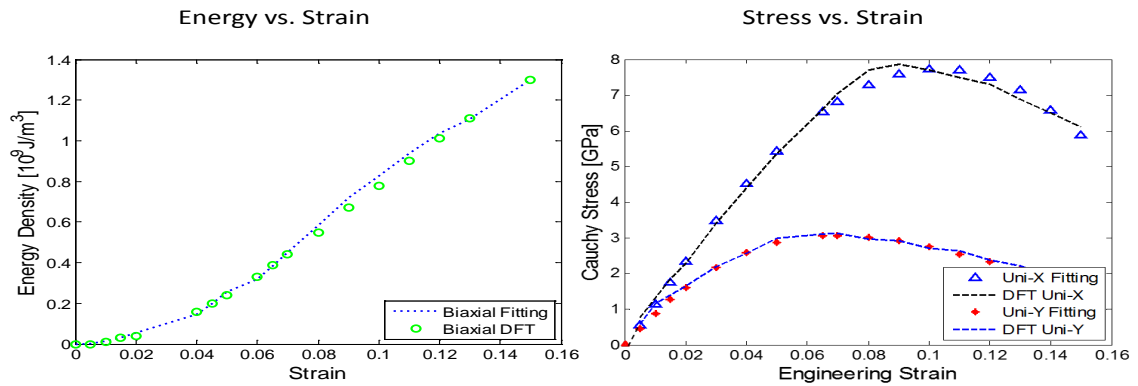
Figure 17: Fitting curve results of biaxial tension of two-dimensional MoO$_3$

Fig. 18 depicts the energy density-strain and stress-strain fitting curves of two-dimensional MoO$_3$ under uniaxial loading while keep the other side free. The fitting curves show that the constitutive model matches well with the DFT results under small strain. Two-dimensional MoO$_3$ is isotropic under strain less than 1 %. It has a Young's modulus near 95 GPa. MoO$_3$ shows its anisotropic properties under large strain.
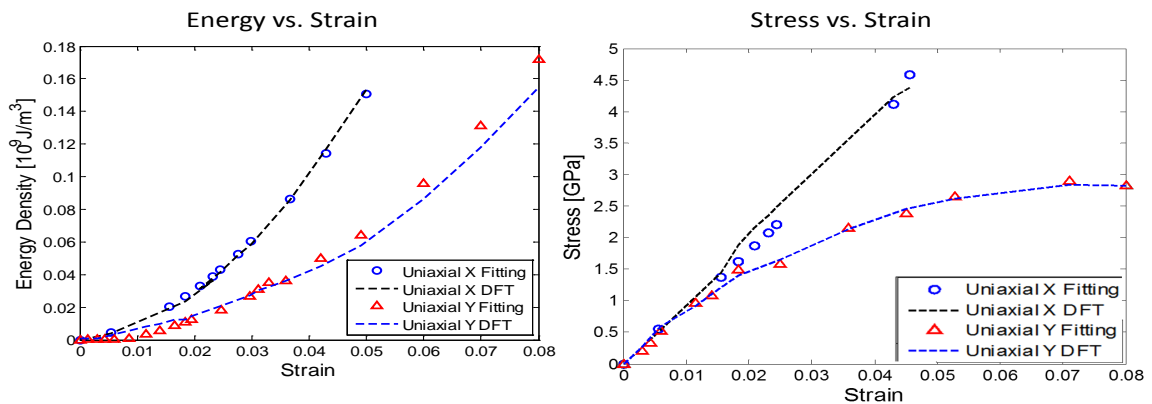
Figure 18: Fitting curve results of uni-X axial tension Y-direction free of two-dimensional MoO$_3$

3.7   Conclusion

The material response of two-dimensional MoO_3 under uniaxial and equal biaxial tensile loadings was computed with DFT simulations. A elastic constitutive model was developed based on the DFT results by applying a least square fit. The constitutive model matches well with the DFT results. The constitutive model is helpful to predict to the mechanical behavior of two-dimensional MoO_3.

MoO_3 is an isotropic material before 1 % strain and its Young's modulus is 95 GPa. MoO_3 becomes anisotropic under large strain conditions.

CHAPTER 4: MECHANICAL PROPERTIES OF GRAPHYNE

In this chapter, a detailed description of the analysis of the mechanical properties of graphyne is presented. First, the background of mechanical analysis on graphyne's current studies and opportunities are stated. Then, we state the research objectives and tasks to investigate the mechanical properties of graphyne. Finally, the issues pertaining to the mechanical properties and its affected key parameters are addressed with molecular dynamics simulation.

4.1   Introduction

Carbon allotropes have been studied for years and still are a subject of interest [41, 66, 167]. There are only two major naturally occurring carbon allotropes: diamond and graphite [38, 79]. Yet there are many other carbon allotropes, such as graphene, graphyne, graphhdiyne and so on. The discovery of two-dimensional graphene expanded the applications of graphite-related carbon materials, including photovoltaic cells, organic light-emitting diodes, field-effect transistors, and chemical sensors [102]. Two-dimensional graphene, as an allotrope having similar structure to graphene, has triggered tremendous interest due to its unique electrical, optical, and mechanical properties [81, 112, 123, 135, 164].

The carbon lattice in graphyne has a rectangular symmetry, unlike the hexagonal symmetry of graphene, as shown in Fig. 19. The zoom-in picture shows the

specific carbon-carbon triple bond, which is different from the carbon-carbon bond of graphene. Graphyne consists of aromatic 6-membered rings and weakly anti-aromatic 12-membered rings comprised of alternating triple bonds and conjugated double bonds [164, 181].
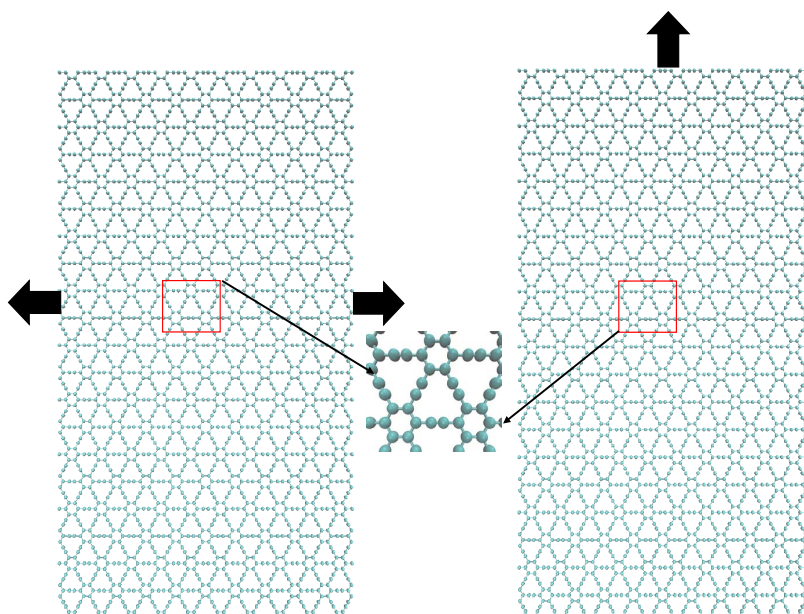
Figure 19: Schematic of two-dimensional graphyne

Considering the similarity of the structure of graphyne to that of graphene, it is likely that graphyne has similar and even superior applications to graphene. Zheng et al. [208] state that two-dimensional carbon derived from graphyne with chemical properties superior to those of graphene. Chen et al. [29] predicated theoretically that graphyne has a higher electron carrier mobility. Furthermore, it is predicated that graphyne can be used as an eletrocatalyst [162, 182, 183, 194]. These remarkable properties make graphyne a promising materials for nanoelectronics and energy storage applications [60, 161, 198].

Graphyne is predicted to have high-temperature stability and similar mechanical

properties to graphite, which might be a semiconductor rather than a metal or semi-metal [123]. Yet there is a big challenge in manufacturing the long-range ordered structure of graphyne. We can not fully understand the functionality of these carbon materials without knowing the structure from a microscopic view [122]. Thus, its essential to understand the mechanical properties of graphyne and its family in order to solve the manufacturing problems.

Shao et al. demostrated that graphene has superior mechanical properties with Young's modulus E=350.01 N/m and ultimate tensile strength of 119.2 GPa at room temperature; while the Young's modulus and ultimate tensile strength of graphyne are only E=250.9 N/m and 81.2 GPa, respectively [156]. However, further studies are needed to fully understand the mechanical properties of graphyne.

Mono-layer graphyne and its family of materials are constructed by replacing one-third of carbon-carbon bonds in two nearest-neighbor hexagonal rings in graphene sheet by acetylenic linkages. These triple bonds open up a potentially limitless array of different geometries beyond the perfect hexagonal lattice of graphene [112].

However, mechanical properties of perfect and defective graphyne have remained largely unsolved. There are mainly three ways to study the microstructure of graphyne. Some researchers investigated the structures of graphyne using density functional theory calculations [23, 85, 106, 135, 161, 165, 182]. Some research groups studied the mechanical properties of graphyne with molecular dynamics simulations [189, 193, 199, 200, 203, 206].

4.2   Purpose

The purpose of this chapter is to resolve the following problems: predict the mechanical properties of pristine graphyne, and find the key parameters that affect the mechanical properties of graphyne. Key parameters include the strain applied on the graphyne, length or width of the graphyne sheet, the percentage and shape or direction of defects in the graphyne.

4.3   Tasks

We address the issues pertaining the mechanical properties of graphyne in the following sections. First, we calculate the mechanical properties of non-defective graphyne and its family materials with molecular dynamics simulations. Secondly, we study the dependence correlations between: (a) mechanical properties and tensile strain and (b) impact of defects on mechanical properties. Third, we study the impact of edge chirality on mechanical properties.

All the molecular dynamics simulations are performed using LAMMPS (Large-scale Atomic Molecular Massively Parallel Simulator) code with the Reax potential [139]. The Reax potential has been shown to be capable of computing the carbon-carbon bond interaction, bond breaking and even bond reforming in the carbon atoms.

In molecular dynamics simulations, we use the Velocity-Verlet algorihthm to integrate the motions of atoms using a timestep of 0.1 fmsec. The tensile loading is applied by applying increment strain in either armchair or zigzag direction, from 0 % up to 20 %. The strain increment is added after every 50 time steps. The molecular dynamics simulations are carried out in a canonical ensemble. The Nose-Hoover

thermostat is used here to control the temperature at 300 K.

4.4   Graphyne without Defects

There are two type of edges in graphene and graphyne: armchair and zigzag edges [46, 122]. In this study, two uniaxial tensile tests are applied on the graphyne sheets, as shown in Fig. 20, by fixing the boundaries in the armchair direction or zigzag direction, respectively.
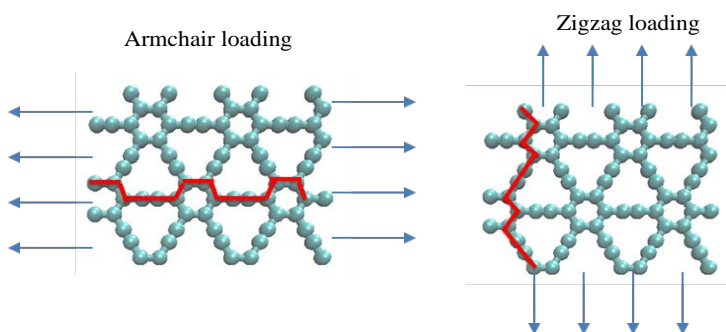
Figure 20: Graphyne with tensile loading

In order to test the effect of the number of triple bonds on the strength of graphyne, single acetylenic are replaced by two triple bonds (diacehtylenic), three triple bonds (graphyne-3) and up to four triple bonds (graphyne-4), as shown in Fig. 21. The same loading conditions are applied onto the graphyne sheets with replaced triple-bonds. The length of triple, single, and aromatic bonds are 1.19 Å, 1.48 Å and 1.49 Å, respectively [38].
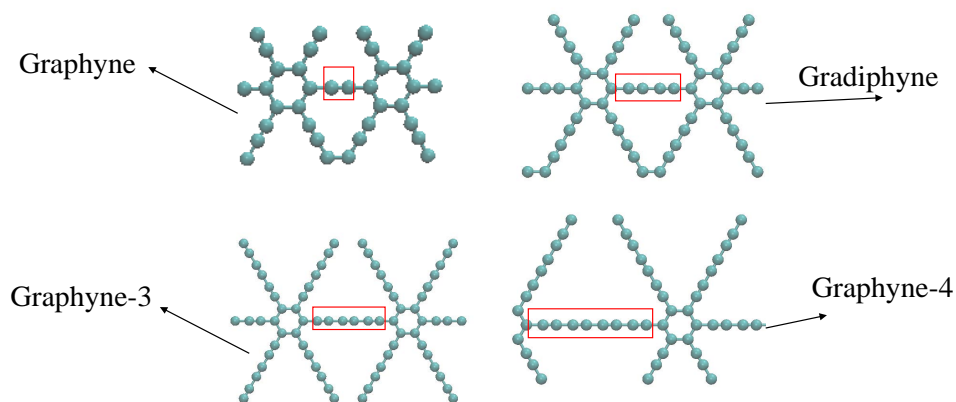
Figure 21: Graphyne and its family of materials
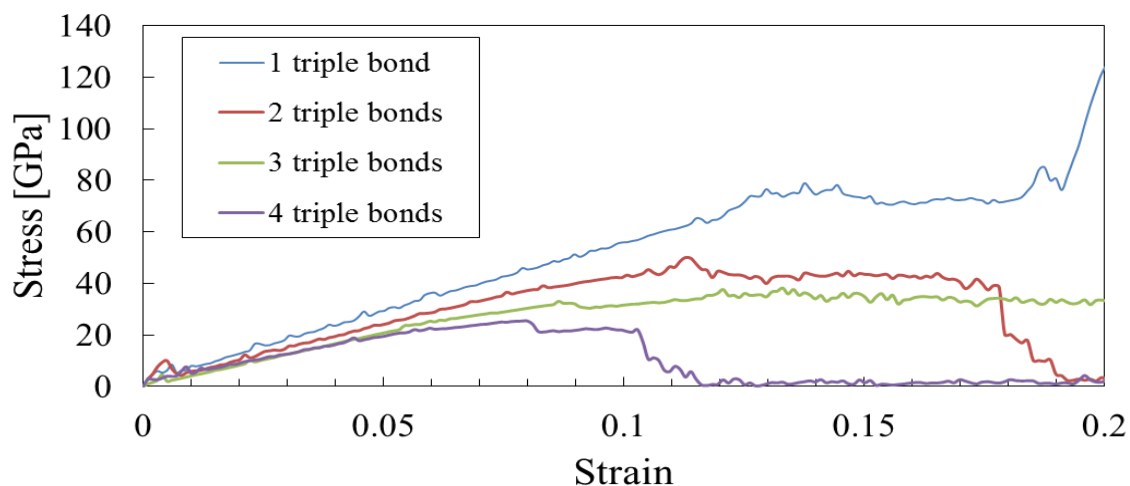
Figure 22: Pristine graphyne with uniaxial tensile loading in the armchair direction

Fig. 22 illustrates the stress-strain curves of pristine graphyne under uniaxial tensile loading in the armchair direction.By increasing the total number of triple bonds between the neighboring hexagonal rings, the maximum strength of graphyne and its family of materials decreases. The longer the triple bond is, the weaker the strength of the bond between the two neighboring hexagonal rings will be. Increasing the

number of triple-bond also make graphyne reaches its maximum strength at an early strain condition. For example, graphyne with single triple-bond reaches its maximum strength around 13% while the maximum strength of double triple-bond sheet occurs around 11%.
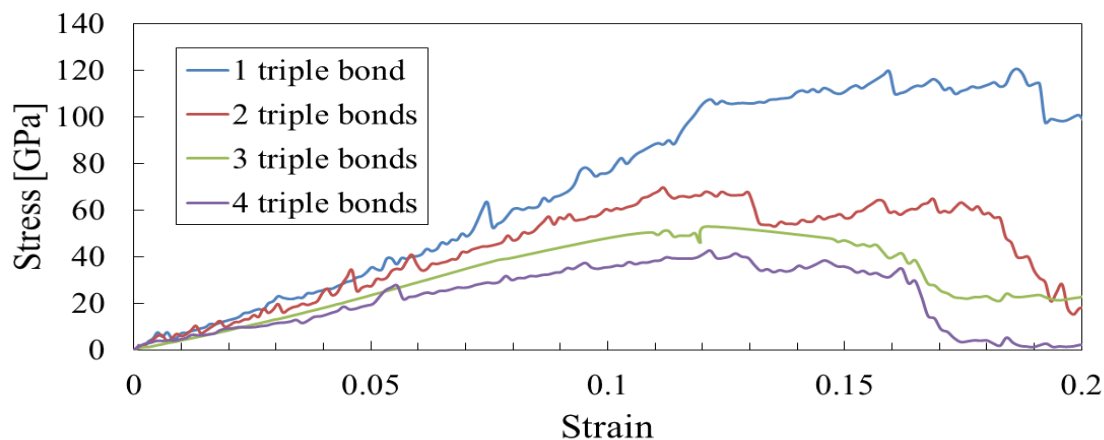
Figure 23: Pristine graphyne with uniaxial tensile loading in the zigzag direction

Fig. 23 demonstrates the stress strain curves of pristine graphyne under uniaxial tensile loading in the zigzag direction. Similar behavior is observed for loading in the zigzag direction compared to the results of loading in the armchair direction. Young's modulus decreases with the increment in the number of triple bonds between the neighboring hexagon rings, which is shown in Fig. 24.
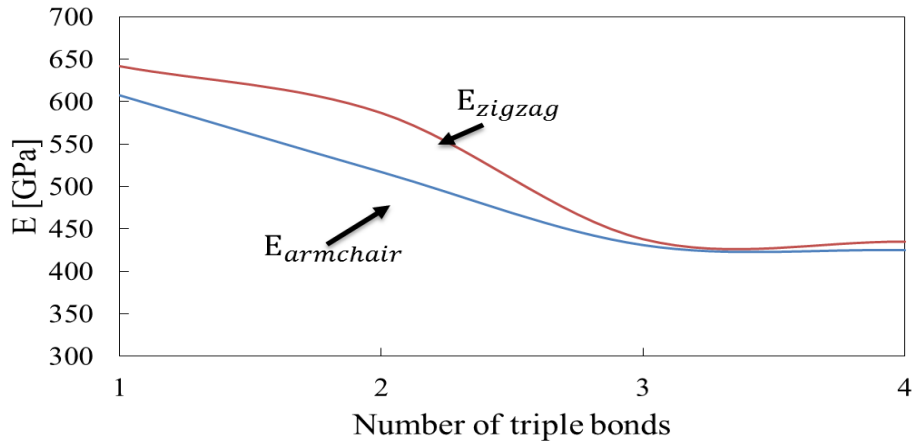
Figure 24: Young's modulus of graphyne with variable number triple bonds

The results show that graphyne is an anisotropic material. Both Young's modulus and yield strength is greater in the zigzag direction compared to the ones in the armchair direction. Graphyne with single triple-bond reaches its maximum strength at the strain of 13% for the uniaxial armchair direction loading while 15% for the uniaxial zigzag direction loading.

4.5   Graphyne with Defects

The formation of different kinds of defects such as incomplete bonding defects, topological defects and heterogeneous defects during the manufacturing of graphyne sheets is inevitable [2]. It is important to study how defect affect the stress strain behavior of two-dimensional graphyne.

Defects in the graphyne sheet are created by deleting certain number of carbon atoms. Fig. 25 shows defects on zero degree links, sixty degree links, mixing defects on zero and sixty degree links and area defect 0 degree defect, shown from left to right, respectively.

| 0 degree | 60 degree | Mix 0 and 60 degree | Area defect |
| (5% defects) | (5% defects) | (5% defects) | (0.25% defects) |
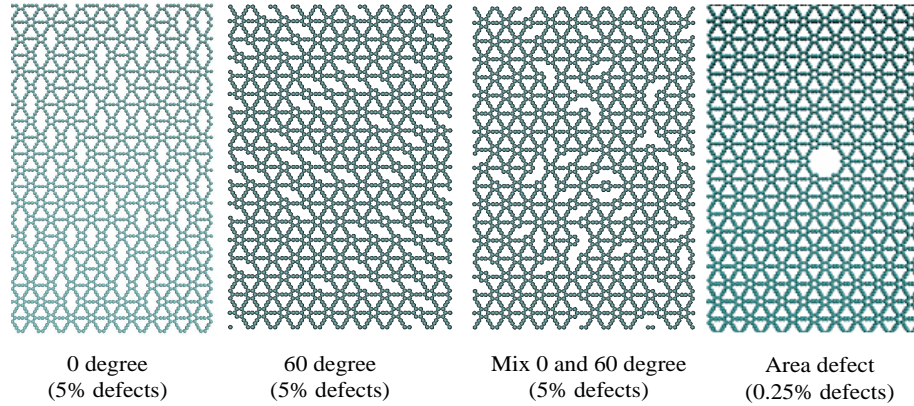
Figure 25: Variable defects type in graphyne

Defect on zero degree link is created in the graphyne sheet by deleting two carbon atoms lying in the zero degree carbon-carbon triple bond. Defect on sixty degree link means deleting the two atoms lying on the carbon-carbon triple bond, which has a sixty degree angle with armchair direction. Area defect is created by deleting a number of atoms in the same neighboring area to make a hole in the graphyne sheet. The percentage of defect is defined as the number of deleted atoms divided by the total number of atoms of the pristine graphyne sheet. The positions of defects on zero and sixty degree links are randomly chosen. All the following results of defective graphyne are obtained by averaging the results of three to six different simulations.

4.5.1 Defects on zero degree links

In this section, we study the mechanical properties of defected graphyne with single triple-bond linkage.
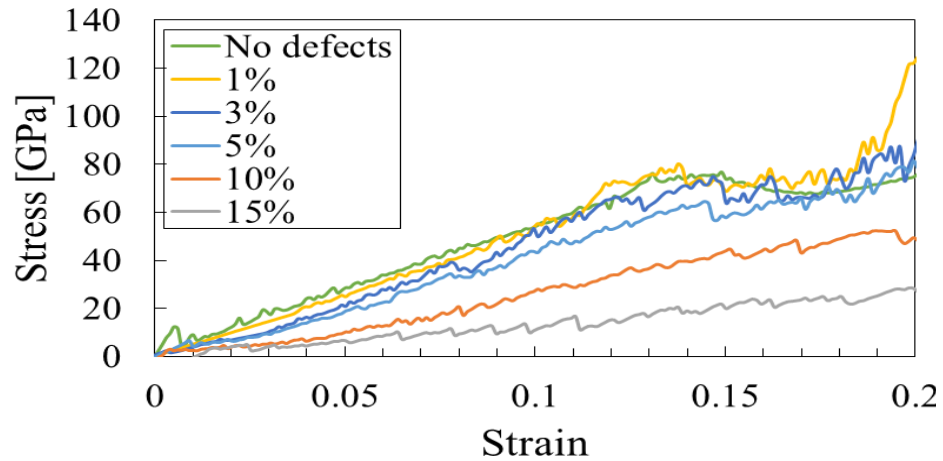
Figure 26: Stress-strain results of uniaxial tension in armchair direction for defects on zero degree links

Fig. 26 and Fig. 27 are the stress-strain curves of defected graphyne under tensile loading in armchair and zigzag direction, respectively. The results show that as the defects percentage increases, both Young's modulus and yield strength decreases.
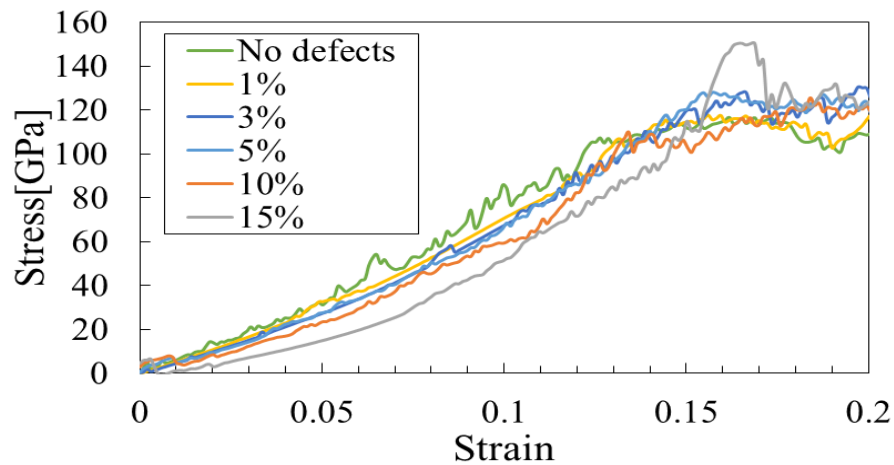
Figure 27: Stress-strain results of uniaxial tension in zigzag direction for defects on zero degree links

When the defects are less than 1%, Young's modulus and yield strength of the defected graphyne are almost the same compared to the sample with no defects. When the defects reach up to 5%, graphyne become more fragile in the armchair

direction then in the zigzag direction. With the same defects, graphyne in the Y-direction have higher strength and Young's modulus.
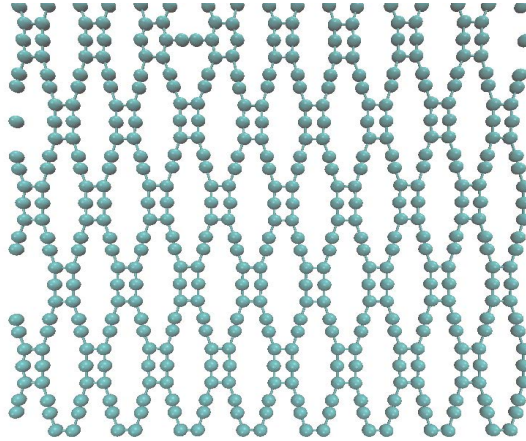
Figure 28: Result of 0 degree 15% defective graphyne with zigzag direction loading

4.5.2   Defects in sixty degree links

In this section, we study the mechanical properties of defective graphyne by creating defects in sixty degree links. The defects are created by deleting sixty degree triple bonds randomly in the two-dimensional graphyne. Fig. 29 and Fig. 30 are the stress-strain curves of defected graphyne under tensile loading in armchair direction and zigzag direction, respectively.
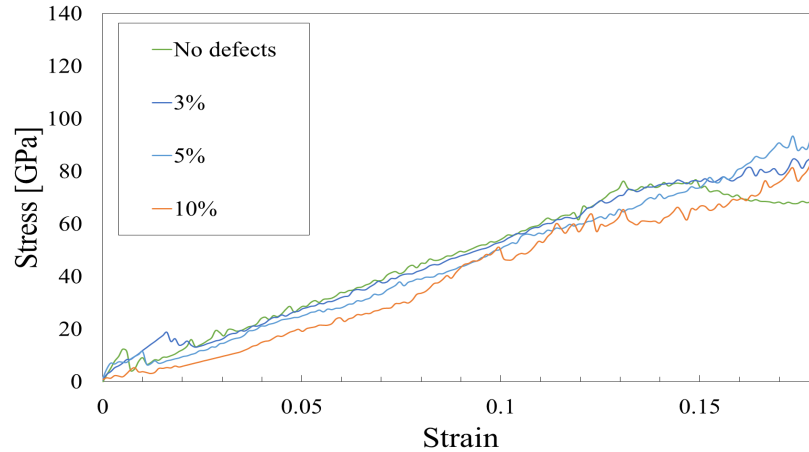
Figure 29: Stress-strain results of uniaxial tension in armchair direction for defects in sixty degree links
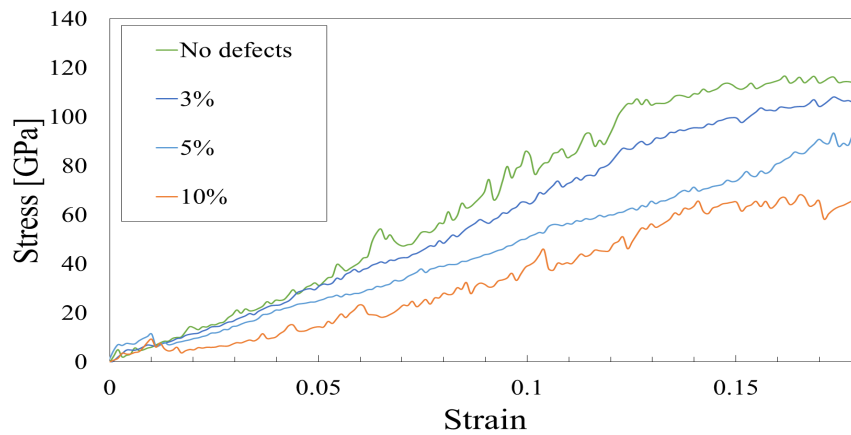
Figure 30: Stress-strain results of uniaxial tension in zigzag direction for defects in sixty degree links

The results show that as the defects percentage increases, both Young's modulus, shown in Fig. 31 and yield strength decreases. When the defects are less than 1%, Young's modulus and yield strength of the defected graphyne are almost the same compared to the sample with no defects. When the defects reach up to 5%, graphyne becomes more sensitive to the strain in the zigzag direction than in the armchair direction.
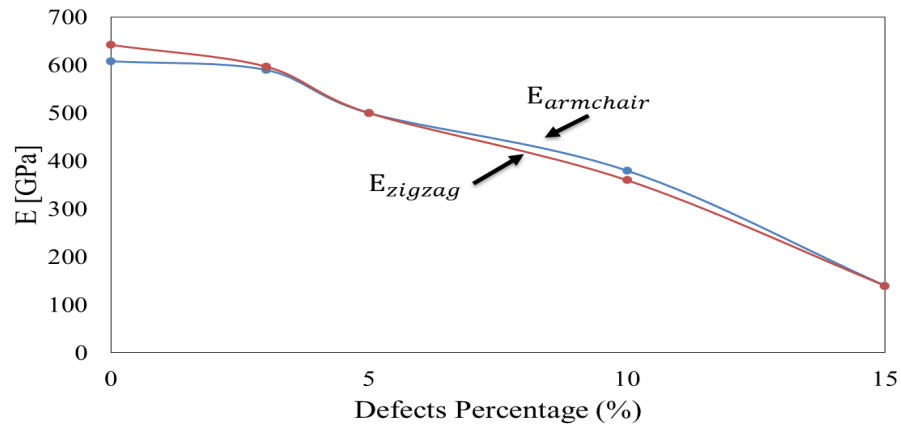
Figure 31: Young's modulus of sixty degree defective graphyne

With the same defects, graphyne sheet with a tensile loading in the armchair direction has higher strength and Young's modulus. Graphyne is more sensitive to the 60 degree defects in the zigzag direction compared to the armchair direction.

4.5.3   Mix Defects

We study the two-dimensional defective graphyne by mixing the defects in zero and sixty degree links. In this section, defects are created by deleting triple bonds randomly in both zero degree links and sixty degree links. The results shown in this section are the average of results six different simulations. Fig. 32 and Fig. 33 show the stress-strain curves of graphyne with variable percentages of defects under tensile loading in the armchair and zigzag direction, respectively.
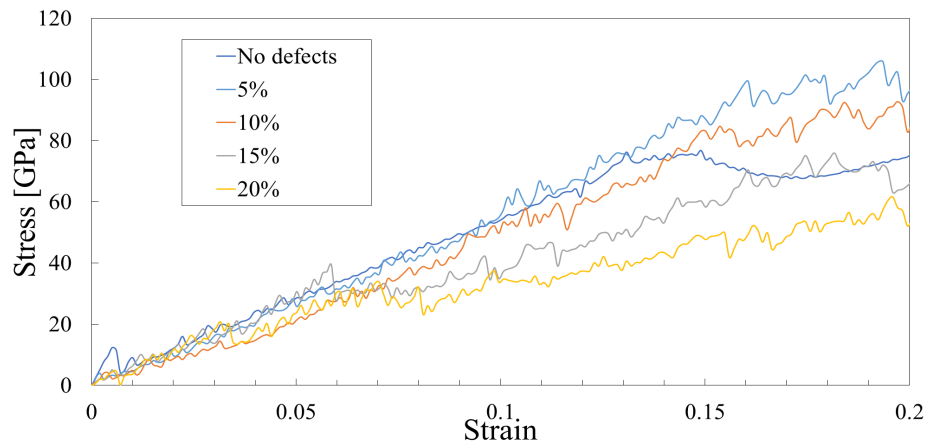
Figure 32: Stress-strain results of uniaxial tension in armchair direction for mix defects
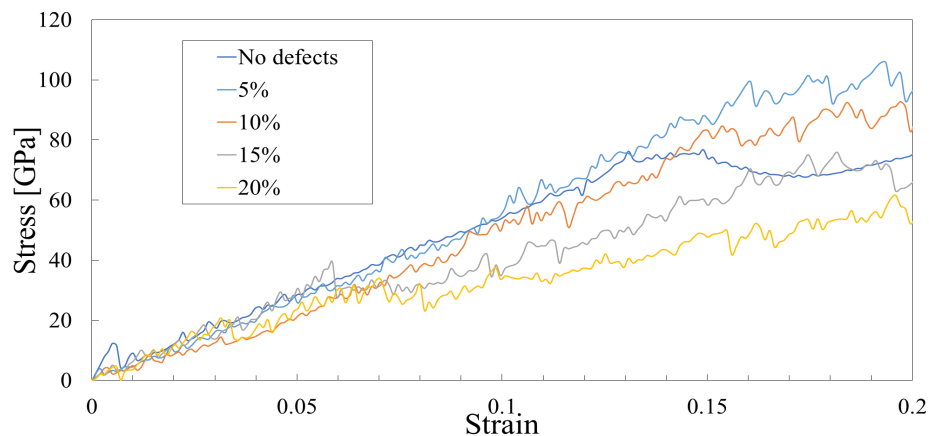
Figure 33: Stress-strain results of uniaxial tension in zigzag direction for mix defects

With similar levels and types of defects, graphyne is more sensitive to the applied strain in the zigzag direction than that in the armchair direction. As the defect area increases, Young's modulus of the graphyne decrease, shown in Fig. 34. Graphyne, with defects under tensile loading in the zigzag direction, has a similar Young's modulus and strength compared with the ones in armchair direction. Graphyne is not sensitive to the mixed defects before strain of 5%. Graphyne, with defects in the armchair direction, reaches its maximum strength around a strain of 15%.
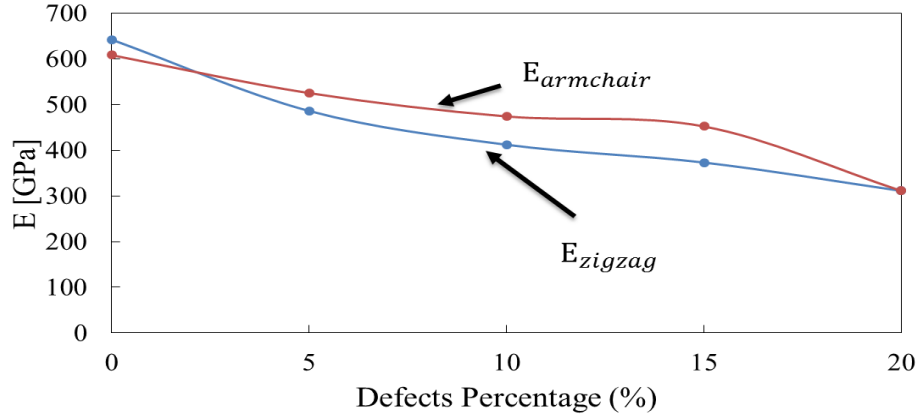
Figure 34: Young's modulus of mix defects for defective graphyne

4.5.4   Honeycomb Shape Defect

In this section, defects are created by deleting the carbon atoms in the shape of honeycomb, which can be considered as an area defect. By increasing the area of defects in the center of the graphyne, we create three types of defects, which are named small, middle and large size defects, respectively. Table 5 shows the percentage of defects of these three types of area defects.

Table 5: Summary of area defect

Area defect	Total atoms	No. of deleted atoms	Defect percentage
Small size	2400	2394	0.25 %
Middle size	2400	2382	0.75 %
Large size	2400	2352	2 %

The strain is applied in the armchair direction from 0 % to 20 %. The stress-strain results of those defective graphyne are shown in Fig. 35. It shows that increasing the size of the central defects does not impact the tensile strength and the yield
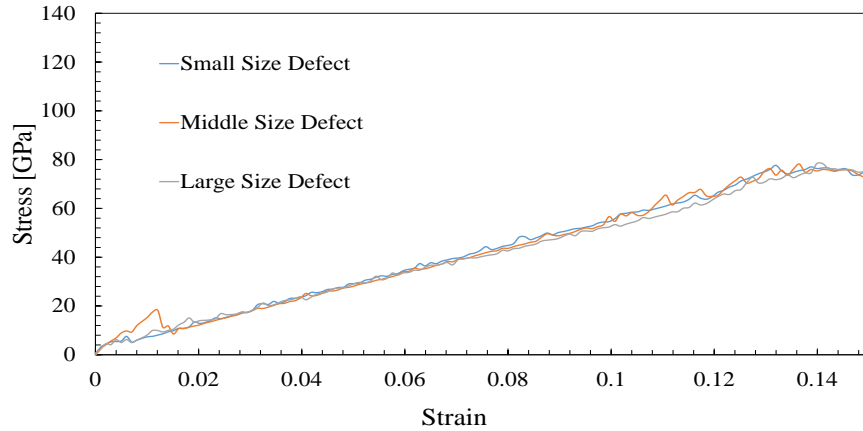
Figure 35: Stress vs. strain curve of graphyne with area defect

strength of the two-dimensional graphyne. The Young's modulus of all those defective graphyne is around 600 GPa. Compared to the previous bond-bond or point defects, the central area defects have a minimum impact on the mechanical strength of the two-dimensional graphyne systems, when the percentage of the defects is below 2 %.

4.6   Conclusion

In this chapter, the mechanical properties of perfect and defective graphyne and its family, were studied using molecular dynamics simulation. The results showed that graphyne has interesting mechanical properties, which is beneficial to engineering design.

The results show that mechanical properties of perfect graphyne and its family of materials are dependent on the number of acetylenic bonds. Both the Young's modulus and yield strength decreases with increasing the number of acetylenic bonds.

For the defective graphyne, Young's modulus and strength are near the perfect condition when percentage of defects is less than 5 %. When the percentage of defects

is over 5 %, both the Young's modulus and strength dropped significantly with an increase in the defects concentration. Perfect graphyne and its family of materials are more sensitive to the applied strain than in the armchair direction. Defective graphyne is more sensitive to the defects in zero degree links in the armchair direction compared with the zigzag direction. Graphyne sheet is more sensitive to the defects in sixty degree links in the zigzag direction compared with the armchair direction. Young's modulus of defective graphyne is affected the most by the defects in zero degree links compared to other defects.

CHAPTER 5: THERMAL CONDUCTIVITY OF GRAPHYNE

In this chapter, we briefly present the study of thermal conductivity of graphyne and its family of materials. First, we review the current achievements and applicable methodologies of graphyne and carbon related materials. Second, we state the research objectives and tasks for studying the thermal conductivity of graphyne and its family of materials. In the end, we solve the problems pertaining the thermal conductivity of graphyne with molecular dynamics.

5.1   Introduction

The increasing demand for the microeletronics requires a fundamental understanding of the thermal behavior of the materials used in these devices [1,47]. The thermal dissipation has become a major issue that challenges the development of microeletronics devices [61, 154, 173]. Efficient heat removal is of great importance to the good performance and stable function of the microscale devices [154]. Good understanding and management of thermal behavior is helpful in tailoring the materials' heat conducting efficiency [14]. Meanwhile, it's useful in improving the performance of thermalelectronic converter systems and optoelectronic devices [31].

Two-dimensional materials such as graphyne and its family of materials have a potential to be used in microelectronics industries, such as graphyne, gradiphyne, graphyne-3 and graphyne-4. Two-dimensional graphyne is a graphite allotrope that

similar to the atomic structure of graphene. Graphyne and its family of materials are produced by replacing the carbon-carbon bond between the neighboring hexagon rings with acetylenic (triple carbon-carbon bond). The thermal conductivity of graphyne can be affected by temperature, strain and substrate [132, 200]. Two-dimensional materials' thermal conductivity can be also affected by defects, impurities, edge chirality, and tailored geometry shapes including size and asymmetry [47, 70, 192]. Yet, until now, few publications have been focused on the study of the thermal conductivity of graphyne and its family of materials.

The study of the thermal conductivity of graphyne and its family of materials still have many gaps, which are due to these reasons. First, it's still difficult to make graphyne. Second, it's very difficult to test the mechanical and thermal properties of graphyne without available graphyne sheets. Third, the current research on thermal conductivity of graphene relies on computational methods, such as molecular dynamics and density functional theory. Yet there are not enough studies of thermal conductivity of graphyne using computational methods.

We use molecular dynamics method to investigate the thermal conductivity of graphyne and its family of materials here.

5.1.1   Background of Thermal Conductivity and Phonon

In 1822, Joseph Fourier published a book stating the complete theory of heat conduction. He stated through the empirical law that the heat flux resulted from the thermal conduction is proportional to the magnitude of the temperature gradient and

opposite to it in the sign [103]. The heat transfer function is shown as follows,

$$J = -\kappa \frac{dT}{dx} \tag{21}$$

where J and κ are the heat flux and the thermal conductivity, respectively. The term $\frac{dT}{dx}$ is the temperature gradient in the x-direction.

In isotropic materials, the thermal conductivity is the same in all the directions while in anisotropic materials, it's dependent on the crystal orientation [15,22,90,129]. Generally, in solid materials heat is carried by acoustic phonons and eletrons. Phonons are considered to be the main heat carriers especially for carbon material [129].

The thermal conductivity of two-dimensional material mainly depends on acoustic phonons, which is very sensitive to the change of the system temperature [68]. As a result, thermal conductivity can be expressed as Eq. (22), in which Kp and K_e are the contributors from phonons and eletrons, respectively.

$$K = K_p + K_e \tag{22}$$

$$\frac{K_e}{\sigma T} = \frac{\pi^2 k_B^2}{3e^2} \tag{23}$$

K_e can be obtained through the Wiedemann-Franz law, shown in Eq. (23); where σ is the electrical conductivity, k_B is the Boltzmann constant and e is the charge of an electron. In metals or degenerately doped semiconductors, K_e is dominant as a result of the numerous density of free carriers [7, 129]. However, in carbon materials such as graphite and graphene, heat conduction is usually dominated by phonons [14, 27, 68, 127, 128].

Table 6: Important elementary excitations in solids [87]

Name	fields
Electron	N/A
Phonon	Elastic wave
Photon	Electromagnetic wave
Plasmon	Collective electron wave
Magnon	Magnetization wave
Polaron	Electron and elastic deformation
Exciton	Polarization wave

5.1.2   Background of Simulation Potentials

We review three different potentials which are widely used to model carbon-carbon interactions: the Airebo penitential, the Tersoff potential, and the ReaxFF potential.

∗ The ReaxFF potential

ReaxFF refers to reactive force field. ReaxFF uses two relationships between bonds: (i) bond distance and bond order and (ii) bond order and bond energy. It's developed to make the molecular dynamics simulation of large scale reactive systems practical [169]. The ReaxFF potentials have already been used for various combinations of chemical elements across the periodic table. For instance, studies of non-metals C,H,O,N, Si and metals Au, Zn, Cu, Al, Mg, Ni, Pt have used the ReaxFF potential [20, 33, 35, 77, 126, 147, 163, 169, 170]. The ReaxFF potential is proved to be capable of providing accurate account of the chemical, mechanical and thermal behavior of hydrocarbons [34, 117, 169], graphene [58, 159], carbon nanotubes [125, 126], nanoribbons [196], nanowiggles [17] and other nanostructures.

∗ The Tersoff potential

The Tersoff potential has been developed and successfully applied in the study of silicon, Si-O systems, hybrid boron nitride, carbon nanotubes [42,113,121]. Compared to the ReaxFF potential, the Tersoff potential is mostly used to study silicon rather than carbon related material. The reason can be attributed to Tersoff is unusable for global structural calculations since bcc structure has lower energy than the diamond structure [42]. Tersoff potential is still used to study the thermal conductivity of carbon nanotubes, carbon fullerenes, graphene ribbons, boron nitride nanotubes [14,47,94,105,116].

The disadvantage of Tersoff potential is it only allows short range of second-nearest-neighbor interactions to be presented [105]. It may cause the thermal conductivity of material to be over predicted or lower predicted.

∗ The Airebo potential

The Airebo potential has been widely used in investigating the thermal properties of graphyne and graphene sheets and nanoribbons, hydrogenated graphene, pillared-graphene, carbon nanotubes and interface among graphene and graphite [100,110, 132,157,179,200]. It has also been used in studying the thermal energy transportation between carbon related materials [69,172]. The Airebo potential has been shown to accurately capture the bond breaking and bond reforming between carbon atoms, which offers a powerful method in modeling the complicated chemistry in carbon-carbon systems [200,204,205].

The ReaxFF potential and the Tersoff potential is predicted to produce similar material behavior under small strain condition, yet deviate greatly under large strain

conditions [20, 169].

In this chapter, we explore the performance of Airebo and Tersoff potentials in modeling the thermal conductivity of graphyne, under various loading and boundary conditions.

5.2   Purpose and Tasks

We first calculate the thermal conductivity of pristine graphyne with molecular dynamics simulations, using LAMMPS [140]. Second, we study the correlations between: (a) thermal conductivity and number of the triple bond, (b) thermal conductivity and tensile strain applied on graphyne, (c) thermal conductivity and defects, (d) thermal conductivity and width of graphyne nanoribbons, and (e) thermal conductivity and length of graphyne nanoribbons.

5.3   Model System and Methodology

We investigate the thermal conductivity of graphyne and its family of materials, using the reverse nonequilibrium molecular dynamics (RNEMD). We calculate the thermal conductivity of graphyne nanoribbons in the armchair and zigzag directions as are shown in Fig. 36.

We use reverse non-equilibrium molecular dynamics method to compute the ribbons thermal conductivity. For this purpose, we divide the graphyne sheet into slabs as is shown. The middle slab is the hot slab and the two edge slabs are cold slabs. The heat flux in Fig. 37 is generated by exchanging the velocity of atom in the cold slab and atom in the hot slab. This leads to an temperature increase in the hot slabs and decrease in the cold slabs.
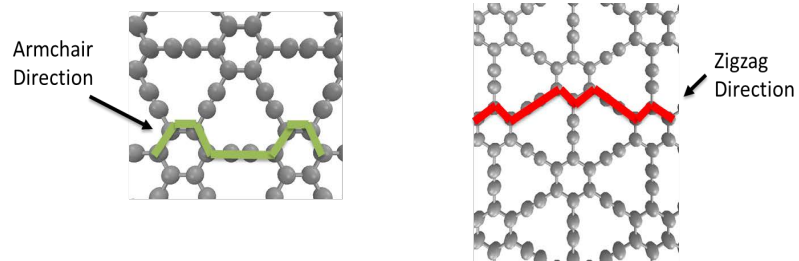
Figure 36: Thermal conductivity vs. number of triple-bond (Airebo)
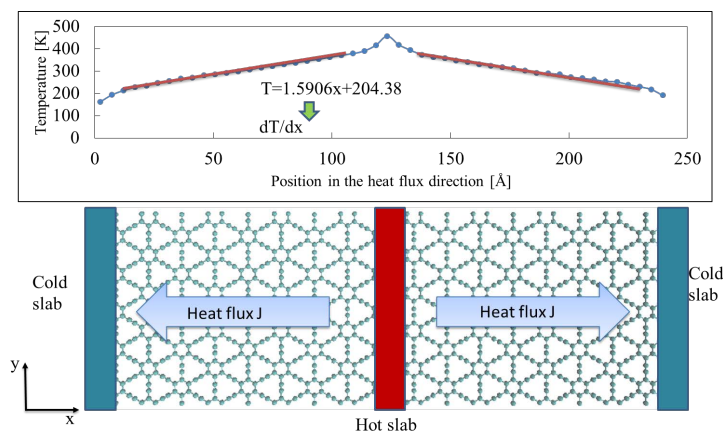
Figure 37: Temperature distribution

Finally, the heat flux is evaluated by adding all the repeated heat transfer,

$$J = \sum_{N_{transfer}} \frac{1}{t} \times \frac{1}{2}(mv_h^2 - mv_c^2) \tag{24}$$

where $N_{transfer}$ is the number of the energy exchanges during the molecular dynamics simulation period, t. v_h and v_c are the velocities of the exchange atoms in the hot slabs and the cold slabs, respectively.

In the end, the thermal conductivity of graphyne is calculated with the Fourier

law:

$$\kappa = -\frac{J}{2 \times A \times \frac{\partial T}{\partial x}} \tag{25}$$

where J is the heat flux in the longitudinal direction; $\frac{\partial T}{\partial x}$ is the temperature gradient, which is obtained as shown in Fig. 37 and A is the cross-sectional area perpendicular to the direction of the heat flow.

5.4   Results and Discussion

In this section, we show the molecular dynamics simulation results on the analysis of graphyne's thermal properties.

5.4.1   Triple Bond Effect on Thermal Conductivity

Using reverse nonequilibrium molecular dynamics, we investigate the influence of number of triple bonds on the thermal conductivity of graphyne. By increasing the number of triple bonds between the hexagon carbon rings in the graphyne from 1 to 4, the graphyne and its family of materials varies in the ribbon structure. The names of graphyne with two triple-bonds is graphdiyne. Similarly, the other graphyne's family of materials are called graphyne-3 and graphyne-4, respectively. In our simulation the ribbon size of the graphyne and its family of materials sample sheets are $length \times width$: 250 Å× 30 Å. Fig. 38 and Fig. 39 are the results obtained using Airebo potential and Tersoff potential, respectively.
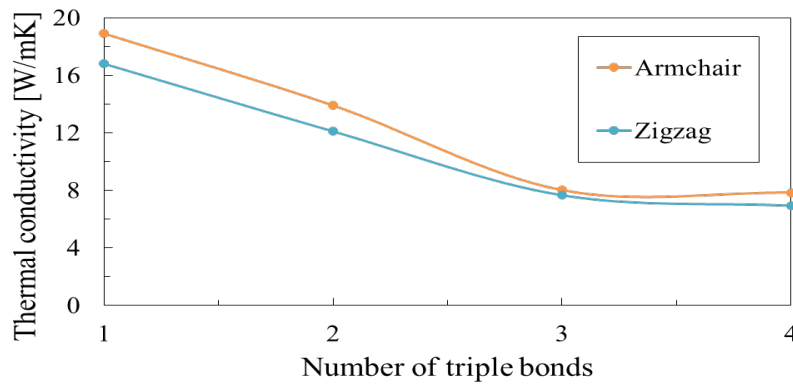
Figure 38: Thermal conductivity vs. number of triple bonds (Airebo)

The curves in Fig. 38 illustrates that graphyne's thermal conductivity decrees with the increasing number of triple bonds. Meanwhile, the plots indicate that the zigzag graphyne has smaller thermal conductivity compared to those of the armchair graphyne. Furthermore, Fig. 38 shows that thermal conductivity drops drastically when the number of triple bonds increases from one to three. Yet the thermal conductivity almost keep the same level when for graphyne with three triple bonds and four triple bonds.

Herein, the results indicate that graphyne's thermal conductivity is very sensitive to the variance of triple-bond. The armchair graphyne has the greatest thermal conductivity, which is 19 W/mK; while the zigzag graphyne-4 has the smallest thermal conductivity around 7 W/mK.
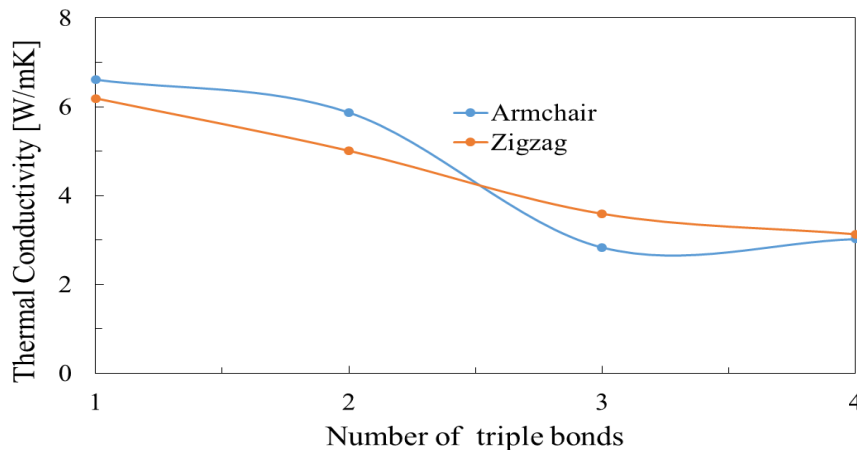
Figure 39: Thermal conductivity vs. number of triple bonds (Tersoff)

The plots in Fig. 39 predict a much lower thermal conductivity for graphyne. The armchair graphyne has the highest thermal conductivity, which is 7 W/mK. Both the armchair and zigzag graphyne-4 shows the same level of thermal conductivity, which is 3.5 W/mK. The armchair graphyne and gradiphyne have larger thermal conductivities compared to those of the zigzag ones. Yet the thermal conductivity of zigzag graphyne-3 and zigzag graphyne-4 surpasses the armchair ones, respectively. As mentioned in the review session in this chapter, the Tersoff potential only considers short range of second-nearest-neighbor interactions to be presented [105]. This may cause the thermal conductivity of the two-dimensional graphyne to be over predicted or lower predicted.

From the results shown in Fig. 38 and Fig. 39, we conclude that the two-dimensional non-defective graphyne has lower thermal conductivity than that of graphene, due to the presence of the triple bonds. We also conclude that the Airebo potential is better than the Tersoff potential in estimating the thermal conductivity dependence on the number of triple bonds.

5.4.2   Defect Effect on Thermal Conductivity

During the manufacturing process of the graphyne sheet, it is inevitable to have various kinds of defects. Understanding the correlation between the defects and graphyne's thermal conductivity is essential for the future utilization of defective graphyne. We introduce random defects by deleting singular atom on the single-layer graphyne. The defects positions are symmetric along the longitudinal axis of the ribbons.
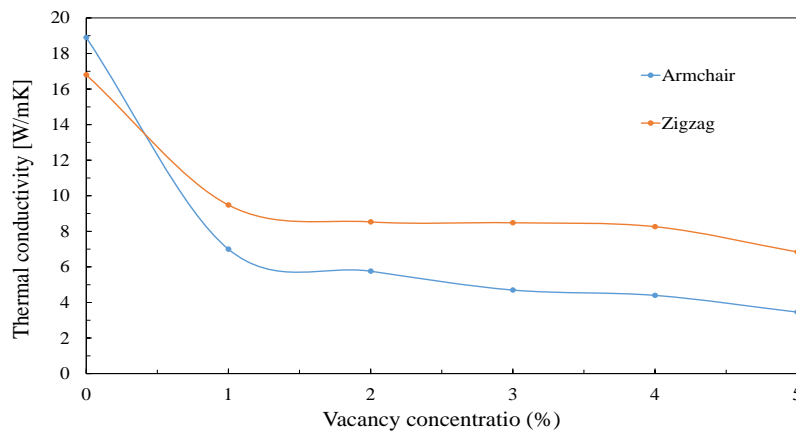
Figure 40: Thermal conductivity vs. defects (Airebo)

The thermal conductivity of the defective graphyne ribbons calculated with the Airebo potential are shown in Fig. 40. The results show that the thermal conductivity of graphyne depends on the percentage of defects. By increasing the percentage of defects the thermal conductivity of graphyne decrease. The curves shown in Fig. 40 indicate that at the same percentage of defects the armchair graphyne thermal conductivity is greater than that of the zigzag graphyne. The pristine graphyne thermal conductivity is 19 W/mK. Adding 1 % defects to the perfect graphyne, it's thermal conductivity is reduced by more than 50 %. Increasing the percentage of defects do

not cause a drastic drop in its thermal conductivity. From 1 % to 5 % in the percentage of defects area, the thermal conductivity of the armchair graphyne decreases from 9 W/mK to 7 W/mK. Similarly, the thermal conductivity of the armchair graphyne decreases from 7 W/mK to 3 W/mK.
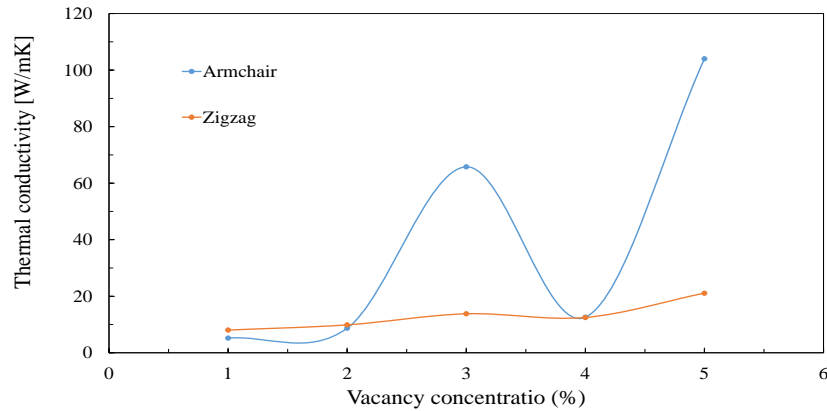
Figure 41: Thermal conductivity vs. defects (Tersoff)

The results shown in Fig. 41 is obtained using the Tersoff potential. The results are obviously odd compared to the results obtained using the Airebo potential. In Fig. 41, the thermal conductivity of 2 % 5 % defective graphyne increases with more defects. It implies that the Tersoff potential is not suitable for the calculation of defective graphyne's thermal conductivity behavior.

5.4.3   Length Effect on Thermal Conductivity

To further understand the intrinsic relationship between the graphyne structure and its thermal conductivity, we study the impact of the nanoribbons length on their thermal conductivity. We increase the length from 80 Å to 1250 Å and keep the width fixed as 30 Å.

Fig. 42 shows that the thermal conductivity of graphyne increases monolithically.

Since phonons are in charge of the heat transportation, the thermal conductivity of graphyne is dependent on the length might be related to the ballistic propagation of low frequency acoustic phonons [28]. Increasing the length of the graphyne nanoribbons induce more phonons to be excited, which increases the thermal conductivity. When the nanoribbons of graphyne are less than 500 Å, the thermal conductivity increases faster.
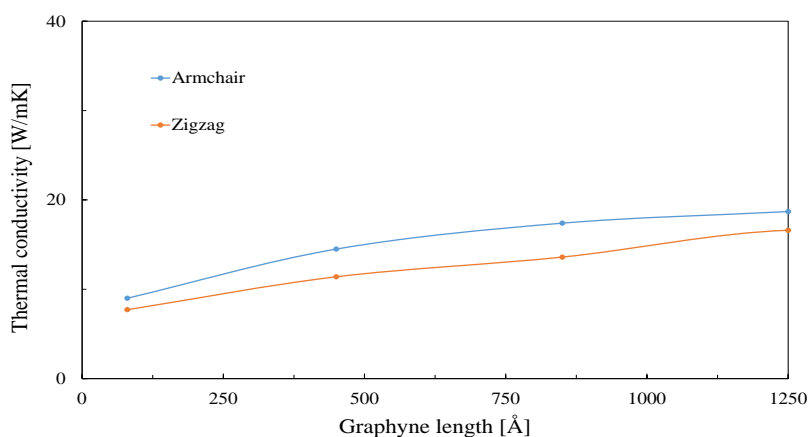
Figure 42: Thermal conductivity vs. length (Airebo)
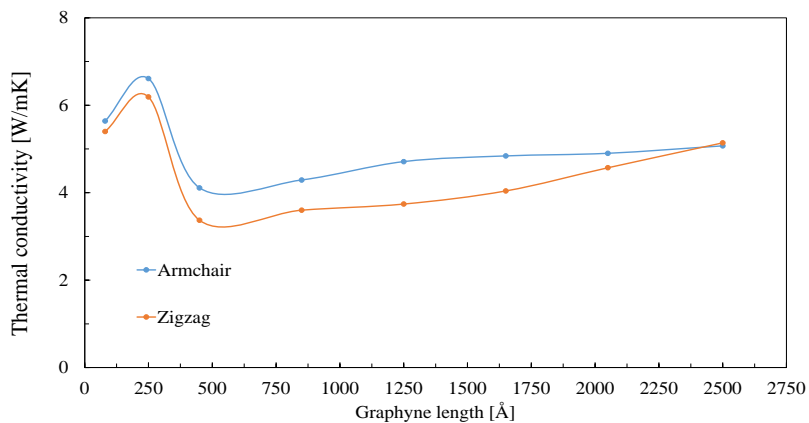
Figure 43: Thermal conductivity vs. length (Tersoff)

Fig. 43 shows the thermal conductivity of graphyne calculated using Tersoff po-

tential. The Tersoff potential predicts that by increasing the length of nanoribbons, graphyne's thermal conductivity is not likely to reduce. The results obtained here by the Tersoff potential are not consistent with the results obtained by the Airebo potential. The Tersoff potential only allows short range of second-nearest-neighbor interactions to be presented [105]. It may cause the thermal conductivity of the two-dimensional graphyne to be lower predicted.

5.4.4   Width Effect of Thermal Conductivity

Fig. 44 and Fig. 45 are the thermal conductivities obtained using the Airebo and the Tersoff potential for ribbons of various width.
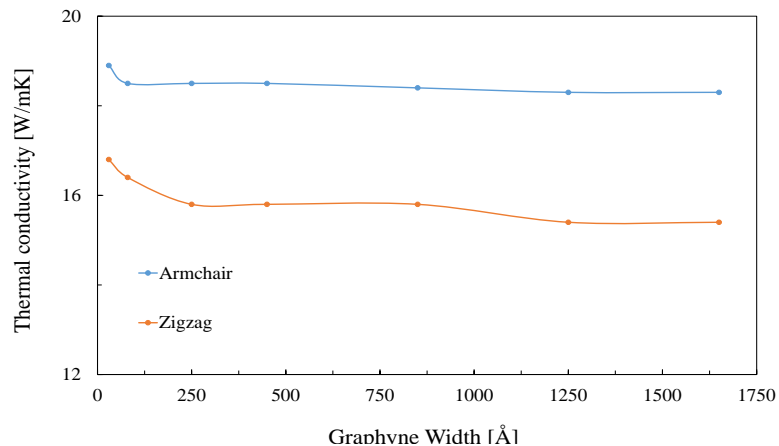
Figure 44: Thermal conductivity vs. width (Airebo)

Keeping the graphyne sheet's length fixed to be 250 Å and increasing the width, we observe in Fig. 44 that the thermal conductivity barely changes after the width reaches to 250 Å. It's concluded that the thermal conductivity of graphyne is not sensitive to the width change compared to the length change. Higher value of thermal conductivity at width smaller than 100 Å is due to the limited number of phonons which are excited in the system. Thus, phonon-phonon combinations, which are

used to satisfy the energy and momentum conservation rules for phonon scattering, are scarce. It prevents phonon-phonon scattering, which prevents the decrease in thermal conductivity [47, 214].
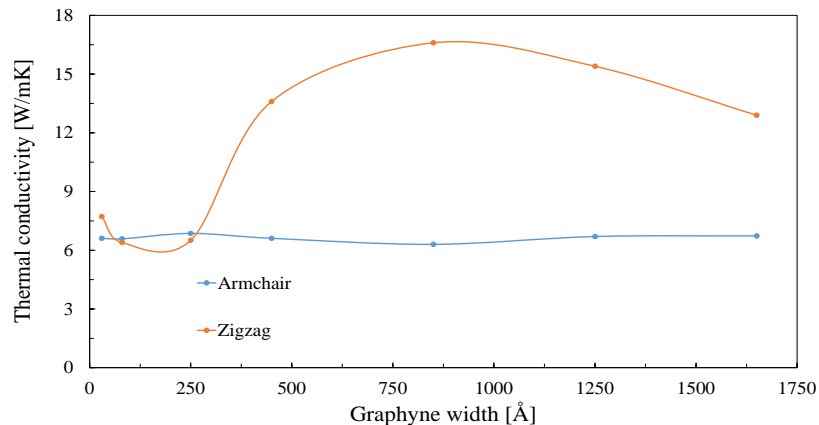
Figure 45: Thermal conductivity vs. width (Tersoff)

Fig. 45 shows the thermal conductivity of graphyne calculated by the Tersoff potential. By increasing the width of nanoribbons, graphyne's thermal conductivity is not likely to fluctuate randomly, as show in Fig. 45. The results obtained here by the Tersoff potential are odd compared to the results obtained by the Airebo potential, which may be caused by the Tersoff potential's limitations.

Conclusion

In this chapter, we have performed simulations to study the thermal conductivity of graphyne and its family of materials, such as gradiphyne, graphyne-3 and graphyne-4. All the calculations are performed using reverse nonequilibrium molecular dynamics (RNEMD) simulation.

Armchair gaphyne's thermal conductivity is greater than the one of the zigzag graphyne. It's apparent that both number of triple-bond and defects impact the

thermal conductivity. Yet graphyne's thermal conductivity dependent more on the defects. Nanoribbons width does not significantly impact the thermal conductivity of ribbons. Increase in the length of graphyne ribbons definitely increases its thermal conductivity.

Each potential (Airebo or Tersoff) has its own strengths and weakness. For the Airebo potential, the thermal conductivity are reasonable and converge with multiple simulations. It takes longer time compared to that using Tersoff potential. However, the results of thermal conductivity obtained by Airebo potential is reasonable while the results of Tersoff potential are not reliable.

CHAPTER 6: STUDY OF THERMAL CONDUCTIVITIES OF HYBRID
GRAPHENE BORON NITRIDE

In this chapter, a detailed description of analysis on the thermal conductivity of

hybrid graphene-boron nitride (HGBN) is presented. We review the current studies

of two-dimensional graphene and boron nitride. Then, we investigate the thermal

conductivity of hybrid graphene-broron nitride using molecular dynamics simulations.

6.1   Introduction

Graphene and boron nitride (BN) have attracted immense interests recently due

to their unique thermal properties. The two-dimensional graphene and boron nitride

have similar nanoribbons, shown in Fig. 46.

A graphene structure   Boron nitride structure
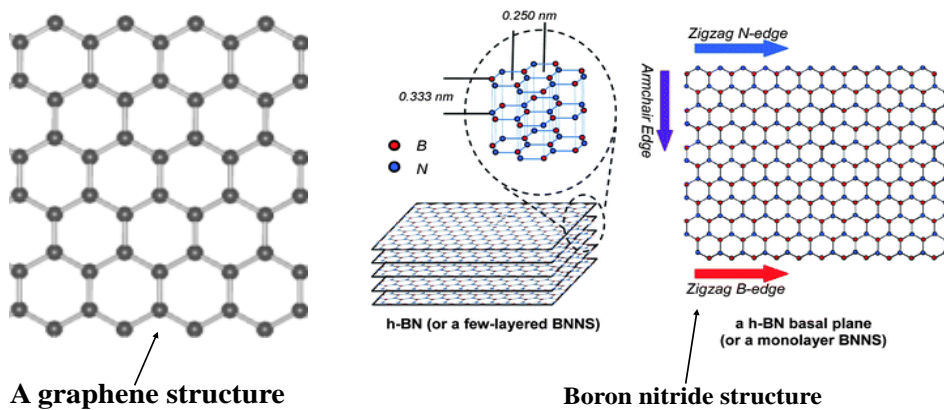
Figure 46: Two-dimensional graphene and boron nitride [104]

Graphene is a superior heat conductor with room temperature thermal conductivity

up to 5000 W/mK, making it an ideal candidate for thermal management applications

in nanoelectronic circuits, even in optoelectronic, photonics, and bioengineering [8, 56, 127, 155, 190].

Two-dimensional boron nitride has a similar atomic structure to that of graphene. Boron nitride has high thermal conductivity and high temperature resistance, which can be used as composite filler to tune the thermal conductivity as required [26, 74, 195, 213]. Boron nitride has smooth surface and light weight and can be used as a substrate of large-scale graphene in nanodevices [26,39,97,187,209]. Boron nitride has showed the unique potential to improve the devices' thermal performance by many researchers [74, 149, 186, 187, 209, 209, 213]. Boron nitride and its nanotubes can increase the thermal conductivity of composites such as BN reinforced polyehthylene and BN particle epoxy-matrix while keep the structural stability [186, 187, 209, 213]. Table 7 shows the previous study on the thermal conductivity of boron nitride. It summarizes the predicted thermal conductivity of boron nitride and also introduces the various methods applicable to the study of thermal conductivity of boron nitride.

Table 7: Summary of thermal conductivity of boron nitride

Material	thermal conductivity (W/mK)	Method
BN filled polybenzoxazine [74]	32.5	Experiment
BN composite [187]	11	Experiment

The thermal conductivity of graphene reduces by applying normal tensile strain, while under tensile strain the thermal conductivity of boron nitride increases [179]. Therefore, it is interesting to know how the thermal conductivity of hybrid graphene-boron nitride (HGBN) changes under the application of normal strain. HGBN is

formed by replacing blocks of the boron nitride sheets by graphene. Although tremendous researches have been used to investigated the thermal conductivity of graphene or boron nitride, there are few publications on the thermal conductivity of HGBN.

6.2   Background of Study Method Framework

We investigate the thermal conductivity of HGBN nanoribbons under uniaxial strain, using the reverse nonequilibrium molecular dynamics(RNEMD) using a Tersoff potential [42, 113, 121]. The MD simulations are conducted using LAMMPS package [139]. We study two types of HGBN nanoribbons : (i) the alternating HGBN and (ii) the laterally HGBN. The nanoribbons are shown in Fig. 47.
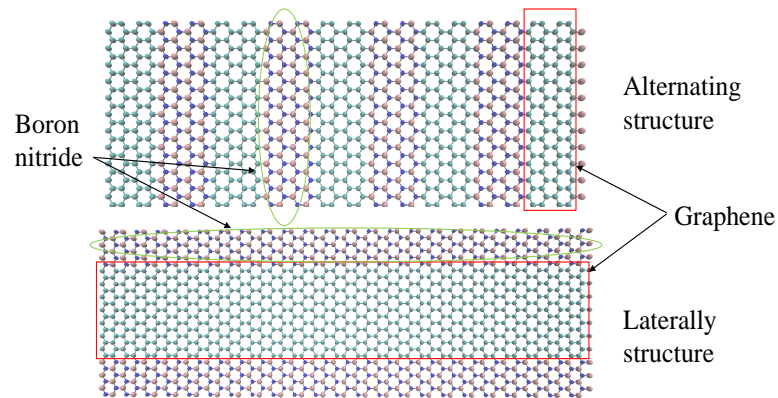
Figure 47: Hybrid graphene-boron nitride

The heat conductivity of the system is calculated using the same procedure as presented in chapter 5.
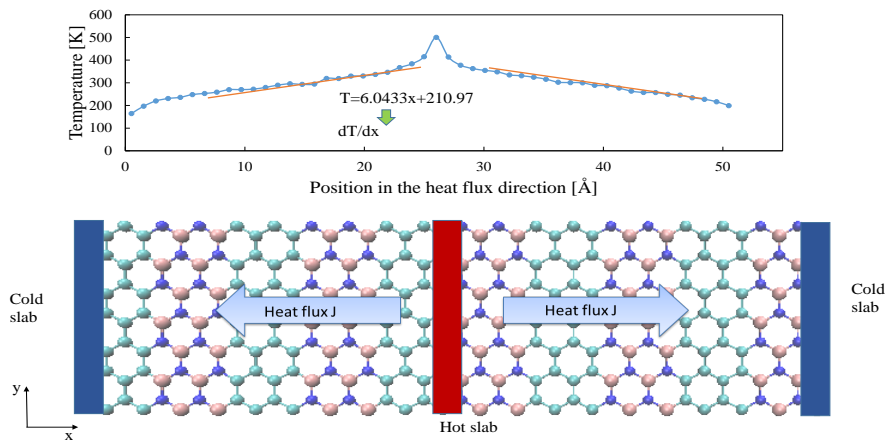
Figure 48: Hybrid graphene-boron nitride

6.3   Results and Discussion

6.3.1   Alternating HGBN

We first calculate the thermal conductivity of alternating HGBN of width of 50 Å
. The alternating HGBN nanoribbon is composed of m graphene unit cells adjacent
to n boron nitrid unit cells along x-direction. We use $m = n = 2, 3, 4$ in this study.
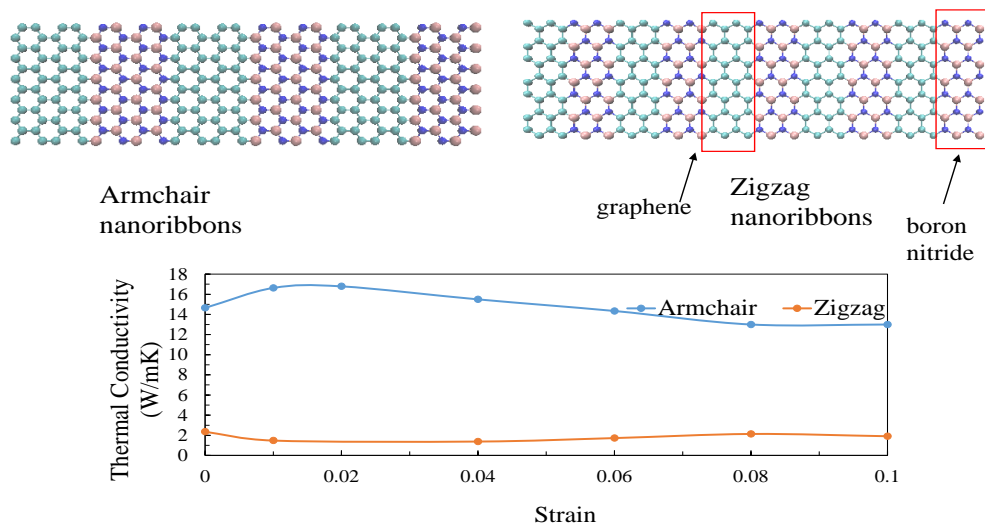
Figure 49: Thermal conductivity of alternating 2 by 2 HGBN

Strain does not dramatically affect the thermal conductivity of HGBN nanoribbons in the zigzag direction compared to its effect in the armchair direction. As shown in Fig. 49, the thermal conductivity of the zigzag HGBN remains almost the same with the increasing applied uniaxial strain in the x-direction.
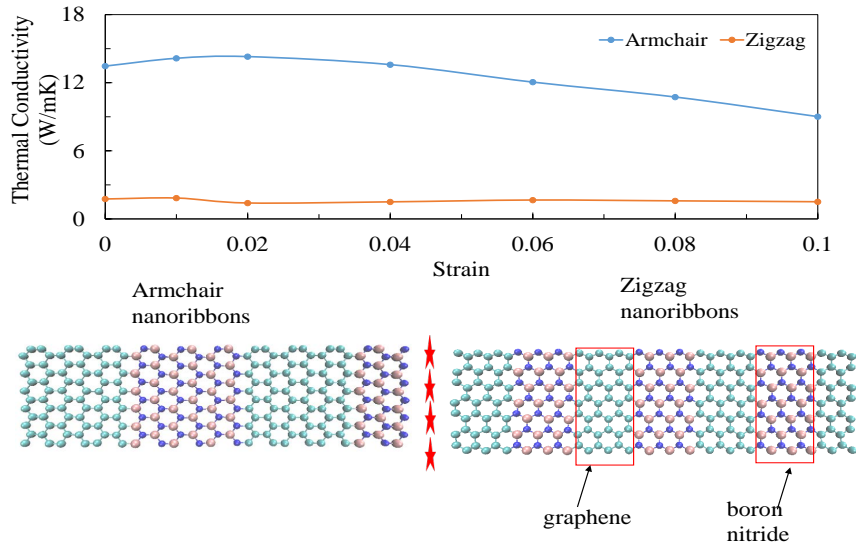
Figure 50: Thermal conductivity of alternating 3 by 3 HGBN

The curves in Fig. 50 shows that alternating armchair HGBN's thermal conductivity is sensitive to the applied strain compared to that of the zigzag nanoribbons. The thermal conductivity of HGBN is greater in the armchair direction compared to those in the armchair direction. By increasing the applied strain from 0 % to 10 % the thermal conductivity in the armchair direction decreases nonlinearly from 14.06 W/mK to 9.02 W/mK. Yet the thermal conductivity of zigzag HGBN maintains almost the same from 0 % to 10 % strain, which is 1.75 W/mK.
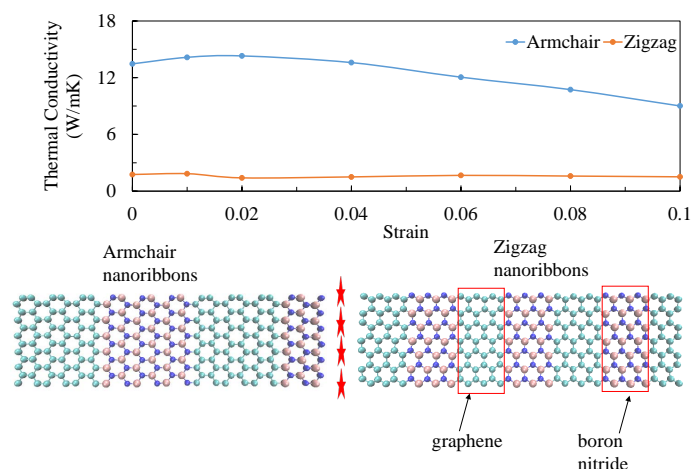
Figure 51: Thermal conductivity of alternating 4 by 4 HGBN

Fig. 51 shows the thermal conductivity of 4 by 4 alternating armchair and zigzag HGBN. The armchair HGBN's thermal conductivity increases by increasing the strain from 0 % to 1 %; however it begins to decreases after 1 %. The zigzag HGBN's thermal conductivity keeps constant with the applied strain.
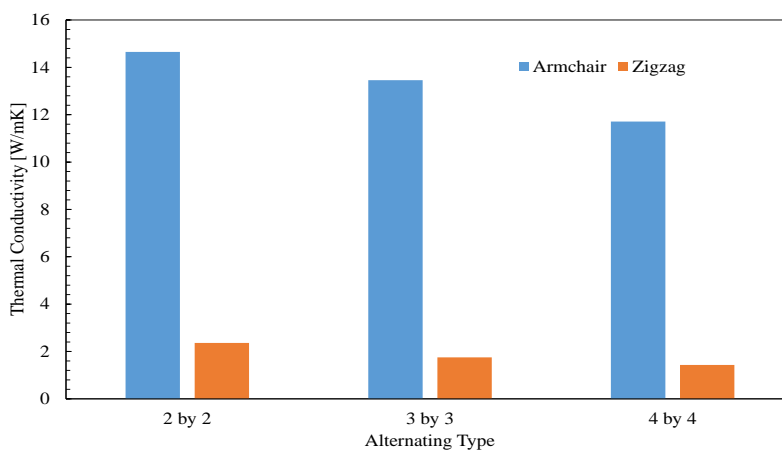
Figure 52: Thermal conductivity of alternating HGBN without strain

Moreover, Fig. 52 shows a summary of the thermal conductivities of all the alternating HGBN without strain. It indicate that the armchair nanoribbons have much

higher thermal conductivities than these of the zigzag nanoribbons. By increasing the number of unit cells in neighboring graphene and boron nitride blocks, the thermal conductivity are reduced.

6.3.2 Laterally HGBN

The plots in Fig. 53 show the laterally HGBN nanoribbons have a much higher thermal conductivity compared to the alternating ones. Both the armchair and zigzag HGBN maintain the same level of thermal conductivity with the variance of strain, which are 63 W/mK and 22 W/mK.
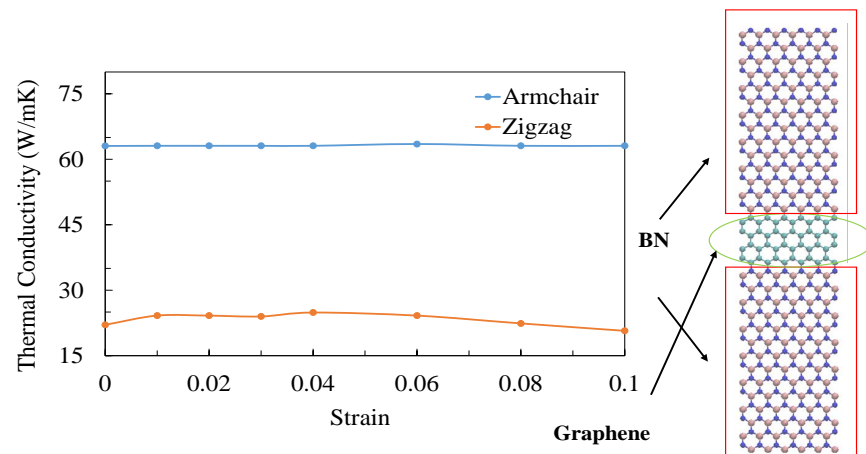
Figure 53: Thermal conductivity of laterally 7 by 3 HGBN

Obviously, the plots in Fig. 54 show the thermal conductivity of HGBN nanoribbons is higher compared to the results shown in Fig. 53. We find that increasing the number of unit cells of graphene between boron nitride can increase the thermal conductivity. Fig. 55 also demonstrates that thermal conductivity does not change a

lot by increasing the applied strain.
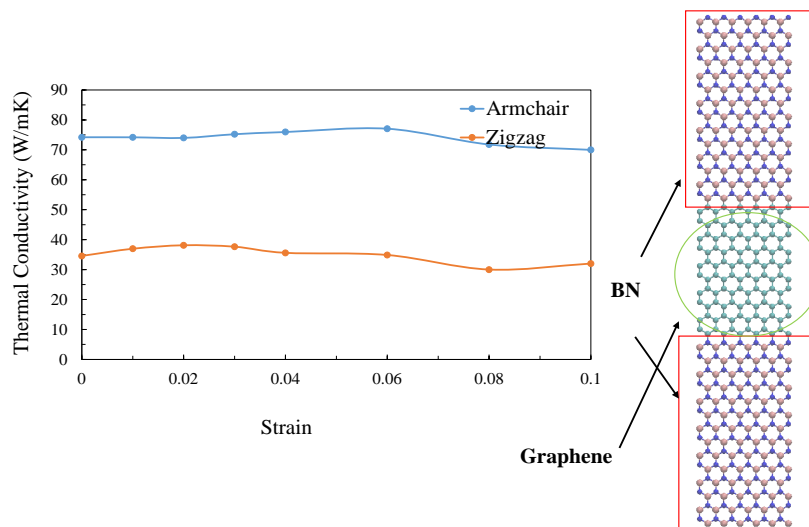
Figure 54: Thermal conductivity of laterally 7 by 5 HGBN
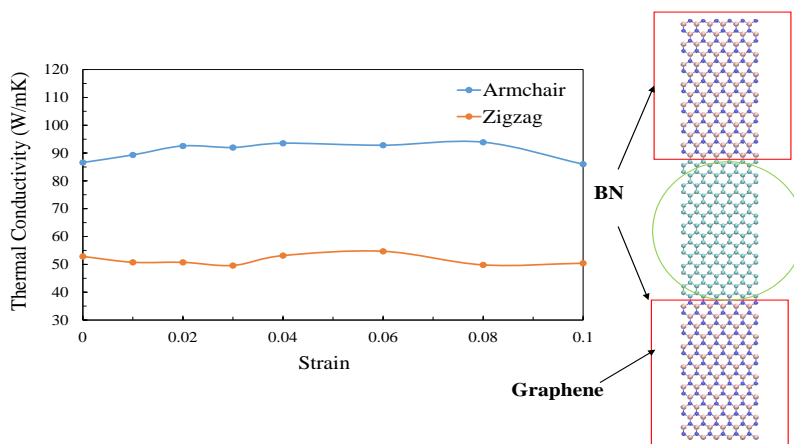
Figure 55: Thermal conductivity of laterally 7 by 7 HGBN

From the results shown in Fig. 53, Fig. 54 and Fig. 55, we conclude that the thermal

conductivity of two-dimensional non-defective HGBN does not change significantly

with increasing strain. This phenomenon happens in both of the armchair and zigzag conditions.
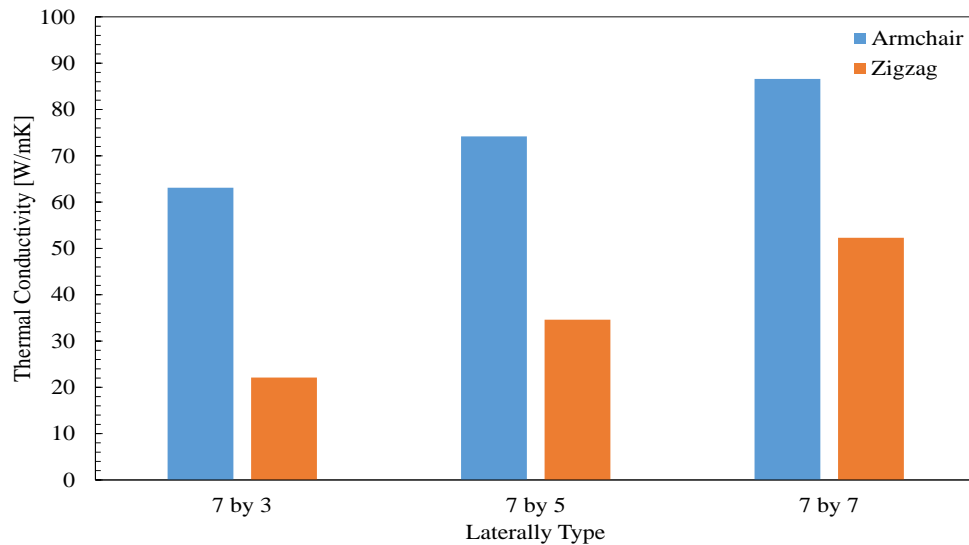
Figure 56: Thermal conductivity of laterally HGBN

Fig. 56 shows a summary of the thermal conductivity of all the alternating HGBN without strain. It indicate that the armchair nanoribbons have a significantly higher thermal conductivities than the zigzag nanoribbons. By increasing the number of unit cells of graphene between the boron nitride nanoribbons, the thermal conductivity increases.

In conclusion, for all the laterally HGBN, the armchair nanoribbons have greater thermal conductivity than the zigzag ribbons. The armchair HGBN's thermal conductivity is more than two times of the zigzag ones.

6.4   Conclusion

In this chapter, we performed extensive simulations to calculate the thermal conductivity of two-dimensional HGBN. All the calculations are performed using the

reverse nonequilibrium molecular dynamics (RNEMD) simulations using the Tersoff potential.

The alternating armchair HGBN's thermal conductivity is greater than that of the zigzag nanoribbon. We found that the alternating HGBN's average thermal conductivity decreases by increasing the number of boron nitride and graphene unit cells.

The laterally armchair HGBN's thermal conductivity is higher than that of the zigzag nanoribbon. The laterally HGBN's average thermal conductivity increases with increasing the number of graphene unit cells between the boron nitride nanoribbons. In another word, increase in the width of HGBN nanoribbons definitely increases the thermal conductivity.

The thermal conductivity of both alternating and laterally HGBN nanoribbons do not change significantly with the applied strain. This can be helpful in developing electronics with constant thermal conductivity under deformation.

CHAPTER 7: CONCLUSION

Computational methodologies, including density functional theory and molecular dynamics, are used to investigate the mechanical and thermal properties of two-dimensional MoO_3, graphyne and its family materials, and hybrid graphene-boron nitride. Mechanical properties of two-dimensional MoO_3 are studied using density functional theory. The energy density-strain and stress-strain correlations of two-dimensional MoO_3 are obtained. In this dissertation, first a constitutive model is developed to model the mechanical behavior of two-dimensional MoO_3. Through the molecular dynamics simulations, the mechanical and thermal properties of graphyne and its family materials, and hybrid graphene-boron nitride are obtained. Based on the computational modeling results, additional analysis were performed to study the key parameters affecting the mechanical and thermal behavior of two-dimensional materials.

7.1   Two-dimensional MoO_3

The study of mechanical properties of two-dimensional MoO_3 shows that MoO_3 is an anisotropic material. MoO_3 is isotropic before 1 % strain with a Young's modulus of 95 GPa. MoO_3 exhibits an anisotropic behavior under large strains. Two-dimensional MoO_3 has higher strength in the x-direction compared to that in the y-direction.

The proposed elastic constitutive model matches well with the DFT results, which pave a reliable and efficient way of investigating the mechanical behavior of two-dimensional MoO_3.

7.2   Graphyne and its Family Materials

The study of mechanical and thermal properties of graphyne and its family of materials, such as gradiphyne, graphyne-3 and graphyne-4, shows that graphyne has high mechanical strength and thermal conductivity. Both mechanical and thermal properties of graphyne and its family materials depend on the nanoribbon size (width and length), edge chirality, defects and number of triple carbon-carbon bonds.

Defects, length and triple carbon-carbon bonds are the predominant factors, affecting the mechanical and thermal properties of graphyne and its family materials. The applied strain changes the thermal conductivity of graphyne and its family of materials, which paves the area of tunable microelectronic applications. The various properties of graphyne and its family of materials make it is possible to design tunable microelectronic devices, which require certain mechanical and thermal properties.

7.3   Hybrid Graphene-Boron Nitride

The thermal conductivity of hybrid graphene-boron nitride (HGBN) nanoribbons depends on ribbons structure and the applied strain. We found that the thermal conductivity of armchair HGBN is greater than the thermal conductivity of zigzag nanoribbons. It's apparent that the average thermal conductivity of alternating HGBN decreases if the number of boron nitride unit cells increases. However, the average thermal conductivity of lateral HGBN increases if the number of graphene

unit cells confined between the boron nitride nanoribbons increases.

REFERENCES

[1] A. R. Abramson, C.-L. Tien, and A. Majumdar. Interface and strain effects on the thermal conductivity of heterostructures: A molecular dynamics study. *Journal of Heat Transfer*, 124(5):963–970, 2002.

[2] S. Ajori, R. Ansari, and M. Mirnezhad. Mechanical properties of defective γ-graphyne using molecular dynamics simulations. *Materials Science and Engineering: A*, 561:34–39, 2013.

[3] M. Alaghemandi, E. Algaer, M. C. Böhm, and F. Müller-Plathe. The thermal conductivity and thermal rectification of carbon nanotubes studied using reverse non-equilibrium molecular dynamics simulations. *Nanotechnology*, 20(11):115704, 2009.

[4] S. Arya and A. D'amico. Preparation, properties and applications of boron nitride thin films. *Thin Solid Films*, 157(2):267–282, 1988.

[5] P. Avouris and C. Dimitrakopoulos. Graphene: synthesis and applications. *Materials today*, 15(3):86–97, 2012.

[6] S. Bae, H. Kim, Y. Lee, X. Xu, J.-S. Park, Y. Zheng, J. Balakrishnan, T. Lei, H. R. Kim, Y. I. Song, et al. Roll-to-roll production of 30-inch graphene films for transparent electrodes. *Nature nanotechnology*, 5(8):574–578, 2010.

[7] A. A. Balandin. Thermal properties of graphene and nanostructured carbon materials. *Nature materials*, 10(8):569–581, 2011.

[8] A. A. Balandin, S. Ghosh, W. Bao, I. Calizo, D. Teweldebrhan, F. Miao, and C. N. Lau. Superior thermal conductivity of single-layer graphene. *Nano letters*, 8(3):902–907, 2008.

[9] S. Balendhran, J. Deng, J. Z. Ou, S. Walia, J. Scott, J. Tang, K. L. Wang, M. R. Field, S. Russo, S. Zhuiykov, et al. Enhanced charge carrier mobility in two-dimensional high dielectric molybdenum oxide. *Advanced Materials*, 25(1):109–114, 2013.

[10] S. Balendhran, S. Walia, M. Alsaif, E. P. Nguyen, J. Z. Ou, S. Zhuiykov, S. Sriram, M. Bhaskaran, and K. Kalantar-zadeh. Field effect biosensing platform based on 2d α-moo3. *ACS nano*, 7(11):9753–9760, 2013.

[11] S. Balendhran, S. Walia, H. Nili, J. Z. Ou, S. Zhuiykov, R. B. Kaner, S. Sriram, M. Bhaskaran, and K. Kalantar-zadeh. Two-dimensional molybdenum trioxide and dichalcogenides. *Advanced Functional Materials*, 23(32):3952–3970, 2013.

[12] G. Basile, C. Bernardin, and S. Olla. Momentum conserving model with anomalous thermal conductivity in low dimensional systems. *Physical review letters*, 96(20):204303, 2006.

[13] G. E. Bauer. General operator ground-state expectation values in the hohenberg-kohn-sham density-functional formalism. *Physical Review B*, 27(10):5912, 1983.

[14] S. Berber, Y.-K. Kwon, and D. Tomanek. Unusually high thermal conductivity of carbon nanotubes. *Physical review letters*, 84(20):4613, 2000.

[15] C. M. Bhandari. *Thermal conduction in semiconductors*. John Wiley & Sons, 1988.

[16] S. Bhowmick and V. B. Shenoy. Effect of strain on the thermal conductivity of solids. *The Journal of chemical physics*, 125(16):164513, 2006.

[17] R. Bizao, T. Botari, and D. Galvao. Mechanical properties of graphene nanowiggles. In *MRS Proceedings*, volume 1658, pages mrsf13–1658. Cambridge Univ Press, 2014.

[18] D. W. Brenner, O. A. Shenderova, J. A. Harrison, S. J. Stuart, B. Ni, and S. B. Sinnott. A second-generation reactive empirical bond order (rebo) potential energy expression for hydrocarbons. *Journal of Physics: Condensed Matter*, 14(4):783, 2002.

[19] T. Brezesinski, J. Wang, S. H. Tolbert, and B. Dunn. Ordered mesoporous [alpha]-moo3 with iso-oriented nanocrystalline walls for thin-film pseudocapacitors. *Nature materials*, 9(2):146–151, 2010.

[20] M. J. Buehler, A. C. van Duin, and W. A. Goddard III. Multiparadigm modeling of dynamical crack propagation in silicon using a reactive force field. *Physical review letters*, 96(9):095505, 2006.

[21] K. Burke. Perspective on density functional theory. *The Journal of chemical physics*, 136(15):150901, 2012.

[22] D. G. Cahill. Thermal conductivity measurement from 30 to 750 k: the 3ω method. *Review of Scientific Instruments*, 61(2):802–808, 1990.

[23] X. Cao, Y. Li, X. Cheng, and Y. Zhang. Structural analogues of graphyne family: New types of boron nitride sheets with wide band gap and strong uv absorption. *Chemical Physics Letters*, 502(4):217–221, 2011.

[24] R. Car and M. Parrinello. Unified approach for molecular dynamics and density-functional theory. *Physical review letters*, 55(22):2471, 1985.

[25] E. V. Castro, K. Novoselov, S. Morozov, N. Peres, J. L. Dos Santos, J. Nilsson, F. Guinea, A. Geim, and A. C. Neto. Biased bilayer graphene: semiconductor with a gap tunable by the electric field effect. *Physical Review Letters*, 99(21):216802, 2007.

[26] C. Chang, A. Fennimore, A. Afanasiev, D. Okawa, T. Ikuno, H. Garcia, D. Li, A. Majumdar, and A. Zettl. Isotope effect on the thermal conductivity of boron nitride nanotubes. *Physical review letters*, 97(8):085901, 2006.

[27] J. Che, T. Cagin, and W. A. Goddard III. Thermal conductivity of carbon nanotubes. *Nanotechnology*, 11(2):65, 2000.

[28] G. Chen. Thermal conductivity and ballistic-phonon transport in the cross-plane direction of superlattices. *Physical Review B*, 57(23):14958, 1998.

[29] J. Chen, J. Xi, D. Wang, and Z. Shuai. Carrier mobility in graphyne should be even larger than that in graphene: A theoretical prediction. *The Journal of Physical Chemistry Letters*, 4(9):1443–1448, 2013.

[30] K. Chen, S. Xie, A. T. Bell, and E. Iglesia. Structure and properties of oxidative dehydrogenation catalysts based on moo 3/al 2 o 3. *Journal of Catalysis*, 198(2):232–242, 2001.

[31] Y. Chen, D. Li, J. R. Lukes, Z. Ni, and M. Chen. Minimum superlattice thermal conductivity from molecular dynamics. *Physical Review B*, 72(17):174302, 2005.

[32] Z. Chen, Y.-M. Lin, M. J. Rooks, and P. Avouris. Graphene nano-ribbon electronics. *Physica E: Low-dimensional Systems and Nanostructures*, 40(2):228–232, 2007.

[33] K. Chenoweth, S. Cheung, A. C. Van Duin, W. A. Goddard, and E. M. Kober. Simulations on the thermal decomposition of a poly (dimethylsiloxane) polymer using the reaxff reactive force field. *Journal Of The American Chemical Society*, 127(19):7192–7202, 2005.

[34] K. Chenoweth, A. C. van Duin, and W. A. Goddard. Reaxff reactive force field for molecular dynamics simulations of hydrocarbon oxidation. *The Journal of Physical Chemistry A*, 112(5):1040–1053, 2008.

[35] S. Cheung, W.-Q. Deng, A. C. van Duin, and W. A. Goddard. Reaxffmgh reactive force field for magnesium hydride systems. *The Journal of Physical Chemistry A*, 109(5):851–859, 2005.

[36] A. J. Cohen, P. Mori-Sánchez, and W. Yang. Insights into current limitations of density functional theory. *Science*, 321(5890):792–794, 2008.

[37] R. Cooper, C. Lee, C. Marianetti, X. Wei, J. Hone, and J. Kysar. Nonlinear elastic behavior of two-dimensional molybdenum disulfide. *Physical Review B*, 87:035423, 2013.

[38] S. W. Cranford and M. J. Buehler. Mechanical properties of graphyne. *Carbon*, 49(13):4111–4121, 2011.

[39] C. Dean, A. Young, I. Meric, C. Lee, L. Wang, S. Sorgenfrei, K. Watanabe, T. Taniguchi, P. Kim, K. Shepard, et al. Boron nitride substrates for high-quality graphene electronics. *Nature nanotechnology*, 5(10):722–726, 2010.

[40] P. A. Denis and F. Iribarne. Comparative study of defect reactivity in graphene. *The Journal of Physical Chemistry C*, 117(37):19048–19055, 2013.

[41] F. Diederich and Y. Rubin. Synthetic approaches toward molecular and polymeric carbon allotropes. *Angewandte Chemie International Edition in English*, 31(9):1101–1123, 1992.

[42] B. W. Dodson. Development of a many-body tersoff-type potential for silicon. *Physical Review B*, 35(6):2795, 1987.

[43] X. Dong, X. Dong, J.-H. Liu, J. Yan, J. Wang, and G. Hong. Study of preparation and photochromism of moo3 nanoparticles hydrosol. *Rare Metal Materials and Engineering*, 34(3):421–424, 2005.

[44] R. M. Dreizler and E. Engel. *Density functional theory*. 2011.

[45] J. Eichler and C. Lesniak. Boron nitride (bn) and bn composites for high-temperature applications. *Journal of the European Ceramic Society*, 28(5):1105–1109, 2008.

[46] T. Enoki, S. Fujii, and K. Takai. Zigzag and armchair edges in graphene. *Carbon*, 50(9):3141–3145, 2012.

[47] W. J. Evans, L. Hu, and P. Keblinski. Thermal conductivity of graphene ribbons from equilibrium molecular dynamics: Effect of ribbon width, edge roughness, and hydrogen termination. *Applied Physics Letters*, 96(20):203112, 2010.

[48] M. Fang, K. Wang, H. Lu, Y. Yang, and S. Nutt. Covalent polymer functionalization of graphene nanosheets and mechanical properties of composites. *Journal of Materials Chemistry*, 19(38):7098–7105, 2009.

[49] C. Faugeras, B. Faugeras, M. Orlita, M. Potemski, R. R. Nair, and A. Geim. Thermal conductivity of graphene in corbino membrane geometry. *ACS nano*, 4(4):1889–1892, 2010.

[50] T. Fleisch and G. Mains. An xps study of the uv reduction and photochromism of moo3 and wo3. *The Journal of Chemical Physics*, 76(2):780–786, 1982.

[51] I. Frank, D. M. Tanenbaum, A. Van der Zande, and P. L. McEuen. Mechanical properties of suspended graphene sheets. *Journal of Vacuum Science & Technology B*, 25(6):2558–2561, 2007.

[52] O. Frank, M. Mohr, J. Maultzsch, C. Thomsen, I. Riaz, R. Jalil, K. S. Novoselov, G. Tsoukleri, J. Parthenios, K. Papagelis, et al. Raman 2d-band splitting in graphene: theory and experiment. *Acs Nano*, 5(3):2231–2239, 2011.

[53] S. Furukawa, H. Uji-i, K. Tahara, T. Ichikawa, M. Sonoda, F. C. De Schryver, Y. Tobe, and S. De Feyter. Molecular geometry directed kagome and honeycomb networks: toward two-dimensional crystal engineering. *Journal of the American Chemical Society*, 128(11):3502–3503, 2006.

[54] K. Galatsis, Y. Li, W. Wlodarski, E. Comini, G. Faglia, and G. Sberveglieri. Semiconductor moo 3–tio 2 thin film gas sensors. *Sensors and Actuators B: Chemical*, 77(1):472–477, 2001.

[55] S. Ghosh, W. Bao, D. L. Nika, S. Subrina, E. P. Pokatilov, C. N. Lau, and A. A. Balandin. Dimensional crossover of thermal transport in few-layer graphene. *Nature materials*, 9(7):555–558, 2010.

[56] S. Ghosh, I. Calizo, D. Teweldebrhan, E. Pokatilov, D. Nika, A. Balandin, W. Bao, F. Miao, and C. Lau. Extremely high thermal conductivity of graphene: Prospects for thermal management applications in nanoelectronic circuits. *Applied Physics Letters*, 92(15):151911, 2008.

[57] C. Gómez-Navarro, M. Burghard, and K. Kern. Elastic properties of chemically derived single graphene sheets. *Nano letters*, 8(7):2045–2049, 2008.

[58] S. Goverapet Srinivasan and A. C. van Duin. Molecular-dynamics-based study of the collisions of hyperthermal atomic oxygen with graphene using the reaxff reactive force field. *The Journal of Physical Chemistry A*, 115(46):13269–13280, 2011.

[59] M. S. Green. Markoff random processes and the statistical mechanics of time?dependent phenomena. ii. irreversible processes in fluids. *The Journal of Chemical Physics*, 22(3), 1954.

[60] Y. Guo, K. Jiang, B. Xu, Y. Xia, J. Yin, and Z. Liu. Remarkable hydrogen storage capacity in li-decorated graphyne: theoretical predication. *The Journal of Physical Chemistry C*, 116(26):13837–13841, 2012.

[61] Z. Guo, D. Zhang, and X.-G. Gong. Thermal conductivity of graphene nanoribbons. *Applied physics letters*, 95(16):163103, 2009.

[62] F. Hao, D. Fang, and Z. Xu. Mechanical and thermal transport properties of graphene with defects. *Applied physics letters*, 99(4):041901, 2011.

[63] M. K. Harbola and V. Sahni. Quantum-mechanical interpretation of the exchange-correlation potential of kohn-sham density-functional theory. *Physical review letters*, 62(5):489, 1989.

[64] Y. Hernandez, V. Nicolosi, M. Lotya, F. M. Blighe, Z. Sun, S. De, I. McGovern, B. Holland, M. Byrne, Y. K. Gun'Ko, et al. High-yield production of graphene by liquid-phase exfoliation of graphite. *Nature nanotechnology*, 3(9):563–568, 2008.

[65] J. Hicks, M. Sprinkle, K. Shepperd, F. Wang, A. Tejeda, A. Taleb-Ibrahimi, F. Bertran, P. Le Fèvre, W. De Heer, C. Berger, et al. Symmetry breaking in commensurate graphene rotational stacking: Comparison of theory and experiment. *Physical Review B*, 83(20):205403, 2011.

[66] A. Hirsch. The era of carbon allotropes. *Nature materials*, 9(11):868–871, 2010.

[67] P. Hohenberg and W. Kohn. Inhomogeneous Electron Gas. *Physical Review*, 136:864–871, Nov. 1964.

[68] J. Hone, M. Whitney, C. Piskoti, and A. Zettl. Thermal conductivity of single-walled carbon nanotubes. *Physical Review B*, 59(4):R2514, 1999.

[69] J. Hu, X. Ruan, and Y. P. Chen. Thermal conductivity and thermal rectification in graphene nanoribbons: a molecular dynamics study. *Nano letters*, 9(7):2730–2735, 2009.

[70] J. Hu, S. Schiffli, A. Vallabhaneni, X. Ruan, and Y. P. Chen. Tuning the thermal conductivity of graphene nanoribbons by edge passivation and isotope engineering: A molecular dynamics study. *Applied Physics Letters*, 97(13):133107, 2010.

[71] M. Hu, X. Zhang, and D. Poulikakos. Anomalous thermal response of silicene to uniaxial stretching. *Physical Review B*, 87(19):195417, 2013.

[72] S. Hu and X. Wang. Single-walled moo3 nanotubes. *Journal of the American Chemical Society*, 130(26):8126–8127, 2008.

[73] T. Ikeshoji and B. Hafskjold. Non-equilibrium molecular dynamics calculation of heat conduction in liquid and through liquid-gas interface. *Molecular Physics*, 81(2):251–261, 1994.

[74] H. Ishida and S. Rimdusit. Very high thermal conductivity obtained by boron nitride-filled polybenzoxazine. *Thermochimica Acta*, 320(1):177–186, 1998.

[75] T. Ivanova, K. Gesheva, and A. Szekeres. Structure and optical properties of cvd molybdenum oxide films for electrochromic application. *Journal of Solid State Electrochemistry*, 7(1):21–24, 2002.

[76] W. Jang, Z. Chen, W. Bao, C. N. Lau, and C. Dames. Thickness-dependent thermal conductivity of encased graphene and ultrathin graphite. *Nano letters*, 10(10):3909–3913, 2010.

[77] T. Järvi, A. Kuronen, M. Hakala, K. Nordlund, A. Van Duin, W. Goddard, and T. Jacob. Development of a reaxff description for gold. *The European Physical Journal B-Condensed Matter and Complex Systems*, 66(1):75–79, 2008.

[78] J.-W. Jiang, J.-S. Wang, and B. Li. Young?s modulus of graphene: a molecular dynamics study. *Physical Review B*, 80(11):113405, 2009.

[79] J. Kang, J. Li, F. Wu, S.-S. Li, and J.-B. Xia. Elastic, electronic, and optical properties of two-dimensional graphyne sheet. *The Journal of Physical Chemistry C*, 115(42):20466–20470, 2011.

[80] M. I. Katsnelson. Graphene: carbon in two dimensions. *Materials today*, 10(1):20–27, 2007.

[81] J. M. Kehoe, J. H. Kiley, J. J. English, C. A. Johnson, R. C. Petersen, and M. M. Haley. Carbon networks based on dehydrobenzoannulenes. 3. synthesis of graphyne substructures1. *Organic Letters*, 2(7):969–972, 2000. PMID: 10768199.

[82] S. Kemaloglu, G. Ozkoc, and A. Aytac. Properties of thermally conductive micro and nano size boron nitride reinforced silicon rubber composites. *Thermochimica Acta*, 499(1):40–47, 2010.

[83] U. Khalilov, G. Pourtois, A. v. Duin, and E. Neyts. Self-limiting oxidation in small-diameter si nanowires. *Chemistry of Materials*, 24(11):2141–2147, 2012.

[84] R. Khare, S. L. Mielke, J. T. Paci, S. Zhang, R. Ballarini, G. C. Schatz, and T. Belytschko. Coupled quantum mechanical/molecular mechanical modeling of the fracture of defective carbon nanotubes and graphene sheets. *Physical Review B*, 75(7):075412, 2007.

[85] B. G. Kim and H. J. Choi. Graphyne: Hexagonal network of carbon with versatile dirac cones. *Physical Review B*, 86(11):115435, 2012.

[86] K. S. Kim, Y. Zhao, H. Jang, S. Y. Lee, J. M. Kim, K. S. Kim, J.-H. Ahn, P. Kim, J.-Y. Choi, and B. H. Hong. Large-scale pattern growth of graphene films for stretchable transparent electrodes. *Nature*, 457(7230):706–710, 2009.

[87] C. Kittel, P. McEuen, and P. McEuen. *Introduction to solid state physics*, volume 8. Wiley New York, 1976.

[88] P. Klemens. Theory of the a-plane thermal conductivity of graphite. *Journal of Wide Bandgap Materials*, 7(4):332–339, 2000.

[89] P. Klemens. Theory of thermal conduction in thin ceramic films. *International journal of thermophysics*, 22(1):265–275, 2001.

[90] P. Klemens, F. Seitz, and D. Turnbull. Solid state physics, vol. *F. Seitz and D. Turnbull (New York: Academic)*, 1958.

[91] W. Kohn. Nobel lecture: Electronic structure of matter-wave functions and density functionals. *Reviews of Modern Physics*, 71(5):1253–1266, 1999.

[92] R. Kubo. Statistical-mechanical theory of irreversible processes. i. general theory and simple applications to magnetic and conduction problems. *Journal of the Physical Society of Japan*, 12(6):570–586, 1957.

[93] Y. Kubota, K. Watanabe, O. Tsuda, and T. Taniguchi. Deep ultraviolet light-emitting hexagonal boron nitride synthesized at atmospheric pressure. *Science*, 317(5840):932–934, 2007.

[94] Y.-K. Kwon, S. Berber, and D. Tománek. Thermal contraction of carbon fullerenes and nanotubes. *Physical review letters*, 92(1):015901, 2004.

[95] C. Lee, X. Wei, J. W. Kysar, and J. Hone. Measurement of the elastic properties and intrinsic strength of monolayer graphene. *science*, 321(5887):385–388, 2008.

[96] J.-U. Lee, D. Yoon, and H. Cheong. Estimation of young?s modulus of graphene by raman spectroscopy. *Nano letters*, 12(9):4444–4448, 2012.

[97] K. H. Lee, H.-J. Shin, J. Lee, I.-y. Lee, G.-H. Kim, J.-Y. Choi, and S.-W. Kim. Large-scale synthesis of high-quality hexagonal boron nitride nanosheets for large-area graphene electronics. *Nano letters*, 12(2):714–718, 2012.

[98] D. Li, M. B. Mueller, S. Gilje, R. B. Kaner, and G. G. Wallace. Processable aqueous dispersions of graphene nanosheets. *Nature nanotechnology*, 3(2):101–105, 2008.

[99] X. Li, W. Cai, J. An, S. Kim, J. Nah, D. Yang, R. Piner, A. Velamakanni, I. Jung, E. Tutuc, et al. Large-area synthesis of high-quality and uniform graphene films on copper foils. *Science*, 324(5932):1312–1314, 2009.

[100] X. Li, J. Chen, C. Yu, and G. Zhang. Comparison of isotope effects on thermal conductivity of graphene nanoribbons and carbon nanotubes. *Applied Physics Letters*, 103(1):013111, 2013.

[101] X. Li, K. Maute, M. L. Dunn, and R. Yang. Strain effects on the thermal conductivity of nanostructures. *Physical Review B*, 81(24):245318, 2010.

[102] Y. Li, L. Xu, H. Liu, and Y. Li. Graphdiyne and graphyne: from theoretical predictions to practical construction. 43:2572–2586, 2014.

[103] J. H. Lienhard. *A heat transfer textbook*. Courier Corporation, 2013.

[104] Y. Lin and J. W. Connell. Advances in 2d boron nitride nanostructures: nanosheets, nanoribbons, nanomeshes, and hybrids with graphene. *Nanoscale*, 4(22):6908–6939, 2012.

[105] L. Lindsay and D. Broido. Optimized tersoff and brenner empirical potential parameters for lattice dynamics and phonon thermal transport in carbon nanotubes and graphene. *Physical Review B*, 81(20):205441, 2010.

[106] Z. Liu, G. Yu, H. Yao, L. Liu, L. Jiang, and Y. Zheng. A simple tight-binding model for typical graphyne structures. *New Journal of Physics*, 14(11):113007, 2012.

[107] X. W. Lou and H. C. Zeng. Complex α-moo3 nanostructures with external bonding capacity for self-assembly. *Journal of the American Chemical Society*, 125(9):2697–2704, 2003.

[108] J. R. Lukes and H. Zhong. Thermal conductivity of individual single-wall carbon nanotubes. *Journal of Heat Transfer*, 129(6):705–716, 2007.

[109] T. Luo and J. R. Lloyd. Equilibrium molecular dynamics study of lattice thermal conductivity/conductance of au-sam-au junctions. *Journal of Heat Transfer*, 132(3):032401, 2010.

[110] T. Luo and J. R. Lloyd. Enhancement of thermal energy transport across graphene/graphite and polymer interfaces: a molecular dynamics study. *Advanced Functional Materials*, 22(12):2495–2502, 2012.

[111] K. F. Mak, C. H. Lui, J. Shan, and T. F. Heinz. Observation of an electric-field-induced band gap in bilayer graphene by infrared spectroscopy. *Physical review letters*, 102(25):256405, 2009.

[112] D. Malko, C. Neiss, F. Viñes, and A. Görling. Competition for graphene: Graphynes with direction-dependent dirac cones. *Physical review letters*, 108(8):086804, 2012.

[113] K. Matsunaga, C. Fisher, and H. Matsubara. Tersoff potential parameters for simulating cubic boron carbonitrides. *Japanese Journal of Applied Physics*, 39(1A):L48, 2000.

[114] E. McCarron and J. Calabrese. The growth and single crystal structure of a high pressure phase of molybdenum trioxide: Moo 3-ii. *Journal of solid state chemistry*, 91(1):121–125, 1991.

[115] J. Meyer, A. Shu, M. Kroger, and A. Kahn. Effect of contamination on the electronic structure and hole-injection properties of moo 3/organic semiconductor interfaces. *Applied Physics Letters*, 96(13):133308–133308, 2010.

[116] W. H. Moon and H. J. Hwang. Molecular-dynamics simulation of structure and thermal behaviour of boron nitride nanotubes. *Nanotechnology*, 15(5):431, 2004.

[117] J. E. Mueller, A. C. van Duin, and W. A. Goddard III. Development and validation of reaxff reactive force field for hydrocarbon chemistry catalyzed by nickel. *The Journal of Physical Chemistry C*, 114(11):4939–4949, 2010.

[118] J. Muijsers, T. Weber, R. Vanhardeveld, H. W. Zandbergen, and J. Niemantsverdriet. Sulfidation study of molybdenum oxide using moo3/sio2/si (100) model catalysts and mo-iv3-sulfur cluster compounds. *Journal of Catalysis*, 157(2):698–705, 1995.

[119] F. Müller-Plathe. A simple nonequilibrium molecular dynamics method for calculating the thermal conductivity. *The Journal of chemical physics*, 106(14):6082–6085, 1997.

[120] F. Müller-Plathe and D. Reith. Cause and effect reversed in non-equilibrium molecular dynamics: an easy route to transport coefficients. *Computational and Theoretical Polymer Science*, 9(3):203–209, 1999.

[121] S. Munetoh, T. Motooka, K. Moriguchi, and A. Shintani. Interatomic potential for si–o systems using tersoff parameterization. *Computational Materials Science*, 39(2):334–339, 2007.

[122] K. Nakada, M. Fujita, G. Dresselhaus, and M. S. Dresselhaus. Edge state in graphene ribbons: Nanometer size effect and edge shape dependence. *Phys. Rev. B*, 54:17954–17961, Dec 1996.

[123] N. Narita, S. Nagai, S. Suzuki, and K. Nakao. Optimized geometries and electronic structures of graphyne and its family. *Physical Review B*, 58(16):11009, 1998.

[124] F. Neese. Prediction of molecular properties and molecular spectroscopy with density functional theory: from fundamental theory to exchange-coupling. *Coordination Chemistry Reviews*, 253(5):526–563, 2009.

[125] E. C. Neyts, A. C. van Duin, and A. Bogaerts. Changing chirality during single-walled carbon nanotube growth: a reactive molecular dynamics/monte carlo study. *Journal of the American Chemical Society*, 133(43):17225–17231, 2011.

[126] K. D. Nielson, A. C. van Duin, J. Oxgaard, W.-Q. Deng, and W. A. Goddard. Development of the reaxff reactive force field for describing transition metal catalyzed reactions, with application to the initial stages of the catalytic formation of carbon nanotubes. *The Journal of Physical Chemistry A*, 109(3):493–499, 2005.

[127] D. Nika, S. Ghosh, E. Pokatilov, and A. Balandin. Lattice thermal conductivity of graphene flakes: Comparison with bulk graphite. *Applied Physics Letters*, 94(20):203103, 2009.

[128] D. Nika, E. Pokatilov, A. Askerov, and A. Balandin. Phonon thermal conduction in graphene: Role of umklapp and edge roughness scattering. *Physical Review B*, 79(15):155413, 2009.

[129] D. L. Nika and A. A. Balandin. Two-dimensional phonon transport in graphene. *Journal of Physics: Condensed Matter*, 24(23):233203, 2012.

[130] K. Novoselov, A. K. Geim, S. Morozov, D. Jiang, M. Katsnelson, I. Grigorieva, S. Dubonos, and A. Firsov. Two-dimensional gas of massless dirac fermions in graphene. *nature*, 438(7065):197–200, 2005.

[131] J. B. Oostinga, H. B. Heersche, X. Liu, A. F. Morpurgo, and L. M. Vandersypen. Gate-induced insulating state in bilayer graphene devices. *Nature materials*, 7(2):151–157, 2008.

[132] T. Ouyang, Y. Chen, L.-M. Liu, Y. Xie, X. Wei, and J. Zhong. Thermal transport in graphyne nanoribbons. *Physical Review B*, 85(23):235436, 2012.

[133] D. Pacile, J. Meyer, C. O. Girit, and A. Zettl. The two-dimensional phase of boron nitride: Few-atomic-layer sheets and suspended membranes. *Applied Physics Letters*, 92(13):133107–133107, 2008.

[134] C.-N. Pan, X.-K. Chen, L.-M. Tang, and K.-Q. Chen. Orientation dependent thermal conductivity in graphyne nanoribbons. *Physica E: Low-dimensional Systems and Nanostructures*, 64:129–133, 2014.

[135] L. Pan, L. Zhang, B. Song, S. Du, and H.-J. Gao. Graphyne-and graphdiyne-based nanoribbons: Density functional theory calculations of electronic structures. *Applied Physics Letters*, 98(17):173102, 2011.

[136] S. Park, K.-S. Lee, G. Bozoklu, W. Cai, S. T. Nguyen, and R. S. Ruoff. Graphene oxide papers modified by divalent ions?enhancing mechanical properties via chemical cross-linking. *ACS nano*, 2(3):572–578, 2008.

[137] Q. Peng, W. Ji, and S. De. Mechanical properties of graphyne monolayers: a first-principles study. *Physical Chemistry Chemical Physics*, 14(38):13385–13391, 2012.

[138] R. Picu, T. Borca-Tasciuc, and M. Pavel. Strain and size effects on heat transport in nanostructures. *Journal of applied Physics*, 93(6):3535–3539, 2003.

[139] S. Plimpton. Fast parallel algorithms for short-range molecular dynamics. *Journal of computational physics*, 117(1):1–19, 1995.

[140] S. Plimpton. Fast parallel algorithms for short-range molecular dynamics. *Journal of Computational Physics*, 117:1–19, 1995.

[141] P. Poizot, S. Laruelle, S. Grugeon, L. Dupont, and J. Tarascon. Nano-sized transition-metal oxides as negative-electrode materials for lithium-ion batteries. *Nature*, 407(6803):496–499, 2000.

[142] E. Pop. Energy dissipation and transport in nanoscale devices. *Nano Research*, 3(3):147–169, 2010.

[143] E. Pop, V. Varshney, and A. K. Roy. Thermal properties of graphene: Fundamentals and applications. *MRS bulletin*, 37(12):1273–1281, 2012.

[144] M. Pumera, R. Scipioni, H. Iwai, T. Ohno, Y. Miyahara, and M. Boero. A mechanism of adsorption of β-nicotinamide adenine dinucleotide on graphene sheets: Experiment and theory. *Chemistry-A European Journal*, 15(41):10851–10856, 2009.

[145] M. A. Rafiee, J. Rafiee, Z. Wang, H. Song, Z.-Z. Yu, and N. Koratkar. Enhanced mechanical properties of nanocomposites at low graphene content. *ACS nano*, 3(12):3884–3890, 2009.

[146] T. Ramanathan, A. Abdala, S. Stankovich, D. Dikin, M. Herrera-Alonso, R. Piner, D. Adamson, H. Schniepp, X. Chen, R. Ruoff, et al. Functionalized graphene sheets for polymer nanocomposites. *Nature nanotechnology*, 3(6):327–331, 2008.

[147] D. Raymand, A. C. van Duin, M. Baudin, and K. Hermansson. A reactive force field (reaxff) for zinc oxide. *Surface science*, 602(5):1020–1031, 2008.

[148] C. Reddy, S. Rajendran, and K. Liew. Equilibrium configuration and continuum elastic properties of finite sized graphene. *Nanotechnology*, 17(3):864, 2006.

[149] K. Sato, H. Horibe, T. Shirai, Y. Hotta, H. Nakano, H. Nagai, K. Mitsuishi, and K. Watari. Thermally conductive composite films of hexagonal boron nitride and polyimide with affinity-enhanced interfaces. *J. Mater. Chem.*, 20(14):2749–2752, 2010.

[150] D. O. Scanlon, G. W. Watson, D. Payne, G. Atkinson, R. Egdell, and D. Law. Theoretical and experimental study of the electronic structures of moo3 and moo2. *The Journal of Physical Chemistry C*, 114(10):4636–4645, 2010.

[151] F. Scarpa, S. Adhikari, and A. S. Phani. Effective elastic mechanical properties of single layer graphene sheets. *Nanotechnology*, 20(6):065709, 2009.

[152] M. Scarselli, P. Castrucci, and M. De Crescenzi. Electronic and optoelectronic nano-devices based on carbon nanotubes. *Journal of Physics: Condensed Matter*, 24(31):313202, 2012.

[153] F. Schedin, A. Geim, S. Morozov, E. Hill, P. Blake, M. Katsnelson, and K. Novoselov. Detection of individual gas molecules adsorbed on graphene. *Nature materials*, 6(9):652–655, 2007.

[154] P. K. Schelling, S. R. Phillpot, and P. Keblinski. Comparison of atomic-level simulation methods for computing thermal conductivity. *Physical Review B*, 65(14):144306, 2002.

[155] Q. Shao, G. Liu, D. Teweldebrhan, and A. Balandin. High-temperature quenching of electrical resistance in graphene interconnects. *Applied Physics Letters*, 92(20):202108, 2008.

[156] T. Shao, B. Wen, R. Melnik, S. Yao, Y. Kawazoe, and Y. Tian. Temperature dependent elastic constants and ultimate strength of graphene and graphyne. *The Journal of chemical physics*, 137(19):194901, 2012.

[157] V. Shenoy, C. Reddy, A. Ramasubramaniam, and Y. Zhang. Edge-stress-induced warping of graphene sheets and nanoribbons. *Physical review letters*, 101(24):245501, 2008.

[158] M. M. Shokrieh and R. Rafiee. Prediction of young?s modulus of graphene sheets and carbon nanotubes using nanoscale continuum mechanics approach. *Materials & Design*, 31(2):790–795, 2010.

[159] S. K. Singh, S. G. Srinivasan, M. Neek-Amal, S. Costamagna, A. C. van Duin, and F. Peeters. Thermal properties of fluorinated graphene. *arXiv preprint arXiv:1303.2258*, 2013.

[160] J. M. Soler, E. Artacho, J. D. Gale, A. García, J. Junquera, P. Ordejón, and D. Sánchez-Portal. The siesta method for ab initio order-n materials simulation. *Journal of Physics: Condensed Matter*, 14(11):2745, 2002.

[161] K. Srinivasu and S. K. Ghosh. Graphyne and graphdiyne: promising materials for nanoelectronics and energy storage applications. *The Journal of Physical Chemistry C*, 116(9):5951–5956, 2012.

[162] K. Srinivasu and S. K. Ghosh. Transition metal decorated graphyne: An efficient catalyst for oxygen reduction reaction. *The Journal of Physical Chemistry C*, 117(49):26021–26028, 2013.

[163] A. Strachan, A. C. van Duin, D. Chakraborty, S. Dasgupta, and W. A. Goddard III. Shock waves in high-energy materials: the initial chemical events in nitramine rdx. *Physical Review Letters*, 91(9):098301, 2003.

[164] K. Tahara, T. Yoshimura, M. Sonoda, Y. Tobe, and R. V. Williams. Theoretical studies on graphyne substructures: Geometry, aromaticity, and electronic properties of the multiply fused dehydrobenzo [12] annulenes. *The Journal of organic chemistry*, 72(4):1437–1442, 2007.

[165] J. Tan, X. He, and M. Zhao. First-principles study of hydrogenated graphyne and its family: Stable configurations and electronic structures. *Diamond and Related Materials*, 29:42–47, 2012.

[166] T. Terao and F. Müller-Plathe. A nonequilibrium molecular dynamics method for thermal conductivities based on thermal noise. *The Journal of chemical physics*, 122(8):081103, 2005.

[167] P. Timmerman, H. L. Anderson, R. Faust, J. Nierengarten, T. Habicher, P. Seiler, and F. Diederich. Fullerene-acetylene hybrids: Towards a novel class of molecular carbon allotropes. *Tetrahedron*, 52(14):4925–4947, 1996.

[168] M. Topsakal, E. Aktürk, and S. Ciraci. First-principles study of two-and one-dimensional honeycomb structures of boron nitride. *Physical Review B*, 79(11):115442, 2009.

[169] A. C. Van Duin, S. Dasgupta, F. Lorant, and W. A. Goddard. Reaxff: a reactive force field for hydrocarbons. *The Journal of Physical Chemistry A*, 105(41):9396–9409, 2001.

[170] A. C. Van Duin, A. Strachan, S. Stewman, Q. Zhang, X. Xu, and W. A. Goddard. Reaxffsio reactive force field for silicon and silicon oxide systems. *The Journal of Physical Chemistry A*, 107(19):3803–3811, 2003.

[171] G. Van Lier, C. Van Alsenoy, V. Van Doren, and P. Geerlings. Ab initio study of the elastic properties of single-walled carbon nanotubes and graphene. *Chemical Physics Letters*, 326(1):181–185, 2000.

[172] V. Varshney, S. S. Patnaik, A. K. Roy, G. Froudakis, and B. L. Farmer. Modeling of thermal transport in pillared-graphene architectures. *ACS nano*, 4(2):1153–1161, 2010.

[173] A. Vassighi and M. Sachdev. *Thermal and power management of integrated circuits*. Springer Science & Business Media, 2006.

[174] S. Walia, H. Nili, S. Balendhran, D. J. Late, K. Kalantar-zadeh, S. Sriram, and M. Bhaskaran. In situ characterisation of nanoscale electromechanical properties of quasi-two-dimensional mos2 and moo3. *arXiv preprint arXiv:1409.4949*, 2014.

[175] J.-Z. Wang, C. Zhong, S.-L. Chou, and H.-K. Liu. Flexible free-standing graphene-silicon composite film for lithium-ion batteries. *Electrochemistry Communications*, 12(11):1467–1470, 2010.

[176] Q. H. Wang, K. Kalantar-Zadeh, A. Kis, J. N. Coleman, and M. S. Strano. Electronics and optoelectronics of two-dimensional transition metal dichalcogenides. *Nature nanotechnology*, 7(11):699–712, 2012.

[177] Z. Wang, L. Zhou, et al. Metal oxide hollow nanostructures for lithium-ion batteries. *Advanced materials*, 24(14):1903–1911, 2012.

[178] K. Watanabe, T. Taniguchi, and H. Kanda. Direct-bandgap properties and evidence for ultraviolet lasing of hexagonal boron nitride single crystal. *Nature materials*, 3(6):404–409, 2004.

[179] N. Wei, L. Xu, H.-Q. Wang, and J.-C. Zheng. Strain engineering of thermal conductivity in graphene sheets and nanoribbons: a demonstration of magic flexibility. *Nanotechnology*, 22(10):105705, 2011.

[180] X. Wei, B. Fragneaud, C. A. Marianetti, and J. W. Kysar. Nonlinear elastic behavior of graphene: Ab initio calculations to continuum description. *Physical Review B*, 80(20):205407, 2009.

[181] K. B. Wiberg. Antiaromaticity in monocyclic conjugated carbon rings. *Chemical reviews*, 101(5):1317–1332, 2001.

[182] P. Wu, P. Du, H. Zhang, and C. Cai. Graphyne as a promising metal-free electrocatalyst for oxygen reduction reactions in acidic fuel cells: A dft study. *The Journal of Physical Chemistry C*, 116(38):20472–20479, 2012.

[183] P. Wu, P. Du, H. Zhang, and C. Cai. Graphyne-supported single fe atom catalysts for co oxidation. *Physical Chemistry Chemical Physics*, 17(2):1441–1449, 2015.

[184] X. Wu, M. Vargas, S. Nayak, V. Lotrich, and G. Scoles. Towards extending the applicability of density functional theory to weakly bound systems. *The Journal of Chemical Physics*, 115(19):8748–8757, 2001.

[185] X. Xiao, T. Ding, L. Yuan, Y. Shen, Q. Zhong, X. Zhang, Y. Cao, B. Hu, T. Zhai, L. Gong, et al. Wo3- x/moo3- x core/shell nanowires on carbon fabric as an anode for all-solid-state asymmetric supercapacitors. *Advanced Energy Materials*, 2(11):1328–1332, 2012.

[186] Y. Xiao, X. Yan, J. Cao, J. Ding, Y. Mao, and J. Xiang. Specific heat and quantized thermal conductance of single-walled boron nitride nanotubes. *physical Review B*, 69(20):205415, 2004.

[187] Y. Xu and D. Chung. Increasing the thermal conductivity of boron nitride and aluminum nitride particle epoxy-matrix composites by particle surface treatments. *Composite Interfaces*, 7(4):243–256, 2000.

[188] Z. Xu and D. B. Mitzi. [ch3 (ch2) 11nh3] sni3: A hybrid semiconductor with moo3-type tin (ii) iodide layers. *Inorganic chemistry*, 42(21):6589–6591, 2003.

[189] M. Xue, H. Qiu, and W. Guo. Exceptionally fast water desalination at complete salt rejection by pristine graphyne monolayers. *Nanotechnology*, 24(50):505720, 2013.

[190] Z. Yan, G. Liu, J. M. Khan, and A. A. Balandin. Graphene quilts for thermal management of high-power gan transistors. *Nature communications*, 3:827, 2012.

[191] N. Yang, Y. Liu, H. Wen, Z. Tang, H. Zhao, Y. Li, and D. Wang. Photocatalytic properties of graphdiyne and graphene modified tio2: from theory to experiment. *ACS nano*, 7(2):1504–1512, 2013.

[192] N. Yang, G. Zhang, and B. Li. Thermal rectification in asymmetric graphene ribbons. *Applied Physics Letters*, 95(3):033107, 2009.

[193] Y. Yang and X. Xu. Mechanical properties of graphyne and its family–a molecular dynamics investigation. *Computational Materials Science*, 61:83–88, 2012.

[194] H. Yu, A. Du, Y. Song, and D. J. Searles. Graphyne and graphdiyne: Versatile catalysts for dehydrogenation of light metal complex hydrides. *The Journal of Physical Chemistry C*, 117(42):21643–21650, 2013.

[195] K. Yung and H. Liem. Enhanced thermal conductivity of boron nitride epoxy-matrix composite through multi-modal particle size mixing. *Journal of Applied Polymer Science*, 106(6):3587–3591, 2007.

[196] E. Zaminpayma and P. Nayebi. Mechanical and electrical properties of function-alized graphene nanoribbon: A study of reactive molecular dynamic simulation and density functional tight-binding theory. *Physica B: Condensed Matter*, 459:29–35, 2015.

[197] C.-L. Zhang, S. Li, Y. Yuan, W.-X. Zhang, T.-H. Wu, and L.-W. LIn. Aromatization of methane in the absence of oxygen over mo-based catalysts supported on different types of zeolites. *Catalysis letters*, 56(4):207–213, 1998.

[198] H. Zhang, M. Zhao, X. He, Z. Wang, X. Zhang, and X. Liu. High mobility and high storage capacity of lithium in sp–sp2 hybridized carbon network: The case of graphyne. *The Journal of Physical Chemistry C*, 115(17):8845–8850, 2011.

[199] Y. Zhang, Q. Pei, and C. Wang. Mechanical properties of graphynes under tension: A molecular dynamics study. *Applied Physics Letters*, 101(8):081909, 2012.

[200] Y. Zhang, Q. Pei, and C. Wang. A molecular dynamics investigation on thermal conductivity of graphynes. *Computational Materials Science*, 65:406–410, 2012.

[201] Y. Zhang, Y.-W. Tan, H. L. Stormer, and P. Kim. Experimental observation of the quantum hall effect and berry's phase in graphene. *Nature*, 438(7065):201–204, 2005.

[202] Y. Zhang, T.-T. Tang, C. Girit, Z. Hao, M. C. Martin, A. Zettl, M. F. Crommie, Y. R. Shen, and F. Wang. Direct observation of a widely tunable bandgap in bilayer graphene. *Nature*, 459(7248):820–823, 2009.

[203] Y.-Y. Zhang, Q.-X. Pei, C.-M. Wang, Y. Cheng, and Y.-W. Zhang. A molecular dynamics investigation on mechanical properties of hydrogenated graphynes. *Journal of Applied Physics*, 114(7):073504, 2013.

[204] H. Zhao and N. Aluru. Temperature and strain-rate dependent fracture strength of graphene. *Journal of Applied Physics*, 108(6):064321, 2010.

[205] H. Zhao, K. Min, and N. Aluru. Size and chirality dependent elastic properties of graphene nanoribbons under uniaxial tension. *Nano letters*, 9(8):3012–3015, 2009.

[206] J. Zhao, N. Wei, Z. Fan, J.-W. Jiang, and T. Rabczuk. The mechanical properties of three types of carbon allotropes. *Nanotechnology*, 24(9):095702, 2013.

[207] X. Zhao, Q. Zhang, D. Chen, and P. Lu. Enhanced mechanical properties of graphene-based poly (vinyl alcohol) composites. *Macromolecules*, 43(5):2357–2363, 2010.

[208] J.-J. Zheng, X. Zhao, Y. Zhao, and X. Gao. Two-dimensional carbon compounds derived from graphyne with chemical properties superior to those of graphene. *Scientific reports*, 3, 2013.

[209] C. Zhi, Y. Bando, C. Tang, H. Kuwahara, and D. Golberg. Large-scale fabrication of boron nitride nanosheets and their utilization in polymeric composites with improved thermal and mechanical properties. *Advanced Materials*, 21(28):2889–2893, 2009.

[210] W.-R. Zhong, M.-P. Zhang, B.-Q. Ai, and D.-Q. Zheng. Chirality and thickness-dependent thermal conductivity of few-layer graphene: A molecular dynamics study. *Applied Physics Letters*, 98(11):113107, 2011.

[211] J. Zhou, S. Deng, N. Xu, J. Chen, and J. She. Synthesis and field-emission properties of aligned moo3 nanowires. *Applied physics letters*, 83(13):2653–2655, 2003.

[212] L. Zhou, L. Yang, P. Yuan, J. Zou, Y. Wu, and C. Yu. α-moo3 nanobelts: a high performance cathode material for lithium ion batteries. *The Journal of Physical Chemistry C*, 114(49):21868–21872, 2010.

[213] W. Zhou, S. Qi, Q. An, H. Zhao, and N. Liu. Thermal conductivity of boron nitride reinforced polyethylene composites. *Materials Research Bulletin*, 42(10):1863–1873, 2007.

[214] J. M. Ziman. *Electrons and phonons: the theory of transport phenomena in solids*. Oxford University Press, 1960.

APPENDIX A: DFT CODE FOR MoO_3

SystemName MoO3

SystemLabel MoO3

NumberOfAtoms   8

NumberOfSpecies   2 NumberOfSpecies   2

% block ChemicalSpeciesLabel

 1 42 Mo # Species index, atomic number, species label

 2 8 O # Species index, atomic number, species label

% endblock ChemicalSpeciesLabel

 LatticeConstant   1.00 Ang

% block LatticeVectors

 3.75744038   0.000000   0.000000

 0.00000   3.942245   0.000000

 0.000000   0.000000   20.393096

% endblock LatticeVector

 AtomicCoordinatesFormat Ang

% block AtomicCoordinatesAndAtomicSpecies

 0.00005533 $-$0.08350290 $-$0.00528364 2

 0.00001459 0.06448913 1.68187643 1

 1.86019828 $-$0.22130568 2.28126748 2

 $-$0.00003792 $-$0.22064732 4.09466428 2

 1.86022230 0.06541629 4.69457731 1

1.86013745	−0.08233300	6.38186501	2
0.00000058	1.84372378	1.94919227	2
1.86023864	1.84508869	4.42759073	2

% endblock AtomicCoordinatesAndAtomicSpecies

% block kgrid_Monkhorst _Pack

30	0	0	0.0000000
0	30	0	0.0000000
0	0	1	0.0000000

% endblock kgrid_Monkhorst _Pack

MeshCutoff   500 Ry

MD. TypeOfRun   CG

MD. VariableCell   .false.

MD. TargetPressure   −1.0 GPa

% block MD. TargetStress

0.0   0.0   0.0 0.0 0.0 0.0

% endblock MD. TargetStress

MD. NumCGsteps   500

MD. MaxForceTol   0.01 eV/Ang

%%%%%%%%%%%%%%%%%%%%%%%%%%%%%%%%%%%%%%%

PAO. SplitNorm   0.16

SpinPolarized   No

SolutionMethod   diagon

```
XC.functional          GGA

XC.authors             PBE

DM.NumberPulay         9

 MaxSCFIterations      100

 WriteMullikenPop      1

 WriteCoorXmol          .true.

 WriteCoorStep          .true.

 WriteForces            .true.

DM.Tolerance          0.01000000000E-03      #  Default  value
```

APPENDIX B: MD CODE FOR MECHANICAL PROPERTIES

```
#Molecular dynamics input file for graphyne

# INITIALIZATION

 units           real

 dimension       3

 atom_style      charge

 boundary        p p p

# ATOM DEFINITION

 read_data       coord.data

 mass 1 12

# GROUP DEFINE

 region top block INF INF 49.0 INF INF INF

 region bottom block INF INF INF −61 INF INF

 group top        region top

 group bottom     region bottom

 group internal subtract all top # internal atoms

 group internal subtract internal  bottom

# FORCE FIELDS

 pair_style      reax/c  NULL

 pair_coeff      * *  ffield.reax.mattsson C

# OUTPUT

 dump            1 all       xyz 10000 dump.xyz
```

```
dump            2 internal xyz 10000 dump_int.xyz

dump            3 top        xyz 10000 dump_top.xyz

dump            4 bottom     xyz 10000 dump_bottom.xyz

dump_modify 1 element   C

dump_modify 2 element   C

dump_modify 3 element   C

dump_modify 4 element   C

# COMPUTES

compute eng all pe/atom

compute eatoms all reduce sum c_eng

compute stress internal stress/atom   virial

compute xx internal reduce sum c_stress[1]

compute yy internal reduce sum c_stress[2]

compute zz internal reduce sum c_stress[3]

compute yz internal reduce sum c_stress[4]

compute xz internal reduce sum c_stress[5]

compute xy internal reduce sum c_stress[6]

# SETTINGS

thermo 20

thermo_style custom step  time temp pe pxx pyy pzz c_eatoms

   lx ly lz # c_xx c_yy  c_zz

thermo_modify line one format float %20.10f
```

```
timestep    0.1
# Minimize System Energy
min_style   cg
fix relax all box/relax iso 0.0
fix qeq all qeq/reax 1 0.0   10.0    1e−6 param.qeq
run   0
undump 2
undump 3
undump 4
minimize    1e−25 1e−15    50000 10000
unfix relax
# Print out the initial parameters
# Store final cell length for strain calculations
variable tmp equal "lx"
variable L0 equal ${tmp}
variable PE equal "pe"
variable Pxx equal "pxx"
variable Pyy equal "pyy"
variable Pzz equal "pzz"
variable Lx equal "lx"
variable Ly equal "ly"
variable Lz equal "lz"
```

```
variable Step equal "step"

variable strain equal "(lx-v_L0)/v_L0"

variable p1 equal v_strain

print "Initial length Lx is: ${L0}" file data.txt

print "step strain PE lx ly lz Pxx Pyy Pzz " append data.txt

print "${Step} ${p1} ${PE} ${Lx} ${Ly} ${Lz} ${Pxx} ${Pyy} ${
    Pzz} " append data.txt

# Apply the deformation

variable stressx equal c_xx

variable stressy equal c_yy

variable stressz equal c_zz

variable i loop 200

label loopa

    change_box all x scale 1.001 remap

    fix relax all box/relax y 0 z 0

    minimize   1e-25 1e-15   50000 10000

    unfix relax

print "${Step} ${strain} ${PE} ${Lx} ${Ly} ${Lz} ${Pxx} ${Pyy
    } ${Pzz} " append data.txt

next i

jump SELF loopa

print "All done"
```

APPENDIX C: MD CODE FOR THERMAL CONDUCTIVITY

```
# Molecular dynamics input file for armchair graphyne
# INITIALIZATION
units              real
dimension          3
atom_style         charge
boundary p p p
# ATOM DEFINITION
read_data          coord.data
# FORCE FIELDS
pair_style         rebo
pair_coeff         * * CH.airebo C
# GROUPS
region interior block     INF   INF   -20.0   9.0     INF INF
group   interior region     interior
group   boundary subtract all   interior
# COMPUTES
compute eng all pe/atom
compute eatoms all reduce sum c_eng
compute newT all temp
# SETTINGS
thermo 1000
```

```
thermo_style custom step   time temp c_eatoms lx ly lz

thermo_modify line one format float %20.10f temp newT

timestep  0.0005

# OUTPUT

dump 2         all      xyz 50000   dump.xyz

dump_modify    2     element C

# MINIMIZE SYSTEM ENERGY

fix qeq all qeq/reax 1 0.0   10.0    1e−6 param.qeq

min_style   cg

fix    1   all box/relax iso 0 vmax 0.001

minimize    1e−25 1e−15    50000 10000

unfix 1

fix freeze boundary setforce 0.0    0.0    0.0

#fix mom interior momentum 1 angular  # to prevent the

    spurious global rotation of the system

# Equilibrating the system

velocity interior create 300 4928459

fix 1 interior nve

fix 2 interior temp/berendsen 300 300   0.1

run 200000

unfix 1

unfix 2
```

fix 2 interior nvt temp 300 300 0.1

run 500000

unfix 2

2nd Equilibration run

reset_timestep   0

compute ke interior ke/atom

variable temp atom c_ke/1.5*503.219574

fix 1 interior   nve

fix 2 interior   ave/spatial 1 100000 100000 x **lower** 0.02

   v_temp file tmp.profile units reduced

fix 3 interior   thermal/conductivity 400 x 50

variable tdiff equal f_2[26][3] − f_2[1][3]

thermo 100000

thermo_style custom step time temp c_eatoms lx ly lz f_3

   v_tdiff

thermo_modify **line** one **format** float *%20.10f temp newT*

run   3000000

Thermal conductivity calculations

variable t equal time

compute vacf interior vacf

variable v1 equal c_vacf[1]

variable v2 equal c_vacf[2]

```
variable v3 equal c_vacf[3]

variable v4 equal c_vacf[4]

fix 4   interior

print 1 "${v1} ${v2} ${v3} ${v4}" file vacf.dat

fix 3   interior    thermal/conductivity 400 x   50

variable   flux equal f_3

fix   ave   interior    ave/time 1 1 100000   v_tdiff ave
   running

variable   ave equal f_ave

fix flux   interior

print 100000 "$t ${flux} ${tdiff} ${ave}" file flux.dat

thermo_style custom step   time temp c_eatoms lx ly lz f_3
   v_tdiff   f_ave

run 3000000

# SIMULATION DONE

print "All done"
```